SAPIENZA
UNIVERSITÀ DI ROMA

Department of Physics

Accelerator Physics PhD School – XXXII cycle

Studies and Measurements on Cavity Beam Position Monitors for Novel Electron Linacs

Giovanni Franzini

Director of Doctoral School:
Prof. Daniele Del Re

Supervisor:
Prof. Luigi Palumbo

Co-supervisor:
Prof. Andrea Mostacci

A.A. 2018/2019

Studies and Measurements on Cavity Beam Position Monitors for Novel Electron Linacs

G. Franzini

Contents

Introduction

Beam diagnostics is an essential constituent of any accelerator. It is the 'organ of sense' showing the properties and the behaviour of the beam. It deals with the real beam including all possible imperfections of a real technical installation. With the development of acceleration techniques, beam diagnostics have also evolved to provide more precise and faster measurements [1].

There is a large variety of beam parameters to be measured. For each of them, there are various diagnostic devices and measurement techniques which can be used, depending on many different aspects. To name a few, the accelerator type, the beam structure and composition, the resolution and accuracy wanted, the minimum and maximum range of measurements, the interaction with the beam (interceptive/non-interceptive) are all important aspects to take into accounts. There are also many engineering aspects which play a major role in the project and development of beam diagnostics, such as the reliability of the devices involved, their cost, the availability of space along the beam line, the complexity and availability of the read-out electronics.

One of the most fundamental beam parameters to be measured is the beam position. Of all the types of devices used to measure it, Beam Position Monitors (BPM) are the most frequent diagnostics used at nearly all linacs, cyclotrons and synchrotrons [2]. BPMs deliver the center-of-mass of the beam along the transversal plane, by using non-destructive diagnostic devices. There are many types of BPMs which were developed during the last decades. They are based on the presence of electromagnetic pick-ups installed along the beam pipe/trajectory, which are typically used to measure the charge induced by the electric field of the beam particles. Most type of BPMs (e.g. stripline or button BPMs) take advantage of the geometrical disposition of the pick-ups in order to reconstruct the center-of-mass of the beam.

Another type of BPM, whose electromagnetic pick-ups are represented by resonance cavities, is the Cavity BPM (cBPM). This type of BPM and the related read-out electronics are the focus of this thesis. More specifically, most of the studies and development were performed for the installation of four cBPMs for the Extreme Light Infrastructure Nuclear Physics – Gamma Beam System Electron Linac (ELI-NP GBS) [3], whose commissioning and development was carried on in the last years and is now halted due to contract dispute. The latter is a high intensity and monochromatic gamma source under construction at IFIN-HH in Magurele (Romania). The photons will be generated by Compton back-scattering at the interaction between a high power recirculated laser and

a high quality electron beam, accelerated by an electron linac at energies up to 740 MeV. Cavity BPMs play a major role for the generation of the gamma beams, as they are used immediately before and after the two interaction points between the laser and the electron beam. This is done in order to get high resolution position measurements for the latter, which is mandatory to match the strict requirements requested for this facility. Most of the work presented in this dissertation is related to the development and characterization of dedicated read-out electronics for cBPM. The development was carried on in collaboration with Instrumentation Electronics, with the aim of creating a system capable of properly read and process the output signals of the cBPMs and deliver beam position measurements with a resolution and precision which match the requirements of ELI-NP GBS. Read-out electronics is, for many aspects the most critical part of the system. This is due to the fact that if not carefully designed, the accuracy, the resolution and the repeatability of the measures can be heavily affected, reducing the overall performance of the measuring system. Even though the research activities were mainly focused for the ELI-NP GBS application, results obtained are being used as a starting point for the development of the diagnostics for a new electron linac, currently under study for the EuPRAXIA project [4]. The latter aims at designing the world's first accelerator based on advanced plasma-wakefield techniques to deliver 5 GeV electron beams. Research and development presented in this dissertation were conducted mainly at the "Istituto Nazionale di Fisica Nucleare – Laboratori Nazionali di Frascati" (INFN-LNF). The measurements in presence of the beam were performed at the electron linac of FLASH at DESY and will be repeated at the electron linac of SPARC-LAB at INFN-LNF. In the latter case, a test bench for the cBPMs and their read-out electronics was designed, developed and installed in the linac.

Dissertation overview

This dissertation is divided in seven chapters. The first four presents the theory and the description of the devices involved, as well as a general overview of the ELI-NP GBS linac. The last three chapters describe the experiments and the measurements performed with cBPMs and their read-out electronics and the results achieved.

In Chapter 1, a general overview of ELI-NP GBS is presented. We also discuss the main parameters of the electron linac and the reason of using cBPMs. In particular, we will highlight the impact of the project requirements and beam specifications to the design of the measuring system based on cBPM.

In Chapter 2, an overview of the diagnostic systems of ELI-NP GBS, with a particular focus on the non-interceptive devices, is presented. Reasons and requirements on the design of all the measuring system are presented.

In Chapter 3, a general description of the working principle of the cBPM will be discussed. Specifications and features of the cBPM model used will also be presented.

In Chapter 4, we will describe in details the read-out electronics specifically developed for the ELI-NP GBS cBPMs and all its features.

In Chapter 5, the description of the test bench developed in laboratory in order to characterize both the cBPMs and the read-out electronics will be presented. The results obtained by this preliminary characterization will be discussed, as well as the advantages/disadvantages of testing the devices without the beam.

In Chapter 6, beam measurements performed at DESY on the read-out electronics are presented. In this case we used a test-bench already installed at FLASH1 with a different type, but with similar specifications, of cBPMs. This chapter contains also some ideas on possible new upgrades for a future version of the electronics.

In Chapter 7, conclusions, perspectives and future works will be discussed. The test bench developed and installed for the cBPMs at SPARC-LAB will also be presented.

1 Extreme Light Infrastructure – Nuclear Physics – Gamma Beam System

The Extreme Light Infrastructure Nuclear Physics Gamma Beam System (ELI-NP-GBS) is a new Compton source operating in the gamma energy range (0.2-19.5 MeV) that aims to provide gamma beams suitable for different kind of applications, both industrial and scientific. More specifically, gamma beams will allow to probe the matter on microscopic-to-nuclear scales in space and time. They can be used in imaging and nuclear fundamental physics, as well as for many other applications in a large number of fields: medicine, biology, material science, national security and high energy physics.

The ELI-NP GBS project was assigned to the EuroGammas consortium [3], which is formed by European research institutions and commercial companies. The Istituto Nazionale di Fisica Nucleare (INFN) is the project leader, working in collaboration with the "Università di Roma La Sapienza", the Centre National de la Recherche Scientifique (CNRS), ACP S.A.S., Alsyom S.A.S., Comeb Srl and ScandiNova Systems AB. The aim is to install and commissioning the Compton source in Magurele, near Bucharest (RO) [5].

ELI-NP GBS is part of the ELI project [6], an international laser research infrastructure, funded mainly by EU structural funds, that will host high-level research on ultra-high intensity laser, laser-matter interaction and secondary light sources. ELI-NP is one of the three main project of this infrastructure, dedicated on Nuclear Physics research and applications. The other two main project are represented by: "ELI Beamlines" [7], devoted to the development and usage of dedicated beam lines with ultra-short pulses of high energy radiation and particles, to be built in Prague (CZ); "ELI ALPS" [8], designed to conduct temporal investigation of electron dynamics in atoms, molecules, plasmas and solids at attosecond scale, to be built in Szeged (HU).

In ELI-NP GBS, the gamma beams will be generated by inverse Compton back-scattering at the interaction between a high power recirculated laser and a high quality and brightness electron beam, produced by a normal conducting linac [3],[9].

The main specifications of ELI-NP GBS are reported in Table 1.1 and the general layout is presented in Figure 1.1.

Table 1.1: Summary of Gamma ray specifications of ELI-NP GBS

Photon Energy	0.2 – 19.5 MeV
Spectral Density	0.8 – 4 $\cdot 10^4$ ph/s·eV
Bandwidth (rms)	≤ 0.5%
# photons per shot within FWHM BW	≤ 2.6 $\cdot$ 10^5
# photons/s within FWHM BW	≤ 8.3 $\cdot$ 10^8
Source size (rms)	10 – 30 µm
Source divergence (rms)	25 – 200 µrad
Peak Brilliance	10^{20} – 10^{23} ph/(s·mm^2· mrad^2· 0.1%)
Radiation Pulse length (rms)	0.7 – 1.5 ps
Linear Polarization	≥ 99%
Macro repetition rate	100 Hz
# of pulses per macropulse	≤ 32
Pulse to pulse separation	16 ns

To reach these challenging specifications, in particular the high value of spectral density, an innovative interaction point module, used for the collision between the electron beam and the laser was designed. The laser pulses generated (see Table 1.2 for the main specifications) are recirculated 32 times at the interaction point within the Interaction Point Module, in order to collide with a multi-bunch electron beam pulses (constituted by 32 bunches, separated by 16.1 ns). A detailed analysis and description of this new optical device can be found in [10], while a general description of the linac will follow in section 1.2 and can be further deepened in [11].

Table 1.2: Summary of Laser Pulse specifications at the interaction points of ELI-NP GBS

Pulse Energy	0.2 – 0.4 J
Wavelength	515 nm
Energy	2.4 eV
Pulse Length (rms)	1.5 ps
Laser M^2	1.2
Pulse Repetition Rate	100 Hz
Waist	28.3 µm
Collision Angle	172°
Passes through the interaction point	32

ELI-NP GBS will be one of the most performing devices in producing radiation with short wavelength, high power, ultrashort time duration, large transverse coherence and tunability. Since the photon energy gain factor in the high energy inverse Compton scattering mainly depends on the energy of the colliding electron beam, the photon beam energies can be easily extended to cover a wide range from soft X ray to very high

energy gamma ray. Another advantage of Compton sources is that secondary photons emitted by inverse Compton scattering present an energy-angle correlation. Thus, by using a collimation system, it is possible to obtain a quasi-monochromatic photon beam, while the forward focusing ensures high spectral densities in small bandwidths.

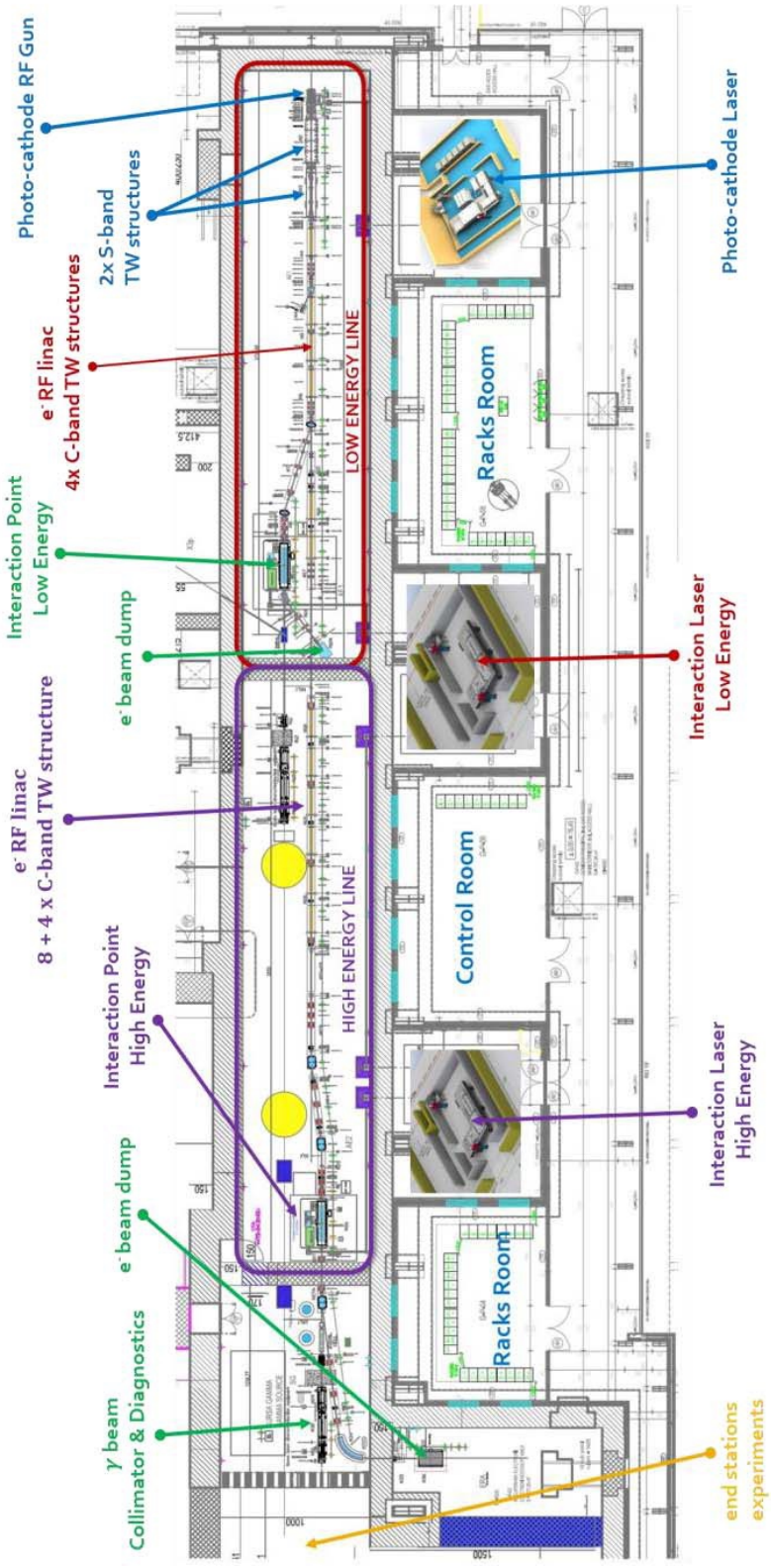

Figure 1.1: Layout of ELI-NP GBS [12].

1.1 Interaction points and Cavity BPMs

At ELI-NP GBS, two interaction points module are foreseen: one for electron energies up to 280 MeV and the other for energies up to 740 MeV. In both modules (which share the same layout), the laser is recirculated up to 32 times in order to collide with the electron beam, constituted by trains of 32 bunches. The laser is injected in the module and will be reflected by means of two Parabolic Mirrors and 31 Mirror Pair Systems, intercepting the interaction point with an angle of 172° in respect to the electron beam (see Figure 1.2) [10].

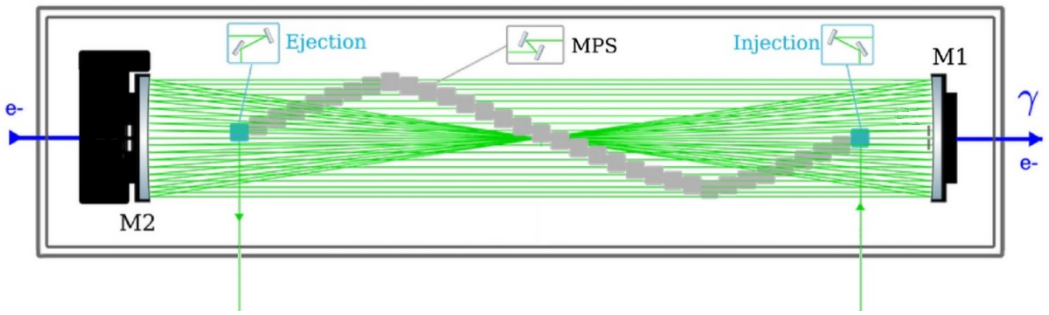

Figure 1.2: Schematic top view of the interaction point module. The green trace represents the laser recirculated 32 times through two parabolic mirrors (M1, M2) and the Mirror Pair System (MPS) [10].

The gamma rays are produced by means of inverse Compton back-scattering. The scattered photon energy E_g is given by [13]:

$$E_g = \frac{(1 - \beta \cos\theta_i) E_{ph}}{\left(1 - \beta \cos\theta_f\right) + \left(1 - \cos\theta_p\right) E_{ph}/E_{el}} \qquad (1.1)$$

where β is the speed of the incident electrons relative to the speed of light; θ_i is the polar angle between the incident photons and electrons directions; θ_f is the scattering angle of the photons; θ_p is the polar angle between the incident and scattered photons directions and is equal to θ_i - θ_f; E_{ph} is the incident photons energy; E_{el} is the electrons energy (refer to Figure 1.3).

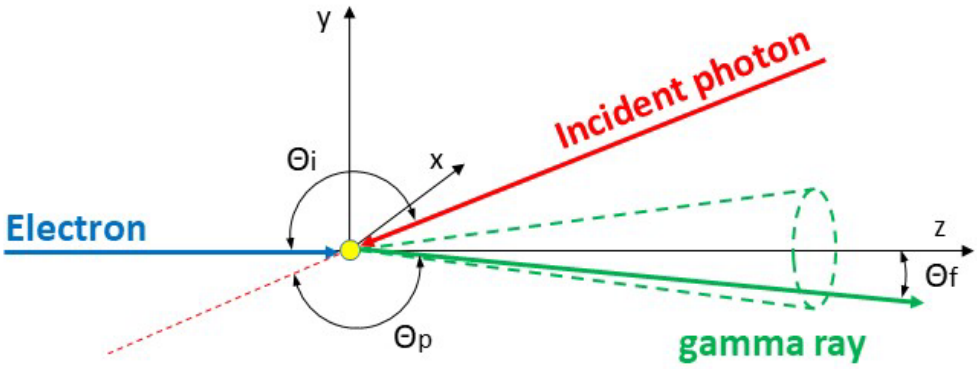

Figure 1.3: Representation of Compton scattering from the collision of an electron beam and incident photons.

To adapt the formula for ELI-NP GBS we can consider the nominal values for the following quantities: E_{el} = 740 MeV (maximum value), E_{ph} = 2.4 eV, θ_i = 172°. By fixing this quantities, it is possible to show the relation between the scattered photon energy E_g and the scattering angle θ_f, plotted in Figure 1.4 [14].

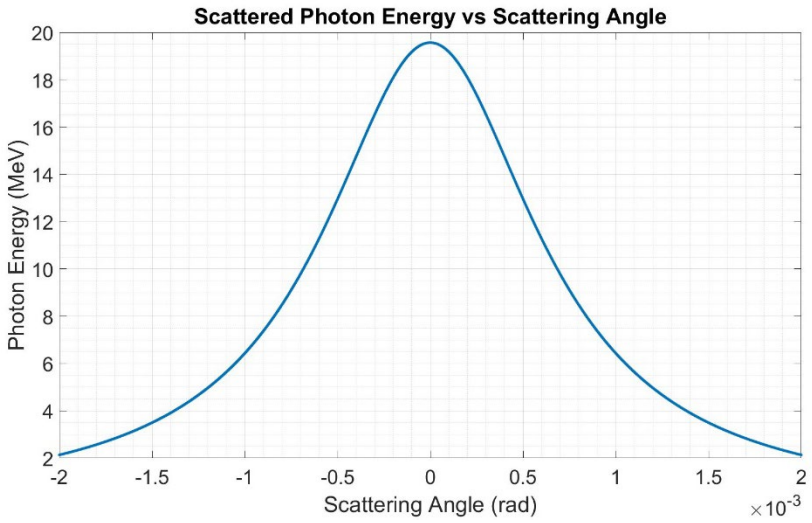

Figure 1.4: Relation between the scattered photon energy (E_g) and the scattering angle (ϑ_f), for a simulated Compton scattering with the nominal parameters of ELI-NP GBS.

It is possible to see that, with a good approximation, the maximum energy (about 19.5 MeV) is obtained for $\theta_f = 0$ and that the higher is the scattering angle, the lower is the photon energy. The energy is independent from the azimuth angle. Thus, by using an observation plane downstream from the collision point and perpendicular to the electron beam direction, photons of equal energies would be disposed in concentric circles [13]. From a practical point of view this energy distribution is exploited in ELI-NP

GBS by using a gamma-ray collimator in order to achieve a scattered photon beam with a small energy spread. The intensity of the scattered photons is also dependent on the scattering angle. The maximum intensity is achieved at $\theta_f = 0$ and decrease for higher values of θ_f [13].

Given the dependency of Energy and Intensity from the scattering angle and the tight specifications on the gamma beam (see Table 1.1), an alignment system for the Interaction Point module and the collimators is foreseen. Precise position measurements of the electron beam at the interaction point are also mandatory. The problem is not only to the transversal position of the electron bunches, which should be optimized to fully intercept the recirculated laser, but also for the angle of the electron beam, that is important for the energy and spatial distribution of the gamma rays produced. To fulfil this requirements, Cavity BPMs will be installed immediately before and after the two Interaction points modules, as depicted in Figure 1.5. This would give the opportunity to measure the position and the angle of the beam at the Interaction points for each of the 32 bunches of the electron macro pulses. The resolution requirement for the transversal beam position, as measured by the Cavity BPM, was estimated to 1 μm, over a measurable range of ±1 mm.

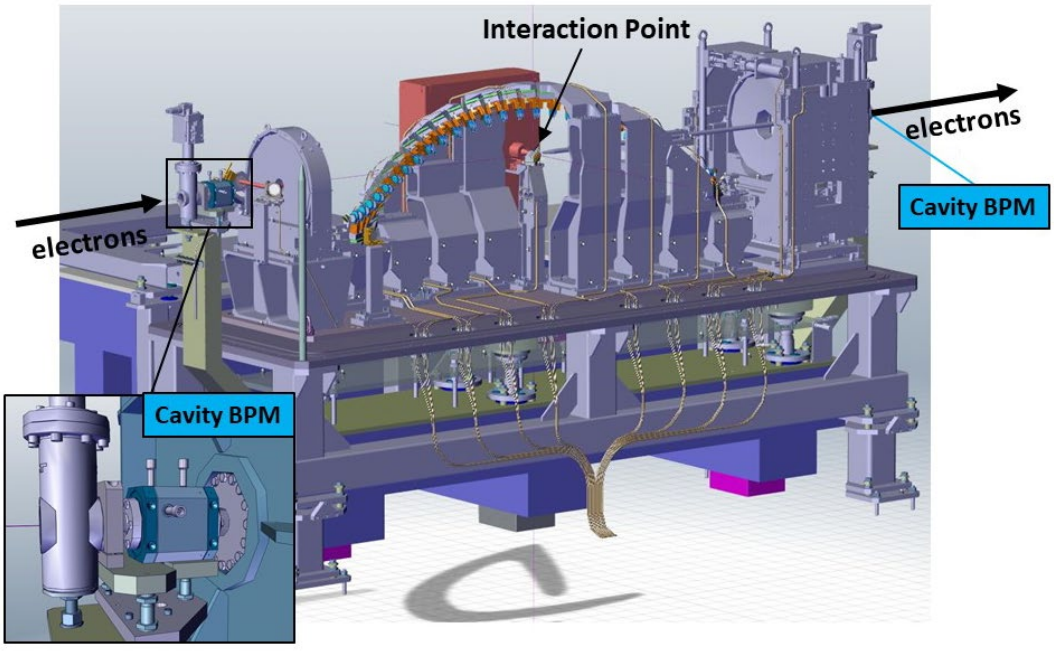

Figure 1.5: 3D view of the complete interaction point module. Cavity BPMs are installed immediately before and after the module [10].

1.2 ELI-NP-GBS LINAC overview

The Gamma Beam System (GBS) [2] is based on a warm RF linear accelerator operated at the C-band mode, with S-band photo-injector. The general layout of the machine is shown in Figure 1.1. The linac will deliver electron beams in the energy range of 80 – 740 MeV. It will operate at 100Hz repetition rate with trains of 32 electron bunches, separated by 16.1 ns and a 250 pC nominal charge (see Figure 1.6). The requirements of the electron beam at Interaction Points are reported in Table 1.3.

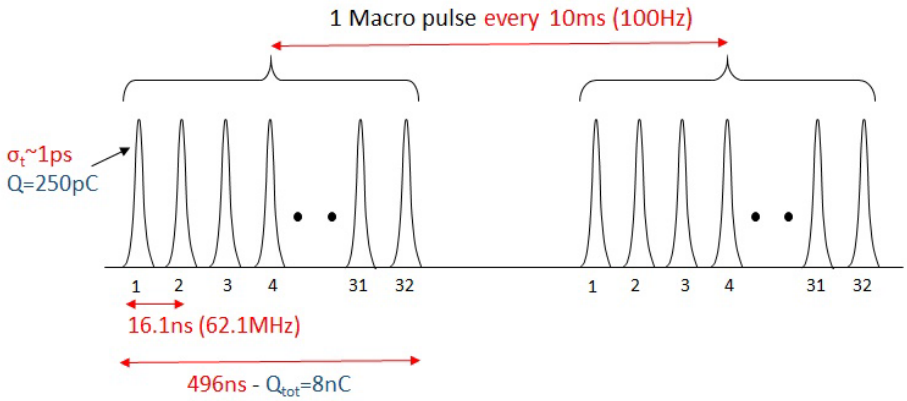

Figure 1.6: ELI-NP GBS electron beam representation in multi-bunch operation mode.

There are two stages, the first stage will produce electrons with energy up to 280 MeV (low energy line), and the second stage the electrons will be accelerated up to 740 MeV (high energy line). At the end of both energy lines, the two Interaction Point Modules are foreseen. The electron beam at the GBS will be generated in the laser-driven photocathode mounted in 1.6 cell standing-wave cavity what all together constitutes the RF gun. It will operate with high electric field gradients 120 MV/m. By illumination of the cathode with laser pulses, the electron bunches, each with the length of 10 ps, will be emitted. The high gradient of radio-frequency field will provide rapid acceleration to relativistic energies. In the first two travelling wave accelerating structures the beam will gain the energy approximately 80 MeV. These are the constant gradient (22 MV/m) structures and will operate at 2.856 GHz (S-band), with the cell phase advance of $2\pi/3$. They will also act as a bunch compressor, decreasing the bunch length from 10 ps to 1 ps, by employment of the velocity bunching.

The linac booster will be composed of 12 travelling wave structures working at 5.712 GHz (C-band) in TM_{01} mode with the cell phase advance of $2\pi/3$, and quasi-

constant accelerating field gradient 33 MV/m. For a deepening on the Linac, refer to [11].

Table 1.3: Summary of Electron Beam Parameters at Interaction Points of ELI-NP GBS

Energy	80 – 740 MeV
Bunch Charge	25 – 250 pC
Bunch Length	100 – 400 µm
ε_n_x,y	0.2 – 0.6 mm·mrad
Bunch Energy spread	0.04 – 0.1 %
Focal Spot Size	> 15 µm
# of bunches in the train	≤ 32
Bunch separation	16 ns
Energy Variation along the train	0.1 %
Energy jitter shot-to-shot	0.1 %
Emittance dilution due to beam break-up	< 10 %
Time Arrival Jitter	< 0.5 ps
Pointing Jitter	1 µm

2 Diagnostics for ELI-NP GBS

2.1 Overview

Various diagnostics devices have been foreseen to be installed in the LINAC, in order to measure the properties of both the macro-pulses and the single bunches. The devices used for the intercepting type of measurements are Optical Transition Radiation (OTR) and YAG screens. A total of 23 stations will be installed along the LINAC: 12 on the Low Energy LINAC, 11 on the High Energy LINAC. They will be used to measure the Beam Position (Centroid) and the Spot Size of the beam. They will also be used to measure the beam energy and its spread, the bunch length and the Twiss parameters, in conjunction with a dipole, an RF deflector and quadrupoles respectively [15]. The devices used for non-intercepting measurements are Beam Charge Monitors (BCM) and Beam Position Monitors (BPM) (see Figure 2.1). The former ones are based on the Integrating Current Transformers (ICT) [2], which will be installed in 4 different positions (3 in the low energy LINAC, 1 in the high Energy LINAC). Concerning the Beam Position Monitors, two different types will be installed: Stripline Beam Position monitors are the most common. 29 of them will be installed, specifically 13 in the Low Energy LINAC, 16 in the High Energy LINAC. Near the interaction points (both at low energy and high energy), a total of 4 Cavity Beam Position Monitors will be installed.

A quick overview of the non-interceptive diagnostics used in ELI-NP GBS is described in the next sections.

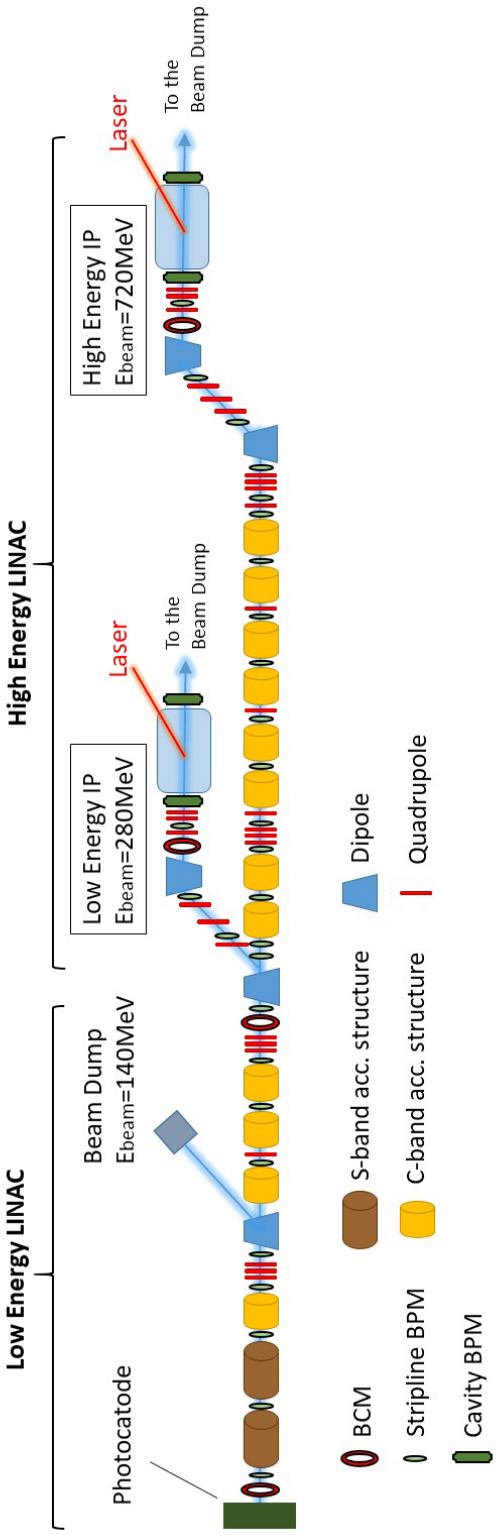

Figure 2.1: Simplified layout of ELI-NP GBS. Both dump lines after the interaction points and some accelerator components are not depicted (e.g. corrector magnets and beam screens).

2.2 Beam Charge Monitors

Beam charge monitors (BCM) will be installed in four positions: the first one will be located right before the first S-band accelerating structure; the second one will be located at the end of all the accelerating structures of the Low Energy LINAC, before the so-called “dogleg”; the third and the fourth will be installed before the low energy and the high energy interaction points. These four locations will allow studying the losses of charge of the beam at the key-points of the LINAC.

Figure 2.2: Integrating Current Transformer from Bergoz Instrumentation for ELI-NP GBS.

BCMs will have the capability to measure the charge of every single bunch, within the macro pulse. The devices which will be installed along the linac are the Integrating Current Transformers (ICT) from Bergoz Instrumentation (see Figure 2.2), whose specifications are reported in Table 2.1. The ICT generates a pulse signal with a nominal duration of 5 ns when a beam bunch pass through it. By integrating the pulse and applying a scale factor (the inverse of the ICT Sensitivity), it is possible to calculate the bunch charge, as shown in Eq. (2.1).

$$Q_{bunch} = \frac{1}{S} * \int_{0}^{16ns} V_{out}(t)dt \qquad (2.1)$$

The ICT operates as a band-pass filter on the signal generated by the passage of a beam bunch through the toroid. The latter could be considered as the input signal of the system. As such, a bunch of ~1 ps will induce an output signal with a duration of 5 ns, by maintaining a proportionality between the charge of the output signal and the charge

of the bunch. The duration of the output signal is short enough to measure the charge bunch by bunch.

Table 2.1: Main parameters of the ICTs for GBS. In parenthesis the measured values in laboratory.

Parameter	Value
Sensitivity (S) in a 50Ω load	5 Vs/C *(4.96 Vs/C)*
Beam charge to output charge ratio in 50Ω load	~10:1
Output pulse duration (6σ)	5 ns *(5.6 ns)*
Output signal droop	3.59 %/µs *(3.57 %/ µs)*
f_{low} / f_{high}	5.3kHz/191MHz *(4.5kHz/180MHz)*

The output signals are digitized with 10bit 4GS/s ADC (Agilent M9210A) and processed by a cPCI crate embedded system with a dedicated control software written in EPICS. The latter will calculate the charge for each bunch window, by applying a calibration factor and offset compensation chosen by the user. For a detailed overview of the system refer to [15].

2.3 Stripline Beam Position Monitors

A total of 29 Stripline BPMs will be installed in ELI-NP GBS. They are the main devices used to measure the average position of the macro pulse along the LINAC. The design is the same for all of them (Figure 2.3), except for the one installed on the dump line after the low energy interaction point, which was designed in order to have a larger beam acceptance range (Ø100 mm) [15].

Stripline BPMs are composed of four stainless steel electrodes of length L = 140mm and width w = 7.7 mm, mounted with a π/2 rotational symmetry at a distance d = 2mm from the vacuum chamber, to form a transmission line of characteristic impedance Zo=50 Ω with the beam pipe. Their acceptance is Ø34mm.

The amplitude of the frequency response presents a sinusoidal shape with maxima at odd multiples of c/4L (~535MHz), selected to be as close as possible to the operating

frequency of the detection electronics and to present non-zero response at the LINAC frequency of 2856 MHz.

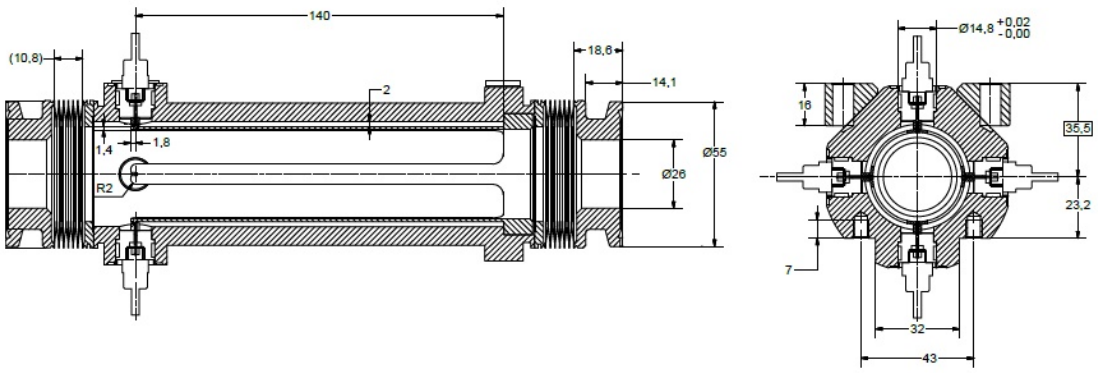

Figure 2.3: Stripline BPM schematics for ELI-NP GBS.

The read-out electronics is represented by Instrumentation Technologies "LIBERA Single pass E" modules. The latter provides analogue front-end electronics to handle the pulse-like signals generated by the passage of the beam on the striplines. The signals are then digitized and processed by an FPGA, in order to calculate the average position of each train of bunches. Horizontal and vertical positions are calculated in first approximation with a difference over sum algorithm applied to the measured amplitude of the signals coming from the corresponding pair of striplines (horizontal and vertical). For ELI-NP GBS, in order to use the full BPM acceptance area without accuracy losses due to non-linearities, we plan to use correction algorithms, developed on the basis of simulations and measurements of BPMs response. In particular, suitable high-order surface polynomials will be used. The calibration factors, used in the polynomial equations, will be extrapolated from the measurements and calibration performed at ALBA laboratories [16] for each BPM and will be implemented directly in the LIBERA Single Pass E modules.

There is also the plan to calculate the charge of each train of bunches by using the output signals of the BPM, in order to increase the number of the charge measurements all along the LINAC [17].

2.4 Cavity Beam Position Monitors

The importance of having high resolution measurements for the beam position at the Interaction points was discussed in section 1.1. Cavity BPMs were selected as the devices which could guarantee the best performances, also in presence of low charge beams, in terms of position resolution for bunch by bunch measurements. Moreover, they give the possibility to measure the charge of each bunch. The cavity pick-up is the PSI BPM16 model, consisting of two resonators with low quality factor (Q = 40) and a resonance frequency of 3.3 GHz [18],[19].

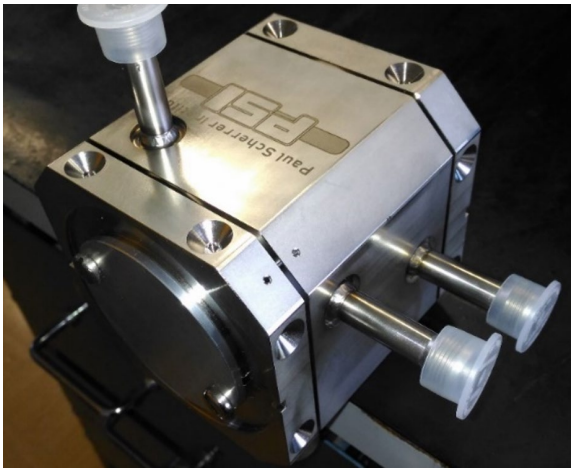

Figure 2.4: Picture of the Cavity BPM model PSI BPM16 used for ELI-NP GBS

The low Q allows to measure the charge and the position of the beam bunch by bunch. In fact, the output signals associated to the passage of a single bunch will decay faster than the time interval between bunches (16 ns). An in-depth discussion of the working principles and features is presented in Chapter 3.

The readout electronics has been specifically designed for the cavity BPM of ELI-NP GBS in collaboration with Instrumentation Technologies. A detailed description of the read-out electronics, as well as the characterizations performed in laboratory and in presence of beam are discussed in Chapter 4, 5, 6.

3 Cavity Beam Position Monitors

The basic idea of the Cavity Beam Position Monitor (cBPM) is quite old, which backs to 1960's. When SLAC was built, this type of BPMs were installed in the drift session along the accelerator and in the beam switchyard [20]. From that time, various configuration of BPM cavities and read-out electronics have been developed in many laboratories and widely used to monitor the beam trajectory mostly in linacs. The type of cBPM that will be discussed in this dissertation is one of the most diffused and is based on the presence of two pillbox cavities.

3.1 Theory and Working principle

Cavity BPM is based on the resonant modes excited in the pillbox cavities when a bunch transit through them. For a cavity with L < 2.03R, where L is its length and R is its radius, the monopole mode TM_{010} is the fundamental oscillation of the cavity [21]. For beams near the center of the cavity, the monopole mode is symmetric and is proportional to the charge of the excitation bunch (see Figure 3.1, left picture). This constitutes the first piece of information used for the beam position calculation, as will be described later. The beam bunch will excite also higher order modes of the cavity, in particular the dipole mode TM_{110}. Its amplitude has a linear dependence on the charge of the bunch as well as on the transverse offset of the beam relative to the electromagnetic (e.m.) center of the cavity. Its phase depends on the direction of the beam offset.

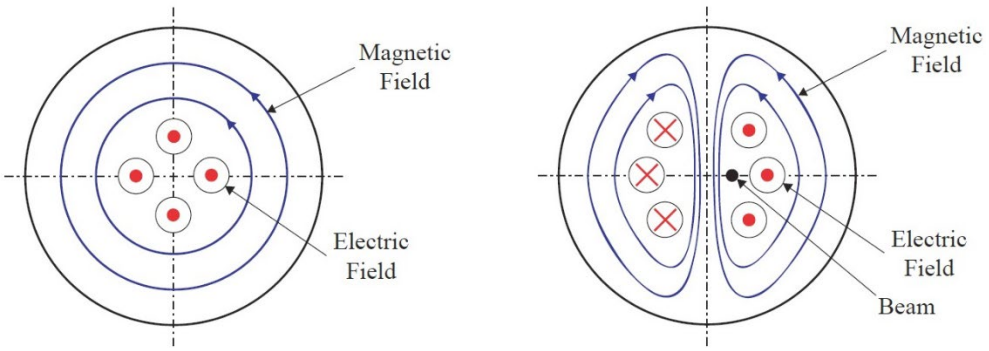

Figure 3.1: Representation of a pillbox cavity section. The electromagnetic fields of the TM_{010} (left) and TM_{110} (right) modes are shown, as excited by the passage of a beam bunch.

Beam position calculation is based on the measurements of the amplitudes of these two modes. Two cavities, placed one after the other in respect to the beam direction, are used: one, named “reference” cavity (or resonator) to measure the amplitude of the monopole mode; the other, named “position” cavity to measure the amplitude of the dipole mode. The monopole mode measurement is used as a reference for two reasons:

1. the amplitudes of the two modes are compared (i.e. the ratio is calculated) in order to obtain a quantity which is dependent only on the beam position, regardless of the bunch charge.
2. The phase of the two modes are compared in order to obtain the direction of the beam offset. This is possible because the monopole mode has always the same phase, while the dipole mode phase depends on the direction of the beam offset.

The explicit expressions for the fields of the TM_{010} (eq.(3.1)) and TM_{110} (eq.(3.2)) are reported in [20] and [21], for the simple case of a pillbox cavity with radius R and length L. These expressions can be considered an approximation of the real case, because they do not take into accounts the presence of the beam pipe and of the waveguides (see later on this paragraph) or other factors, such as the crosstalk between the fields excited in the two cavities. For a short introduction on pillbox cavities for particle accelerators, refer to [22].

$$\begin{aligned} E_z &= A \cdot J_0(j_{01} r) \cdot e^{i\omega_{010} t} \\ H_r &= 0 \\ H_\phi &= -i \frac{A \cdot j_{01}}{\omega_{010} \mu} \cdot J_1'(j_{01} r) \cdot e^{i\omega_{010} t} \end{aligned} \qquad (3.1)$$

$$\begin{aligned} E_z &= A \cdot J_1(j_{11} r) \cdot \cos(\phi)\, e^{i\omega_{110} t} \\ H_r &= -i \frac{A}{\omega \mu} \cdot \frac{J_1(j_{11} r)}{r} \cdot \sin(\phi)\, e^{i\omega_{110} t} \\ H_\phi &= -i \frac{A \cdot j_{11}}{\omega_{110} \mu} \cdot J_1'(j_{11} r) \cdot \cos(\phi)\, e^{i\omega_{110} t} \end{aligned} \qquad (3.2)$$

J_0 and J_1 are the Bessel functions of the first kind of order 0 and 1; j_{01} and j_{11} are their roots; ω_{010} and ω_{110} are the resonant angular frequencies, calculated with eq.(3.3), where c is the speed of light;

$$\omega_{mnp} = c\sqrt{\left(\frac{j_{mn}}{R}\right)^2 + \left(\frac{p\pi}{L}\right)^2} \qquad (3.3)$$

A_0 and A_1 are equal to E_0/J_{0max} and E_1/J_{1max}. J_{0max} and J_{1max} are the maximum value of the Bessel functions and E_0, E_1 are the maximum value of the electric fields at a radius (r_I) corresponding to the maximum of the Bessel function (refer to Figure 3.2).

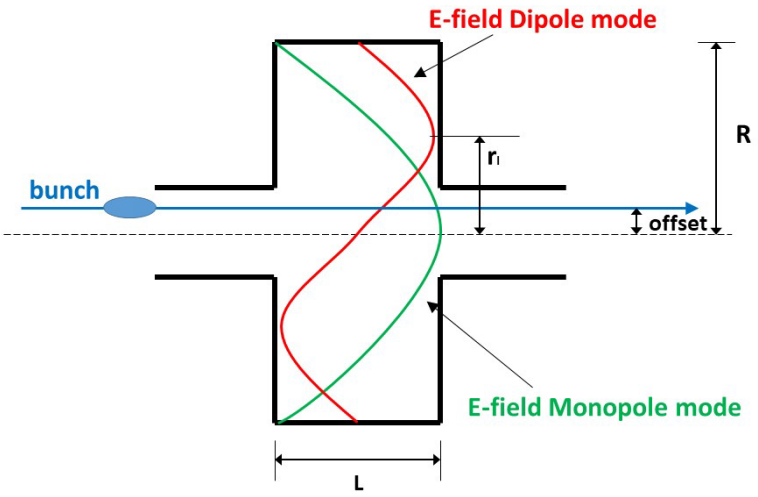

Figure 3.2: Representation of the excitation of the monopole and dipole mode at the passage of a beam bunch. The dipole mode is excited only if the beam has an offset in respect to the electromagnetic center of the cBPM.

To calculate how the modes of the cavity are excited by the beam bunch, we need to calculate the energy released by the latter. This depends entirely on the geometry of the cavity and the properties of the bunch (i.e. in first approximation, direction, offset and charge). The key parameter for the cavity is the normalized shunt impedance, defined as:

$$\frac{R}{Q} = \frac{V^2}{\omega W} \qquad (3.4)$$

where W is the energy transferred and stored in the cavity and the potential V is defined as:

$$V = \left| \int_{-L/2}^{L/2} E_z dz \right| \qquad (3.5)$$

By calculating the energy transfer from the beam bunch to an initially empty cavity, it is possible to calculate the voltage V_{out} (eq.(3.6)) in an output line with impedance Z

(assuming the presence of properly designed couplers). Refer to [20] and [21] for a full explanation.

$$V_{out} = \frac{q \cdot \omega_{110}}{2} \sqrt{\frac{Z}{Q_{ext}} \left(\frac{R}{Q}\right)_m} \cdot T(\theta) \cdot \frac{J_1(j_{11} r)}{J_{1max}} \sin(\omega_{110} t)\, e^{-t/\tau} \qquad (3.6)$$

Q_{ext} is the external-Q of the external coupling; $(R/Q)_m$ is the shunt impedance defined for the potential calculated with the maximum electric field E_1; $T(\vartheta)$ is the transit time factor (usually negligible); τ is the decay constant equal to:

$$\tau = \frac{2Q_L}{\omega} \qquad (3.7)$$

where Q_L is the loaded Q.

For beam around the electromagnetic center, the Bessel function $J_1(j_{11}r)$ is proportional to the beam offset. Thus, V_{out} is a sine signal, decaying in time, whose amplitude can be used to measure the beam position (see Figure 3.3)

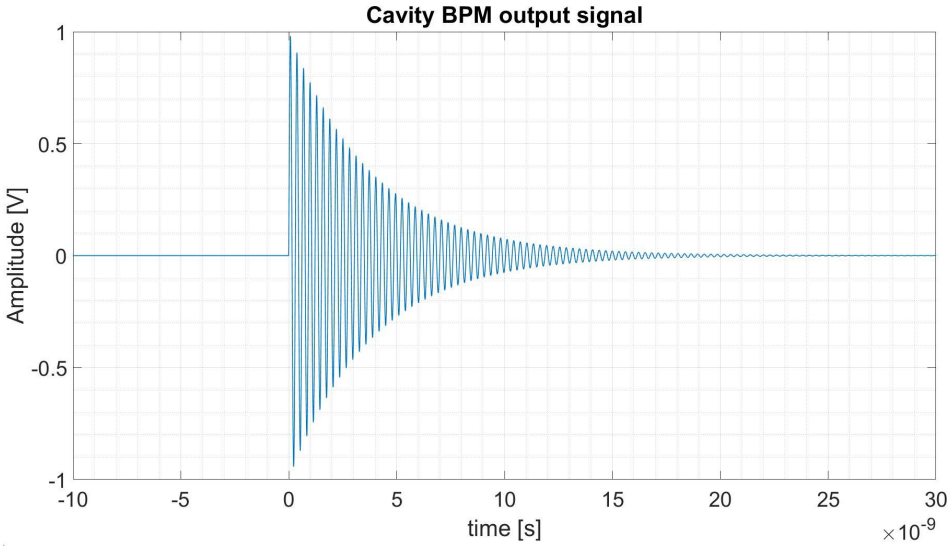

Figure 3.3: Simulation of the cBPM output signal associated to the excitation of the dipole mode. The signal is a sinewave, decaying in time, whose amplitude is proportional to the beam charge and offset of the beam bunch. The parameters which define the signal (frequency and decay constant) depends on the geometry of the cavity and on its Q_L. The simulation is based on the parameter of the cBPM used for ELI-NP GBS (see section 3.2)

The dipole mode is also dependent on the beam angle. In commonly used beam optics, the signal level dependent on the beam angle is usually much smaller than the beam

position signal. Nevertheless, it should be taken into consideration, as it could bring to problems on the measurement accuracy of the beam position. An analysis of the angle dependency can be found in [20] and [21], while a detailed analysis of the response of Cavity BPM to more complex beam profiles is discussed in [23].

Concerning the dipole mode, it is possible, by taking advantage of the horizontal and vertical polarization of the fields and with an adequate design of the cavity, to measure the horizontal and vertical displacement separately.

One possible design is illustrated in Figure 3.4. Four rectangular waveguides are matched to the position cavity by coupling ports. Due to their geometric configuration the X-ports will couple only with the X dipole mode, rejecting the Y dipole mode and the monopole mode; same applies for the Y-port (Figure 3.5).

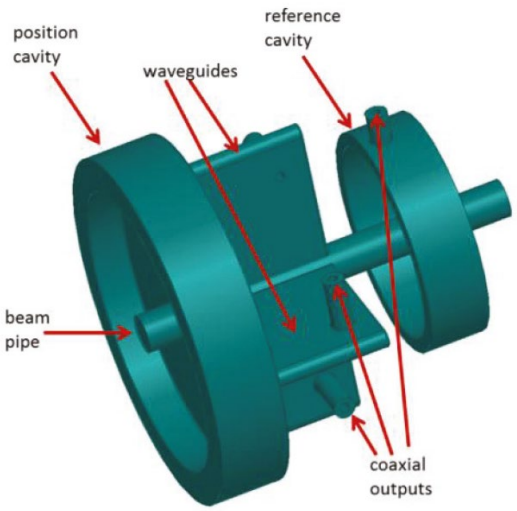

Figure 3.4: Cavity BPM schematic view [18].

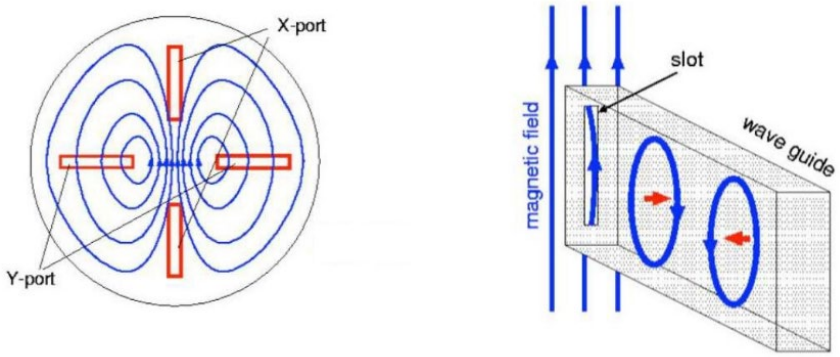

Figure 3.5: Representation of a pillbox cavity section with magnetic (blue) field lines. Due to their geometry, the X-ports will couple only with the X dipole mode, rejecting the Y dipole mode and the monopole mode. Same applies for the Y-port.

Antennas, connected to a coaxial output, are placed inside the waveguides and will couple with the field of the extracted mode. The reason to use four waveguides, two for X and two for Y, is to keep the symmetry of the cavity BPM. Moreover, it is possible to sum the signals in pairs, once extracted, doubling the amplitude of the final signal for X and for Y and to further reduce the contribution of the monopole mode on them.

The reference cavity is simpler in design. Antennas are directly inserted in the cavity, without the implementation of waveguides. This is due to the fields distribution within the cavity and the fact that the monopole mode is the fundamental one (i.e. the contribution of higher order modes to the output signal is marginal).

The output signal is similar in shape as the one descripted for the dipole mode (see Figure 3.3), with the exception that its amplitude is proportional only to the bunch charge.

In general, the radius of the two resonators is chosen in such a way that the resonance frequencies of the monopole mode for the reference cavity and the dipole mode for the position cavity are the same. Thus, the two signals have the same frequency facilitating the design of the readout electronics and simplifying the measurement of the phase difference between the two signals. For general readings on cBPM and their related performances, refer to [24], [25],[26] and [27]. For an example of the design process of a cBPM and its related issues refer to [28] and [29].

3.2 Cavity Beam Position Monitors for ELI-NP GBS

Cavity Beam Position Monitor (cBPM) that will be used for ELI-NP GBS is the PSI model "BPM16". This model was designed for the SwissFEL linac, but its features fit well for the ELI-NP GBS implementation. Thus, four additional cBPMs were produced in collaboration with PSI and delivered at INFN-LNF. A detailed description and analysis of their design can be found in [18] and [19].

The main nominal parameters of the cBPM are reported in Table 3.1, while a picture and a 3D model are reported in Figure 2.4 and Figure 3.6. The cBPM has five N-type connectors, two for signals associated to position X (carrying the same signals), two for position Y and one for the reference signal.

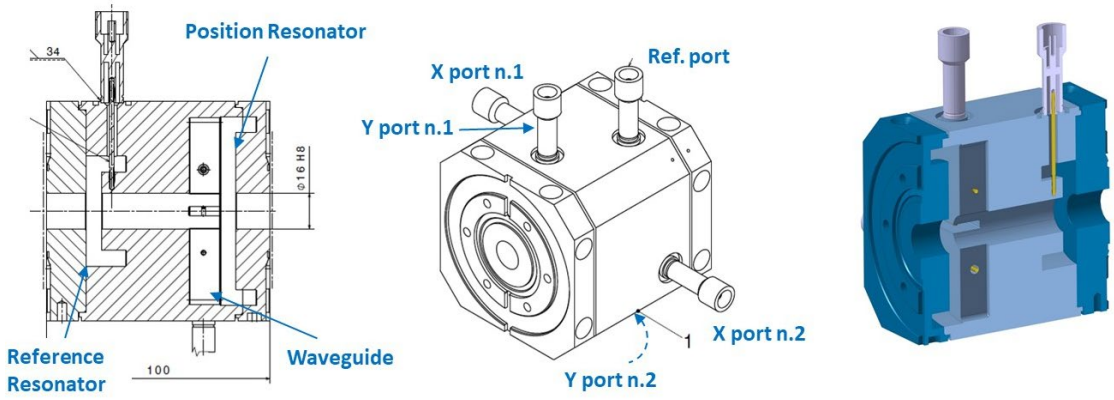

Figure 3.6: Layout and 3D representation of the cBPM PSI model "BPM16". Courtesy of B.Keil. There are two ports for X and Y, which can be used independently.

Table 3.1: Main parameters of the cBPM, PSI model "BPM16", used for ELI-NP GBS.

Parameter	
Material	Stainless Steel 316LN
Beam Acceptance [mm]	Ø16
Total length [mm]	100
Distance between the two resonators [mm]	60
Position Cavity Resonator	
Length [mm]	7
Q_L	40
TM_{110} frequency [GHz]	3.284
TM_{010} frequency [GHz]	2.252
Position Signal Sensitivity [V/(mm·nC)]	7.07
Angle Signal Sensitivity [µm/mrad]	4.3
Reference Cavity Resonator	
Length [mm]	7
Q_L	40
TM_{010} frequency [GHz]	3.284
Reference Signal Sensitivity [V/nC]	135

The main reason to use this cBPM model is related to the low loaded quality factor. As described in Eq. (3.7), by taking into account that $Q_L = 40$ and $\omega = 2\pi \cdot 3.284$ GHz, the resulting decay constant of the output signals, for both resonators, is $\tau = 3.87$ ns, which is lower than the time interval between bunches in ELI-NP GBS (16.1 ns). Nevertheless, a small portion of each signal, associated to the passage of a single bunch (the "tail"), will interfere with the signal of the subsequent bunch. This issue and its solution will be later described in section 4.2.2. The PSI model "BPM16" has a high enough position

signal sensitivity (see Table 3.1) to be applicable for ELI-NP GBS. Results obtained at SwissFEL [30], show that a resolution of 1 μm for beam bunch charges as low as 10 pC are obtainable.

Preliminary radio-frequency measurements performed at PSI for the four cBPM to be used in ELI-NP are reported in Table 3.2.

Table 3.2: Radio-frequency measurements of the cBPM, PSI model "BPM16", used for ELI-NP GBS, performed at PSI. Results were obtained by measuring the scattering parameters of the five ports.

Parameter	**f_{res} [GHz]**	**Q_L**
cBPM no. B-004		
X-plane	3.2897	43.1
Y-plane	3.2901	42.1
Reference	3.2793	37.5
cBPM no. B-012		
X-plane	3.2881	42.3
Y-plane	3.2881	43.3
Reference	3.2774	38.3
cBPM no. B-013		
X-plane	3.2894	43.3
Y-plane	3.2886	42.4
Reference	3.2809	38.4
cBPM no. B-014		
X-plane	3.2889	41.9
Y-plane	3.2891	42.8
Reference	3.2793	37.8

Table 3.3: Average and maximum variation of the resonance frequency and QL for the reference and position resonators.

	Position Resonator	**Reference Resonator**
Mean f_{res} [GHz]	3.2890	3.2792
Variation range of f_{res} [GHz]	0.0020	0.0035
Mean Q_L	42.65	38
Variation range of Q_L	1.4	0.9

In Table 3.3, the average values and the maximum variation for the resonance frequency and loaded Q are reported for both resonators, taking into accounts the measurements performed on the four Cavity BPMs. The small differences for these parameters could be considered negligible for the position measurements.

4 Readout Electronics for Cavity BPM

Readout Electronics design is of critical importance in a Cavity Beam Position Monitor measuring system. This is due to the fact that if not carefully designed, the accuracy, the resolution and the repeatability of the measures can be heavily affected, reducing the overall performance of the measuring system. The readout electronics main task is to collect signals from the Cavity BPM, elaborate them and present an estimation of the beam position.

The majority of readout electronics used for Cavity BPMs is nowadays based on the down-conversion of the Cavity BPM signals and the digital transformation of them, by means of Analog to Digital Converters (ADC). The digital signals will then be elaborated in order to present the estimation of the beam position. Different signal processing schemes can be adopted in order to do so. One of the most used is based on the I-Q demodulation, which will be described later.

The readout electronics which will be implemented in ELI-NP GBS for the Cavity BPMs is represented by the "LIBERA Cavity BPM" modules, recently developed (2017) by Instrumentation Technologies (Figure 4.1) [31],[32],[33]. The initial concept and the development were elaborated and executed by taking into accounts the ELI-NP GBS requirements. The development and the final stage of testing and validation where performed in strict collaboration with INFN-LNF and represent part of the work discussed in this thesis.

The module has three independent input channels (SMA connectors), named "X", "Y", "I", which are used for the output signal coming from a single Cavity BPM. "X" and "Y" are used for the signals of the "position" resonator, "I" is used for the reference resonator. The channels and the related electronics are the same for each channel. The only difference is related in how the digital data related to the signals are used to compute the beam position. The signals are filtered, down-mixed and attenuated/amplified by means of front-end electronics, independently for each channel. They are then digitized and the beam position is calculated with algorithms performed by an FPGA. An external trigger is used to synchronize the acquisition with the beam bunches. The module needs also an external reference signal, i.e. a sinewave with the same frequency of the bunches (62.087 MHz), that is in common for the three channel and is used to down-mix the input signals and to lock the ADC sampling frequency. A full explanation of all the sub-systems of the module will follow in the next sections, while the main parameters of it are shown in Table 4.1.

Table 4.1: Main parameters of the "LIBERA Cavity BPM".

Parameter	
General	
Number of RF inputs	3
Input connector type	SMA
Maximum Input Range	16 dBm
Signal Frequency for ELI	3.3 GHz
FPGA /CPU (model)	Zynq-7035 / Dual Core ARM Cortex –A9
ADC (model)	Analog Device AD9680-500
Channels no.	4
Number of bits	14
Bandwidth	2 GHz
Sampling Rate	500 MS/s
Maximum Input Range	2.06 V_{p-p}
Trigger signal	Single Ended lvTTL
Trigger connector type	LEMO
Max. Trigger frequency	100 Hz
Trigger frequency for ELI	100 Hz
Reference Signal	Continuous sine-wave
Ref. Signal connector Type	SMA
Signal Level Range	0-10 dBm
Signal frequency for ELI	62.087 MHz

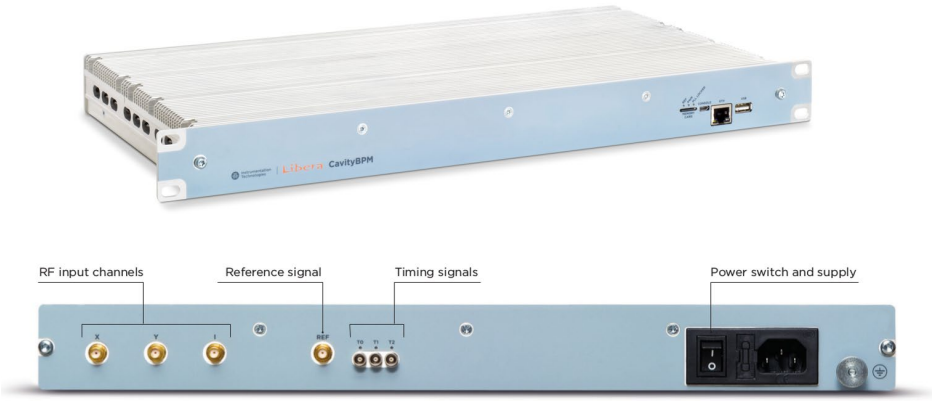

Figure 4.1: "LIBERA Cavity BPM", developed by "Instrumentation Technologies" as the readout electronics for Cavity BPM signals. Front and back panels view.

4.1 Front end electronics and digitizer

The working principle of the front end electronics can be explained by looking at Figure 4.2.

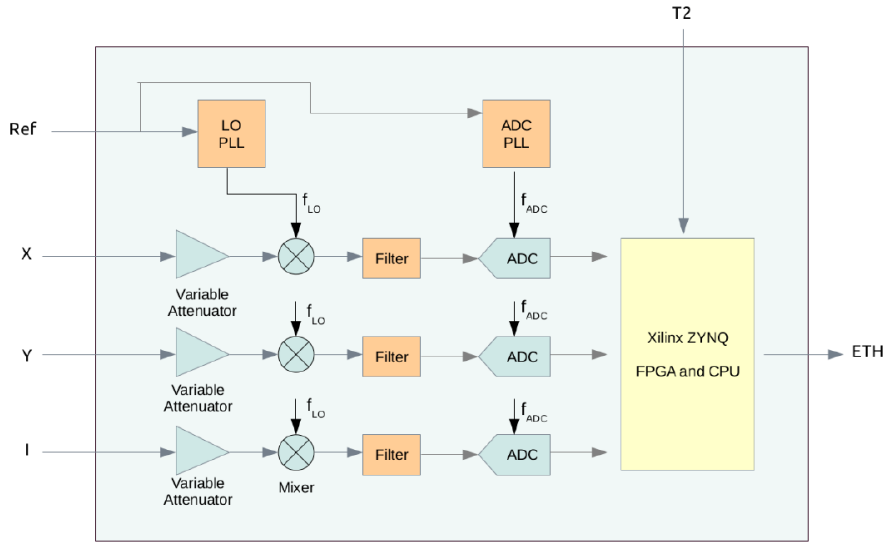

Figure 4.2: Block diagram of "LIBERA Cavity BPM" [32].

Each module is capable to acquire the signals produced by the "position" resonator ("X", "Y") and by the "reference" resonator ("I") of one Cavity BPM.

4.1.1 Variable attenuators

At the front-end stage, the signals are filtered from unwanted frequency component and their amplitudes are adjusted by means of variable attenuators (0 dB / 32 dB), depending on the beam conditions (e.g. charge, position). After the variable attenuators, a series of fixed-gain amplifiers [33] and internal attenuators are used to further adjusting the signals level (not depicted in Figure 4.2).

The choice of the attenuation levels plays an important role in the determination of the resolution of the measurements. The main objective is to adjust them in order to exploit all the dynamic range of the read-out electronics and at the same time avoiding the saturation of the channels. For example, by knowing the maximum possible charge of the bunches during a specific accelerator operation, it is possible to adjust the attenuators of channel "I", in such a way that with the maximum bunch charge, the

signal on the “I” channel will take 90% of the input range. This will improve the Signal to Noise ratio (SNR) and will help to achieve the best resolution possible on the measurement. For channel “X” and “Y”, the choice relies not only on the maximum charge of the bunches, but also on the maximum observable range of the bunch position. Once the maximum bunch charge is fixed, it is possible to choice the maximum observable range, by selecting the attenuations of “X and “Y” channels (the higher the attenuation chosen, the higher the observable range). By selecting low attenuation values, the maximum observable range will decrease, but (since the signal will have higher amplitudes) the SNR will increase and so will do the resolution of the system. As such, adjusting the attenuators gives the possibility to the user to adjust the level of the resolution wanted at the cost of the maximum observable range. This holds true if two conditions are verified.

- Noise introduced by the read-out electronics is dominant, if compared to the thermal noise inherent to the Cavity BPM (see section 5.2). In the opposite case, SNR is fixed, irrespective to the attenuation used.
- The Cavity BPM signals are strong enough (depending on the charge and position of the beam) to cover at least 100% of the input range of the readout electronics channels (without the use of attenuations). If this not holds, the attenuation level should be simply put to zero in order to exploit the input range at best.

Concerning the second point, each channel of the “LIBERA CavityBPM” has an input range of -15 dBm (V_{max}= ±56 mV) without any attenuation. The sensitivity of the resonators of the ELI-NP GBS Cavity BPM are S = 7.07 V/nC/mm and S = 135 V/nC (see Table 3.1).

As such, for example, with bunches of 100 pC and transversal beam offsets in the order of hundreds of μm (which is a realistic case for the foreseen operation at ELI-NP GBS), the signals would be strong enough to cover more than the maximum input range of all the channels of the “LIBERA Cavity BPM”.

4.1.2 Down conversion and digitization

Down-conversion is applied to the cBPM signals by using the reference signal provided to the system. The main reason to down-mix the signal is to relax the requirements on the ADC.

The reference signal ("Ref") at the bunch repetition frequency (62.087 MHz) is provided by the timing system to two Phase Locked Loops (PLLs) (refer to [35],[36]), which generate the ADC sampling frequency (f_{ADC} = 496.7 MHz) and the down-conversion mixer components (f_{LO} = 3.663 GHz). The cavity input signal (f_{res} = 3.284 GHz with a bandwidth of 82.1 MHz) is adjusted by a series of attenuators and amplifiers (not depicted in Figure 4.2) and down-converted to an intermediate frequency (f_{IF} = 379 MHz with a bandwidth of 82.1 MHz).

It should be noted that the sampling frequency is not high enough to satisfy the Nyquist criterion. In fact, the signal is under-sampled, falling in the second Nyquist zone, which is delimited by $f_{ADC}/2$= 248.5 MHz and f_{ADC}=496.7 MHz, as shown in Figure 4.3 [37], [38]. A band-pass filter centered at 375 MHz with a bandwidth of 116 MHz is used to ensure that all the harmonic contents of the signal falls entirely into the second Nyquist zone. The effect of under-sampling in the second Nyquist zone is that the digitized signal is an aliased representation of the analogue signal. This means that the digitized signal will have a central frequency (aliased representation of the central frequency of the analogue signal) of:

$$f_{alias} = f_{ADC} - f_{IF} = 117.7\ MHz \qquad (4.1)$$

It should also be noted that by the effects of under-sampling, the frequency content of the aliased representation is inverted compared to the analogue signal frequency content (see Figure 4.3). Nevertheless, by the Nyquist-Shannon sampling theorem, it is possible to fully reconstruct the original signal perfectly from the sampled version.

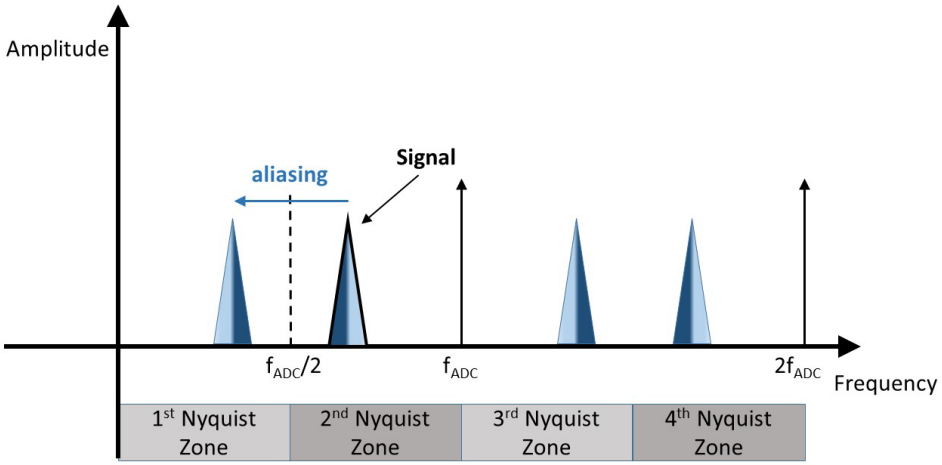

Figure 4.3: Representation of the Nyquist zones and the effects of the under-sampling technique (aliasing). $f_{ADC}/2$ is half of the sampling frequency and coincides with the Nyquist frequency.

The “T2” input (see Figure 4.2) is used for the machine trigger (100 Hz) and it is used to start the acquisition procedure.

The ADC data is continuously transferred through serial interfaces to a Xilinx ZYNQ 7035 System on Chip, which provides all the necessary computing resources, including a FPGA, a CPU and the internal shared memory. Every time a new injection happens, the trigger signal enables the storage of up to 4096 ADC samples in the memory of the device, ready to be further processed.

4.2 Digital processing

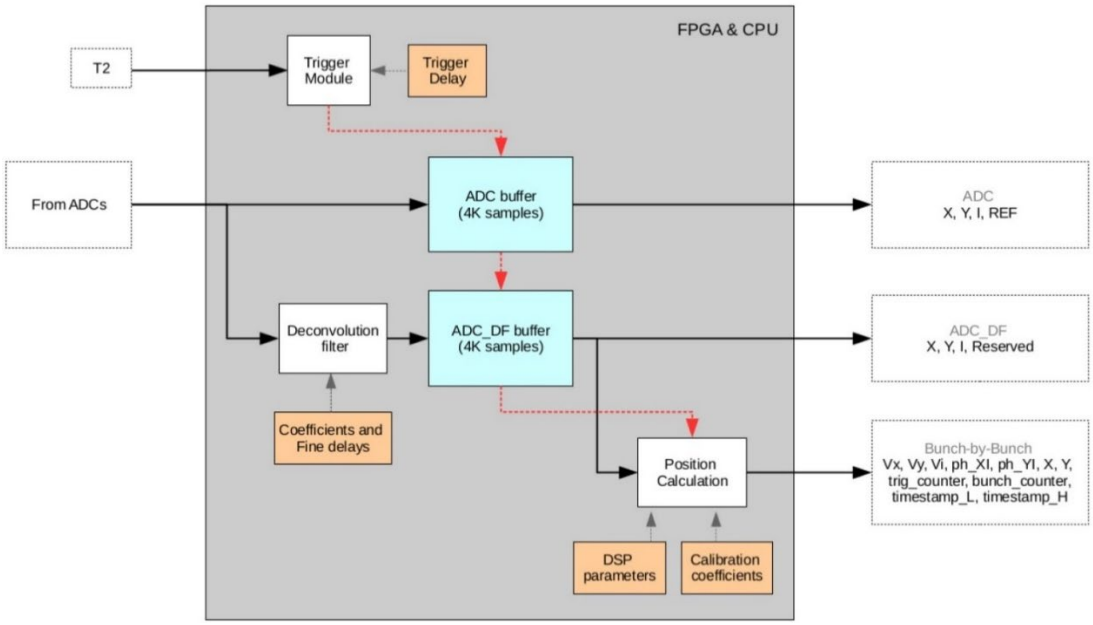

Figure 4.4: Block diagram of “LIBERA Cavity BPM” data-paths

4.2.1 Calculation of the beam position

Once the signals are digitized, their amplitudes is computed. For each channel (“X”, ”Y”, ”I”) the samples are organized in “bunch windows” which are used to calculate the amplitude (V_{Xb}, $V_{Yb,}$ V_{Ib}) of the signals associated to the b^{th} bunch. The number of samples composing a single “bunch window” is adjustable, but during the multi-bunch operation mode in ELI-NP GBS should be fixed at eight, due to the time structure of the beam.

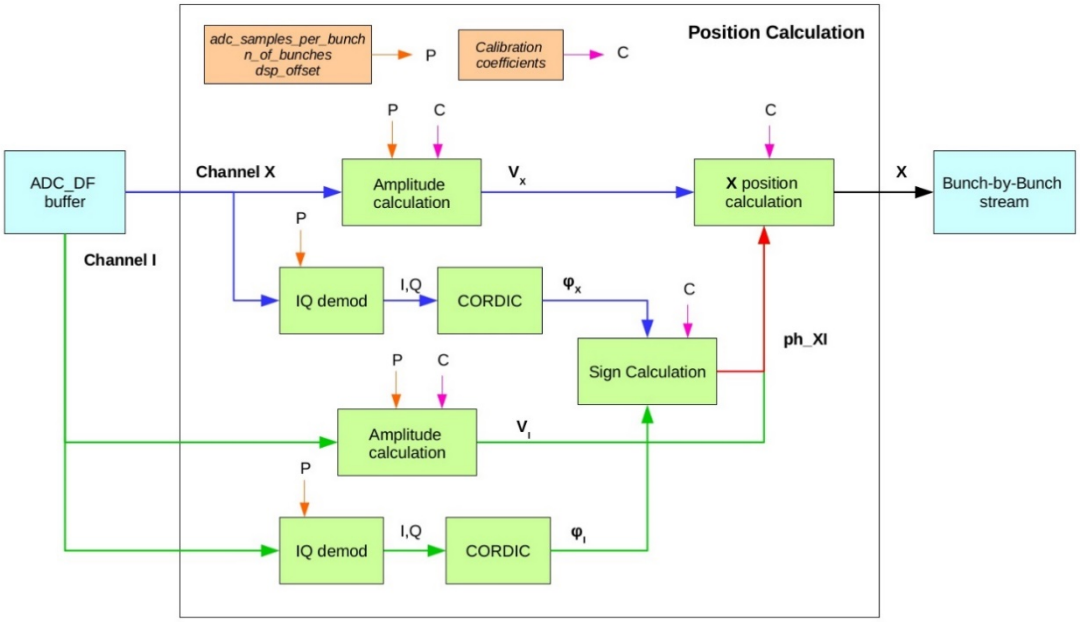

Figure 4.5: Position Calculation block scheme for "X" and "I" channels.

The amplitudes of the signals are calculated as:

$$V_{X_b} = \sqrt{\sum_{bth\ bunch\ window} {x_n}^2}$$
$$V_{Y_b} = \sqrt{\sum_{bth\ bunch\ window} {y_n}^2} \qquad (4.2)$$
$$V_{I_b} = \sqrt{\sum_{bth\ bunch\ window} {i_n}^2}$$

In Eq. (4.2), x_n, y_n, i_n are the n^{th} samples of the X, Y, I channels respectively. "b^{th} bunch window" is the sample window centered on the signals produced by the passage of the b^{th} bunch. V_{Xb}, V_{Yb}, V_{Ib} are proportional to the amplitude of the signal associated to the passage of the b^{th} bunch. The absolute transverse position of each bunch is then obtained as (4.3):

$$X_b = K_x \frac{V_{X_b}}{V_{I_b}} \qquad Y_b = K_y \frac{V_{Y_b}}{V_{I_b}} \qquad (4.3)$$

X_b and Y_b are the calculated transverse distances of the b^{th} bunch in respect to the electromagnetic center (e.m. center) of the "position" resonator in the horizontal and vertical axes respectively. K_x and K_y are user-defined calibration constants which take

into accounts the sensitivity of the resonators, the level of input attenuator used and the attenuation of the cables. A calibration procedure is used to find the correct value for K_x and K_y before the starting of operations.

In order to evaluate the sign of the bunch position on the X and Y axes of the transversal plane, the phase of the signal of the X and Y channels are compared to the phase of the I channel (see section 3.1)

Thus, the samples in each bunch window are also used to calculate the phase of each signal: ϕX, ϕY, ϕI in relation to an internal generated signal. This is done through IQ demodulation applied to the samples in each bunch window. The phase is then calculated with the CORDIC (Coordinate Rotation Digital Computer) algorithm. Once ϕX-ϕI and ϕY-ϕI are calculated, it is possible to evaluate the sign of each bunch position. User-defined calibration constants are also applied in this case to compensate differences in the channel lengths, which could affect the calculated phase for each signal.

4.2.2 Deconvolution filter (for multi-bunch operation)

In multi-bunch operations, as previously described, the digitized samples are divided in bunch windows, each containing 8 samples (for ELI-NP GBS operations), for a total time interval of 16.1 ns. However, In the case of ELI-NP GBS, the resonators of Cavity BPMs produce signals at the passage of a bunch which will last over 16.1 ns, overlapping with the passage of the subsequent bunch. The amplitude of the "tail" of the signal which potentially overlaps is mainly determined by the Quality factor of the Cavity BPM resonators (Q_L= 40) and was calculated to be roughly 1.5% (see eq.(3.6) and (3.7)) of the maximum amplitude of the signal after 16.1 ns. This potential problem could be worsened by the effects of cables used to bring the signal from the Cavity BPM to the readout electronics.

To reduce this inter-bunch interference, the digitized signals can be processed by a digital 100-bin FIR filter, called "Deconvolution" filter. This is used to limit the superposition between signals of consecutive bunches, by compressing them to occupy exactly 8 samples. An example of how the filter is defined and works with a single bunch input signal is presented in Figure 4.7.

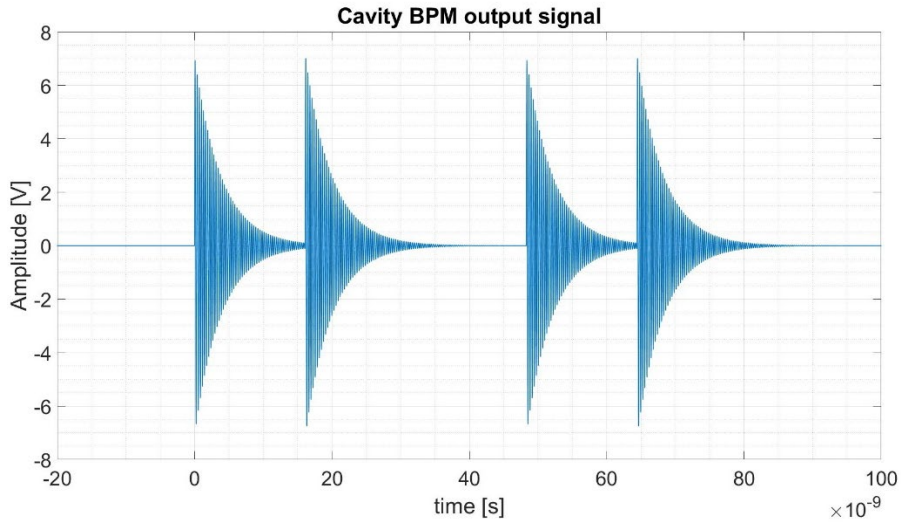

Figure 4.6: Simulated signal shape of ELI-NP GBS Cavity BPM ("X" channels) in multi-bunch operation mode (the third bunch is missing on purpose). It can be noted the small overlaps between signals from consecutive bunches. Amplitudes were simulated by taking into account a "Position" Resonator Sensitivity of 7.07 V/nC/mm for a bunch of 1 nC and a distance of 1 mm on the horizontal axis in respect to the electromagnetic centre of the Cavity BPM.

In order to define the Deconvolution filter response, a calibration procedure is needed before the starting of operations. In order to do this, a goal function has to be defined (G(t)). The latter was chosen to be a rise cosine shape as depicted in Figure 4.7. After that, an input signal produced by the passage of a single bunch in the cavity BPM should be provided (see Figure 4.7, $IN_{std}(t)$). This is considered as the "standard" signal that the cavity BPM will provide. The frequency and impulse response of the deconvolution filter are then calculated as:

$$DF(f) = \frac{G(f)}{IN_{std}(f)} \quad \overset{iFFT}{\Longrightarrow} \quad DF(t) \tag{4.4}$$

Where G(f) and $IN_{std}(f)$ are the Discrete Fourier transforms of G(t) and $IN_{std}(t)$ and *iFFT* indicates the inverse of the Fast Fourier Transformation.

Thus, the deconvolution filter frequency response is calculated as the function that transforms the "standard" signal for the passage of a single bunch to a signal with a rise cosine shape, limited to 8 samples. The filter bins amplitudes are defined in order to guarantee that, once the filter is applied, the overall amplitude of the digitized signal V_x (calculated with eq.(4.2)) remains the same.

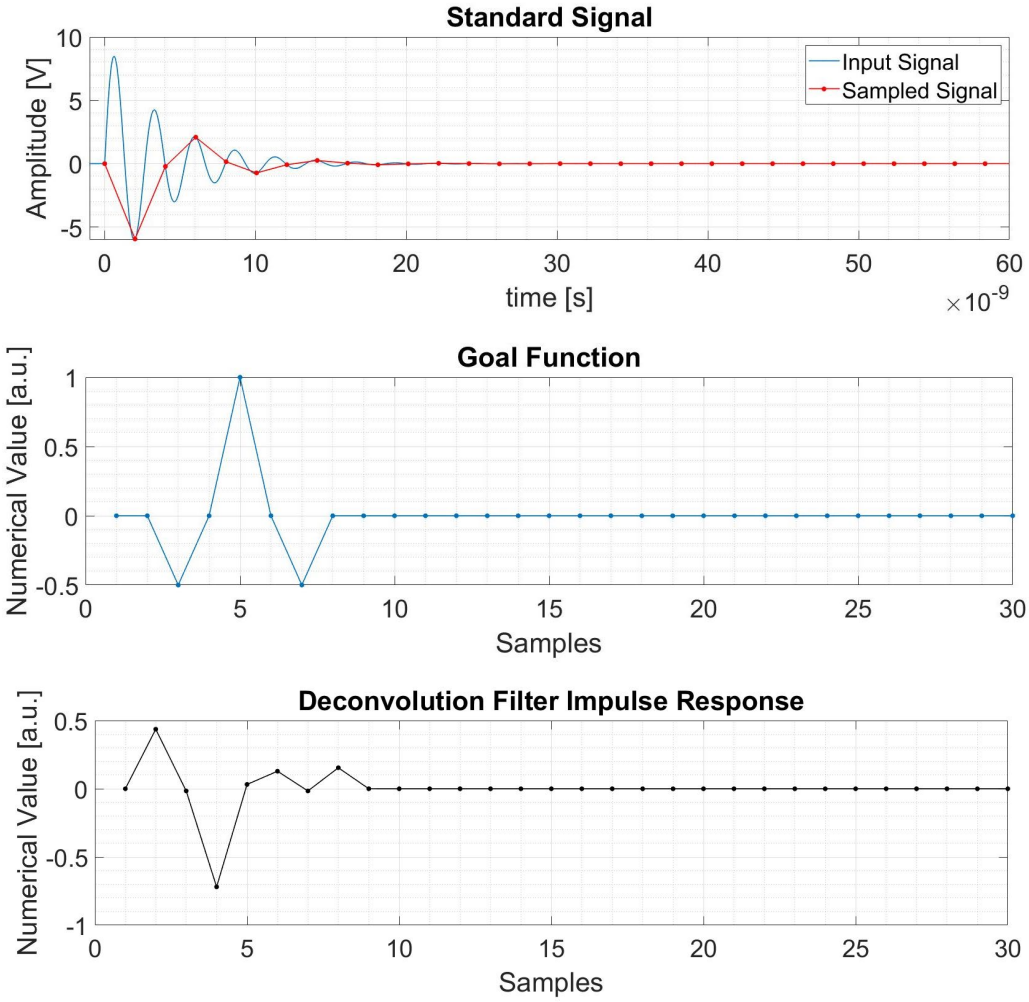

Figure 4.7: Signals (simulated) involved in the calculation of the impulse response of the deconvolution filter. The "standard" signal, $In_{std}(t)$, is the signal produced by the passage of a single bunch in the Cavity BPM. The Goal Function, G(t), is a user-defined rise cosine function. The Deconvolution Filter Impulse Response, DF(t), is calculated as the function which transform $In_{std}(t)$ into G(t).

Since the calculation of the deconvolution filter is based on the definition of a "standard" input signal, the calibration procedure has to be repeated independently for the "X", "Y" and "I" channels, creating three different filters. The application of the deconvolution filter is optional, since it is only used in the presence of multi-bunch pulses operation.

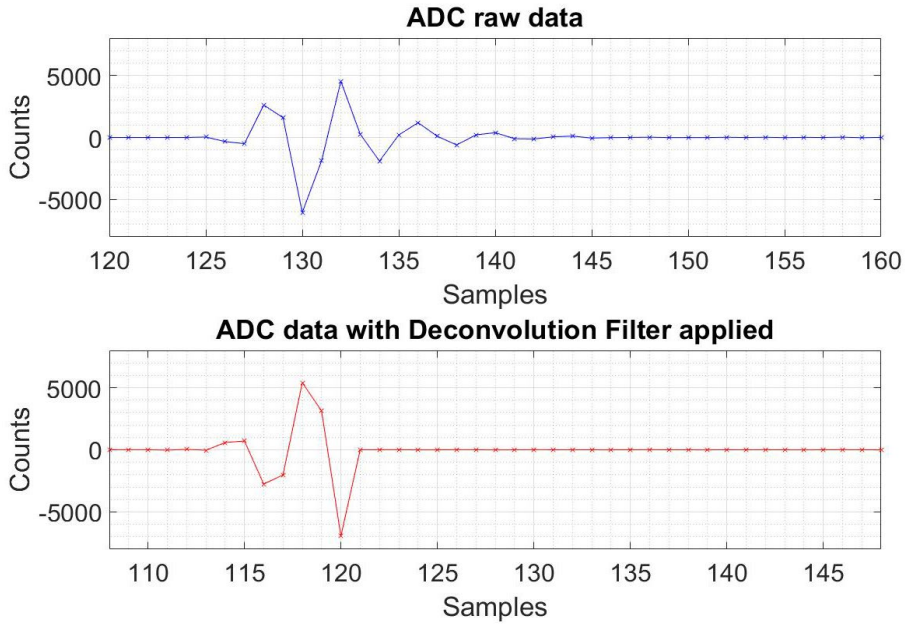

Figure 4.8: Example of the digital signal "X" of the "position" resonator without and with the application of the deconvolution filter (respectively the upper plot and the lower plot). The signal digitized was generated by the "position" resonator of one of the Cavity BPMs of ELI-NP GBS, excited by means of a pulse generator (see chapter 5).

Once created, the deconvolution filter will transform any input signal related to a bunch, ideally by compressing it into 8 samples (and thus, limiting the inter bunch interferences), while keeping constant their overall amplitudes (calculate with eq.(4.2)). Its application on a single bunch signal obtained during measurements performed in laboratory (see chapter 5) is presented in Figure 4.8, while a simulation of its applications on a multi-bunch signal is presented in Figure 4.9. Here, the signals produced by the passage of five consecutive bunches (at a time interval of 16.1 ns) is represented. The five signals have different amplitudes in order to simulate different horizontal positions. From the results presented in Table 4.2, it is clear the effects on the deconvolution filter on the calculation of the amplitude of the signals. Without the deconvolution filter (second column of data) it is possible to see that the calculated amplitudes (Vx) are affected by the "overlapping" of consecutive bunches, due to the tail of the signals.

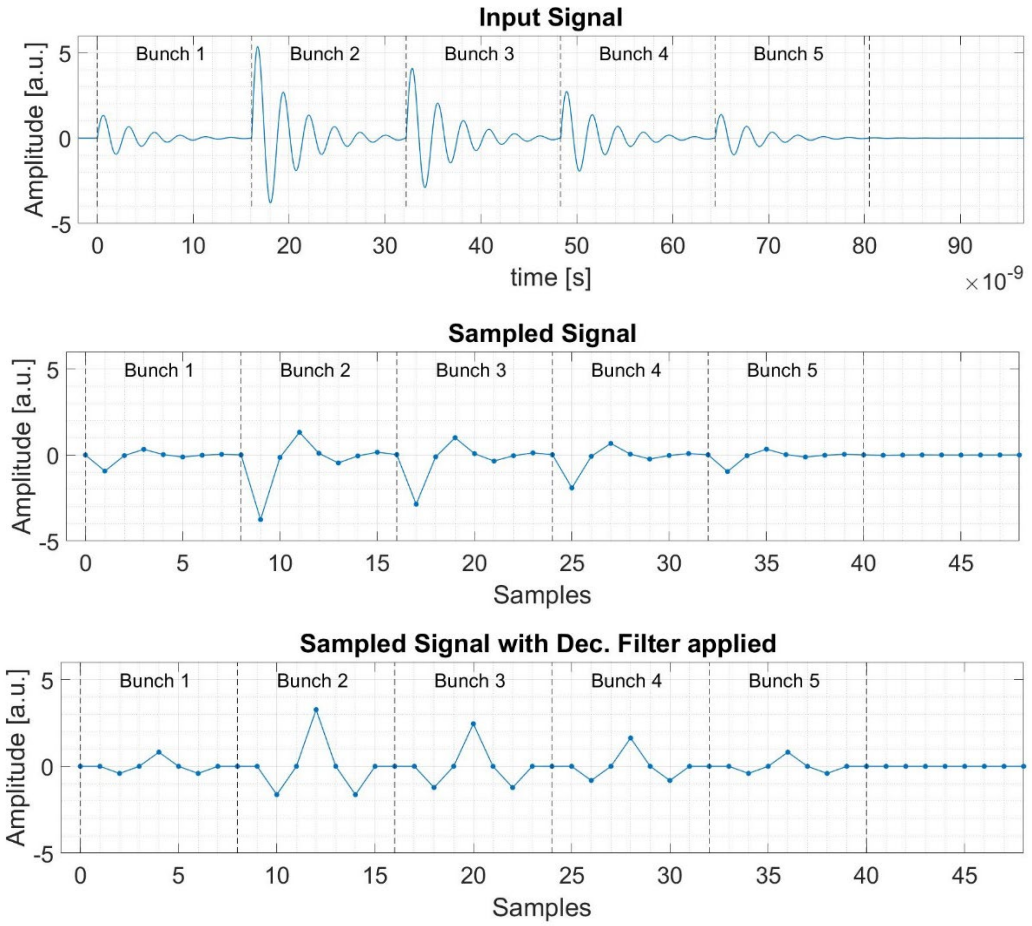

Figure 4.9: Simulation of the application of the Deconvolution filter. "Input signal" represent the Cavity BPM signal already down-converted and filtered. "Sampled signal" is the digitized signal. "Sample Signal with Deconvolution Filter Applied" is the digitized signal with the application of the Deconvolution Filter. The latter was calculated by using a single bunch signal, similar to the one marked as "Bunch 1".

Table 4.2: Results of the simulation presented in Figure 4.9. "Vx" represent the amplitude of the signals, calculated with EQUATION. "Vx (theoretical values)" are the ones which the system, unaffected by noise, would calculate without the problem of the overlapping between consecutive bunches. While the second and the third column of data represent the Vx calculated with and without the application of the Deconvolution Filter (middle and bottom plots of Figure 4.9).

	Vx [a.u.] (expected value)	**Vx [a.u.] (without DF filter)**	**Vx [a.u.] (with DF filter)**
1st bunch	1.000	1.000	1.000
2nd bunch	4.000	4.014	4.000
3rd bunch	3.000	3.060	3.000
4th bunch	2.000	2.045	2.000
5th bunch	1.000	1.031	1.000

5 Bench measurements on Cavity BPM

5.1 Test-stand at LNF-INFN

The validation and the first measurements on the Cavity BPMs and their read-out electronics (the "LIBERA CavityBPM" module) were performed in the SELCED ("Servizio Elettronica, Controlli e Diagnostica") laboratory at INFN-LNF. The first goal for this session of measurements was to test all the functionalities of the "LIBERA Cavity BPM" modules, as the last phase of the development process, that was carried on in collaboration with the Instrumentation Technologies staff. The second goal was to perform measurements on the Cavity BPMs and the readout electronics, characterizing their features and performances as a single measuring system. In order to achieve both goals, we developed a test-stand that includes one cBPM and one "LIBERA for CavityBPM" module. The idea was to develop a system capable to "simulate" the passage of a beam through the cBPM as the one expected at ELI-NP GBS linac [40]. The latter, in multi-bunch operation mode (see section 1.2), is composed by trains of 32 bunches, with a repetition rate of 100 Hz and a time interval between bunches of 16.1 ns.

The setup is developed on the idea of using one cBPM as a filter for a train of pulses generated in laboratory. This was possible because the "position" resonator of the cBPM (model PSI Cavity BPM16, see Figure 3.6) has two ports for the horizontal axes and two for the vertical axes. As such, we used one port (on the horizontal axes) as the input port to excite the "position" resonator and the other horizontal port as the output one.

In order to reconstruct the position of the beam on one axes, the read-out electronics needs the signal from the "position" resonator of that axes (Channel "X" or "Y") and the signal from the "reference" resonator (Channel "I"). With the test-stand used, it is not possible to use the "reference" resonator of the cBPM, as there is only one port associated to it. Thus, in order to provide a signal on channel "I", we split the signal (by means of a balanced resistive splitter) at the port used as the output of the cBPM. As such, half of the signal is provided at channel "X" and half at channel "I". This work around is based on the fact that the resonance frequency of the position resonator and reference resonators of the cBPM have roughly the same frequency and quality factor (see Table 3.2). It also has another benefit: since the position calculation is based on the ratio of the amplitudes on channel "X" and channel "I", by using only one cBPM output signal, split in two halves, the noise associated to the input signal and injected into the

front-end of the readout electronics is greatly reduced, similarly to the case of measuring a noisy signal in differential mode.

The general layout of the test-stand is shown in Figure 5.1.

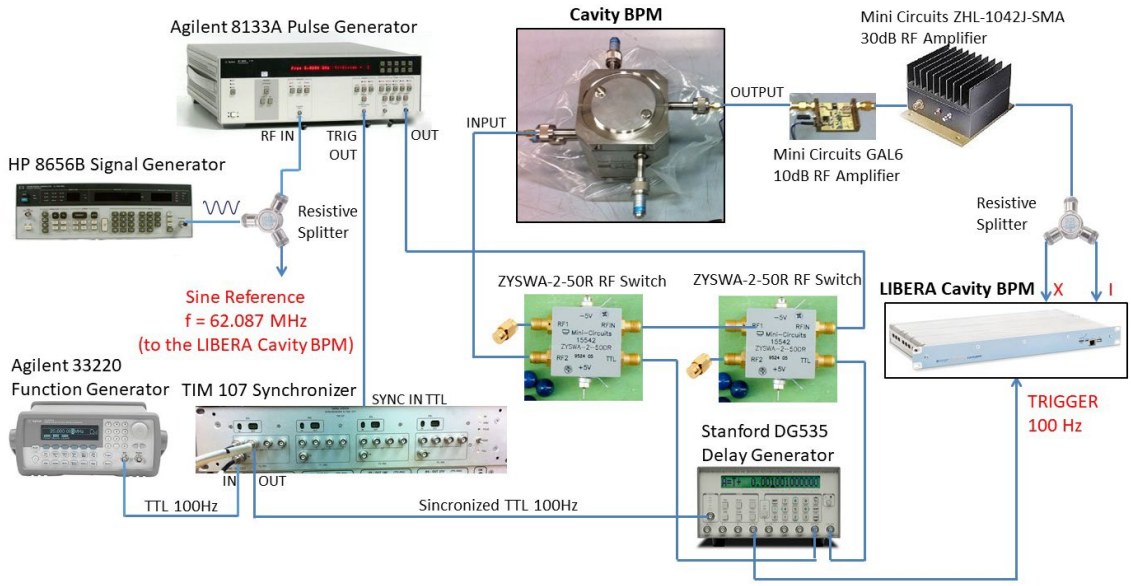

Figure 5.1: Layout of the test-stand used in laboratory at LNF, by using cBPM output signals. Courtesy of Donato Pellegrini.

The Pulse Generator "Agilent 8133A" is used to generate pulses of 2 V with a width of 50 ps and a time interval between them of 16.1 ns, corresponding to a repetition frequency of 62.087 MHz. This signal is gated by means of a cascade of two switches "ZYSWA-2 50R" with the output signal of the Delay Generator "Stanford DG535". The latter provide a variable gate window which could be regulated to overlap in time with a variable number of consecutive bunches, with a repetition rate of 100 Hz. For example, by adjusting its time length to roughly 512 ns, it is possible to allow the passage of 32 consecutive bunches through the switches. The train of pulses is then provided to one of the port of the "position" resonator of the cBPM. The reason to uses two switches in cascade instead of one is to increase the input-output isolation. Due to impedance miss-matching between the RF-switches and the cavity port used as the input port, we detected the effects of unwanted signal reflections on the output signal of the cBPM. These reflections were reduced by installing a 50 Ω - 3dB attenuator at the cBPM input port (not depicted in Figure 5.1). At the other port of the cBPM (used as the output port), two amplifiers are installed (Mini Circuits "GAL6" and Mini Circuits "ZHL-1042J-SMA")

for a total nominal gain of 40 dB. The amplified signal is then provided to the channel "X" and channel "I" of the "LIBERA for Cavity BPM", by means of a resistive splitter.

The reference signal at 62.087 MHz is provided to the "LIBERA for Cavity BPM" by the Signal Generator "HP 8656B". The latter is used also as the input trigger of the Pulse generator, in order to guarantee that the reference signal is synchronized with the train of pulses. The trigger at 100 Hz is provided by the "Stanford DG535" delay generator. Since the trigger and the train of pulses are generated by different devices, synchronization of the two signals is required. In order to achieve this, a Synchronizer device ("TIM 107") is used. It synchronizes two signals: the output trigger of the pulse generator (at a frequency of 62.087 MHz), synchronous with the generation of pulses; the TTL square wave with a frequency of 100 Hz, provided by the function generator "Agilent 33220". Thus, the output of the Synchronizer is a signal with a frequency of 100 Hz, whose rising edges are synchronized with the pulses generated by the pulse generator. This signal is provided to the Delay Generator, which is, as already explained, used to gate the train of pulses and to provide the trigger to the "LIBERA for CavityBPM".

The cBPM output signals produced by the test-stand are shown in Figure 5.2 and Figure 5.3, for the case of single pulse excitation and 32-pulses excitation. We detected high levels of distortion on the signal spectrum, introduced by the two amplifiers installed at the output port of the cBPM. As such, most of the measurements performed with this setup and presented here were performed without them.

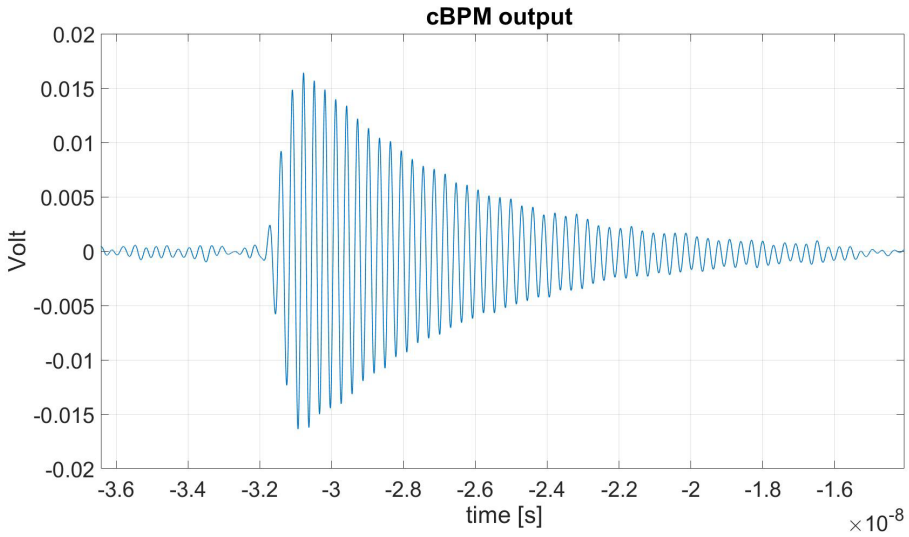

Figure 5.2: cBPM output signal (not amplified) with a single pulse excitation.

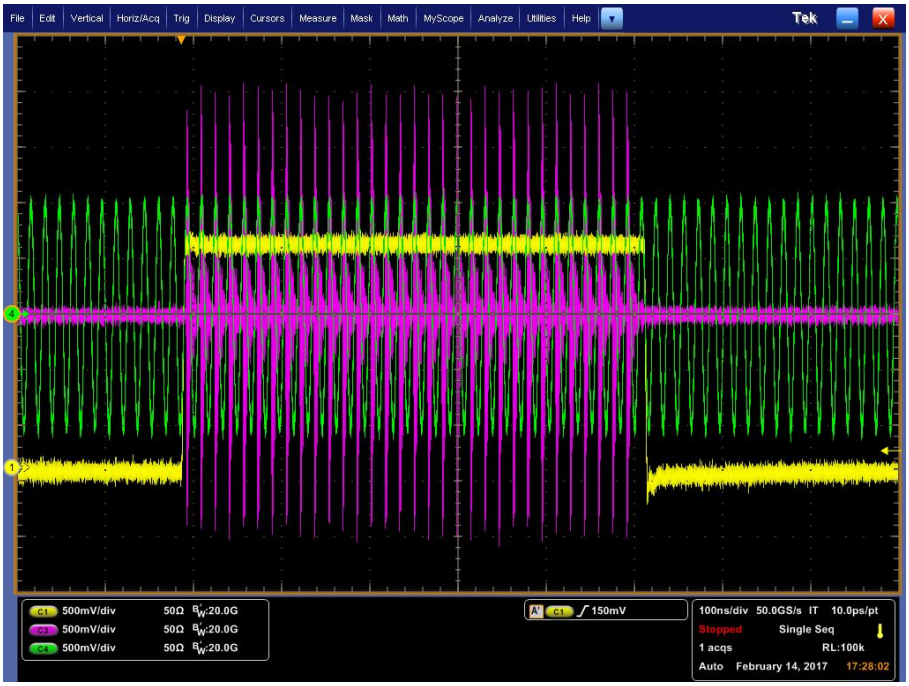

Figure 5.3: Magenta waveform: cBPM output signal with a train of 32 pulses excitation (amplified). Green waveform: sine reference at 62.087 MHz. Yellow waveform: signal used for the gating of the train of pulses.

The amplitude of the signal after the resistive splitter and without the amplifiers has a maximum amplitude of ~ 17 mV, sufficient to reach about ±2000 counts of the ADC used by the "LIBERA Cavity BPM", out of its maximum range of -8191/+8192 counts.

5.1.1 Test-stand at LNF-INFN with sinewave signals

Some of the measurements were performed by using sinewave signals at a frequency of 3.284 GHz (the same value of the resonance frequency of the cBPM). In this case the test-stand used is shown in Figure 5.4. We used a Vector Analyzer (AGILENT E5071B) to produce a sinewave signal at 3.284 GHz. As in the previous case, the signal is split and provided to channel "X" and "I" of the readout electronics. The trigger is provided by the Delay Generator (STANFORD DG535), while the reference signal at 62.087 MHz is provided by the signal generator "HP 8656B". Since we used a continuous waveform, there was no need to synchronize the signal with the reference or the trigger.

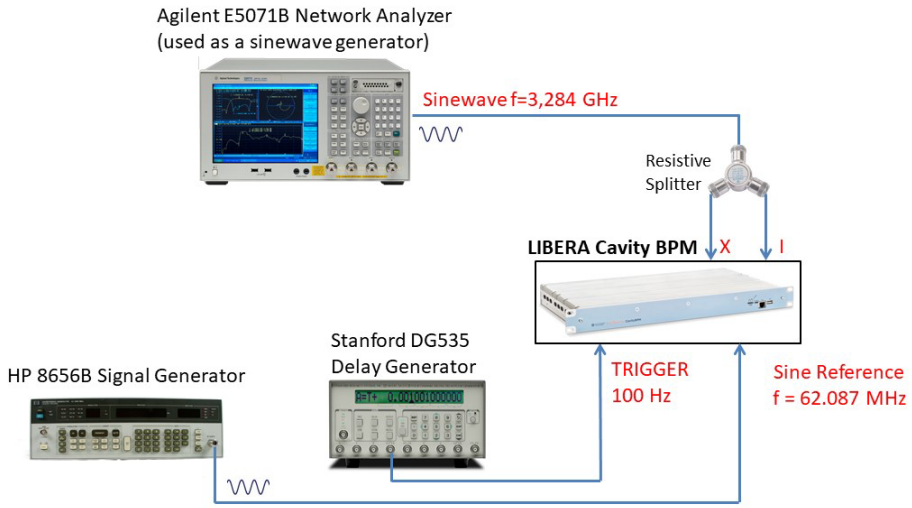

Figure 5.4: Layout of the test-stand used in laboratory at LNF, by using sinewave signals.

5.2 Noise Measurements

Noise measurements performed in laboratory were executed by using 50 Ω SMA terminators on the input port of each channel (X, Y, I). All internal variable attenuators were set to 0 dB. We provided to the "LIBERA Cavity BPM" an external trigger with a frequency of 100 Hz (using the STANFORD DG535 Pulse Generator) and a reference signal with a frequency of 62.087 MHz (using the HP 8656B Signal Generator).

We measured the mean and the standard deviation of noise, by acquiring $40*10^6$ samples. Results are shown in Table 5.1, in Figure 5.5 and Figure 5.6.

The noise signal and the power spectrum for channel Y and channel I are similar to the one of Channel X.

Table 5.1: Mean value and standard deviation of noise for channels X, Y, I of "LIBERA Cavity BPM". All channel input ports were terminated with 50 Ω. The maximum range of the ADC is [-8191, +8192].

Noise measurements		
Channel	**Mean (counts)**	**Standard Deviation σ (counts)**
X	-1.98	3.07
Y	-9.96	3.10
I	-1.84	3.01

The input range of the 14-bit ADC installed in the "LIBERA Cavity BPM), "AD9680-500" is 2 Vp-p [39]. Each count represents 2 V / 2^{14} = 122.1 µV. Thus a standard deviation of 3.07 counts (for Channel X) is the equivalent of a noise amplitude of 374.8 µV at the input port of the ADC.

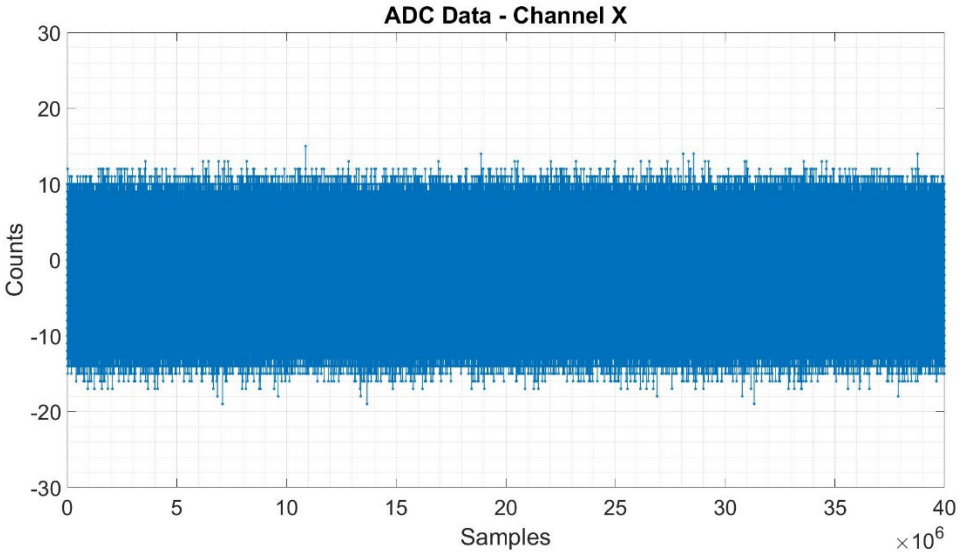

Figure 5.5: Noise of channel X, by terminating the input port with 50 Ω. The maximum range of the ADC is [-8191, +8192].

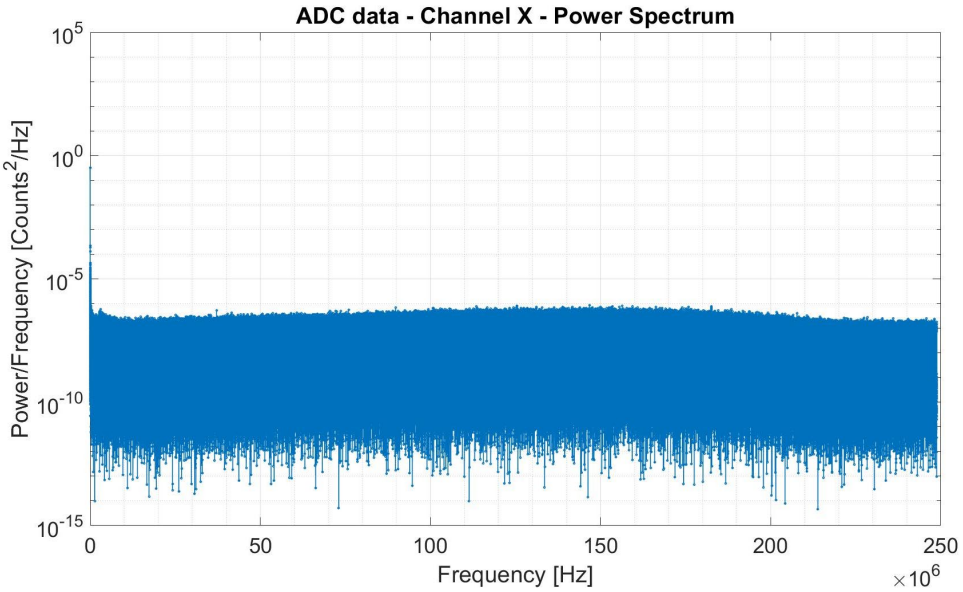

Figure 5.6: Power spectrum of noise for channel X, by terminating the input port with 50 Ω.

It is possible to calculate and compare the thermal noise that would be introduced along with an input signal (for example along with the BPM output signal) to the noise

measured. This analysis is helpful in determining what could be the major limitation for the overall measurement resolution of the system.

The thermal noise power P_N is given by [21]:

$$P_N = kT\Delta f \tag{5.1}$$

Where k is Boltzmann's constant, T is the operating temperature (considered to be 290 °K) and Δf is the noise bandwidth. The latter can be considered to be 100 MHz, corresponding to the tightest band-pass filter in the system. Thus, the thermal noise power calculated at the input port of the channel is -94 dBm. In order to refer it to the ADC input, the amplification introduced by the front-end electronics should be taken into account, which correspond to a total gain of 25 dB, by considering the effects of the mixer and all the amplifiers/internal attenuators of the front-end of each channel.

We considered the variable attenuator to be set to 0 dB. Thus, the thermal noise power present at the ADC input is equal to

$$P_N|_{ADC\ in} = -94\ dBm + 25\ dB = -69\ dBm \tag{5.2}$$

From this calculation and by taking into accounts that the ADC differential input resistance is 50 Ω, the thermal noise voltage is equal to 79.3 µV. This would be the noise at the ADC input introduced with the cBPM output signal with noise-free front-end electronics. This value is much lower than the measured value (374.8 µV). In fact, noise introduced by the electronics component (which can be expressed in terms of Noise Figure [41]) is the dominant one, especially the one introduced by the ADC. By referring to its datasheet [39], the input noise power is -59 dBm (calculated from the ADC SNR value), corresponding to a voltage power of 251 µV, which is the largest contribution to thermal/electronic noise of the system and, in absence of other type of noises or interferences, is the major limitation to the resolution of the measuring system.

An analysis of the effects of noise on the resolution of the horizontal and vertical beam position calculated by the "LIBERA CavityBPM" is presented in section 6.4.3, where a comparison with the measurements performed in presence of beam is also presented.

5.3 Measurements with sinewave signals

5.3.1 Calibration of the variable attenuators

As explained in 4.1.1, each channel (“X”, “Y”, I”) of the “LIBERA Cavity BPM” has a variable attenuator (0 dB – 31 dB) installed at its input. These are used in order to setup the module, in accordance with the signal amplitudes of the two resonators of the cBPM. We performed a characterization of each variable attenuators, in order to evaluate the attenuation values compared to the nominal values for every level of attenuation (0 dB – 31 dB). In order to do so, we used the test-stand shown in Figure 5.4. The signal used for the characterization is a sinewave with an amplitude of -15 dBm, used to test each channel separately. The measured attenuation deviation from the nominal value and the phase shift introduced for each attenuation level are shown in Figure 5.7. The attenuation deviation was calculated by comparing the amplitude of the sinewave as measured by the readout electronics (V_X, V_Y, V_I) to the expected amplitude value. The latter was calculated by taking into accounts the attenuation level used and the amplitude of the sinewave measured without attenuation. Phase of the signals was calculated separately for each channel by applying an I-Q demodulation algorithm to the ADC data and taking the phase of the non-attenuated sinewaves as the reference phase (“0” deg).

The effects of the attenuation deviation and phase shift on the ratio V_X/V_I and V_Y/V_I are shown in Figure 5.8. These quantities, in presence of a beam passing through the resonators of the cBPM, would be proportional to the horizontal and vertical position of the beam (see (4.3)). Thus, it is possible to see that the non-ideal behaviour of the variable attenuator would introduces noticeable effects on the measured beam position. In fact, the relative maximum deviation from the mean value is equal to ±1.25% for V_X/V_I and ±0.5% for V_Y/V_I.

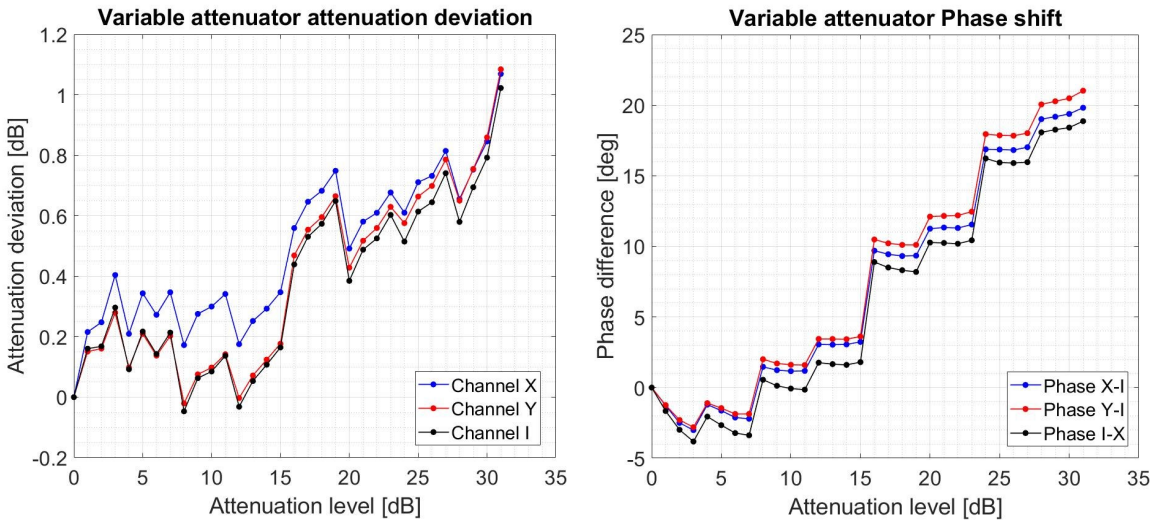

Figure 5.7: Left plot: deviation in attenuation value compared to the nominal value, depending on the value of attenuation applied for the variable attenuators of channel "X", Y", "I" of the "LIBERA Cavity BPM". Right plot: phase shift, calculated as the difference in phase between the three channels ("X-I", "Y-I", I-X"), for different values of attenuation applied for the variable attenuators.

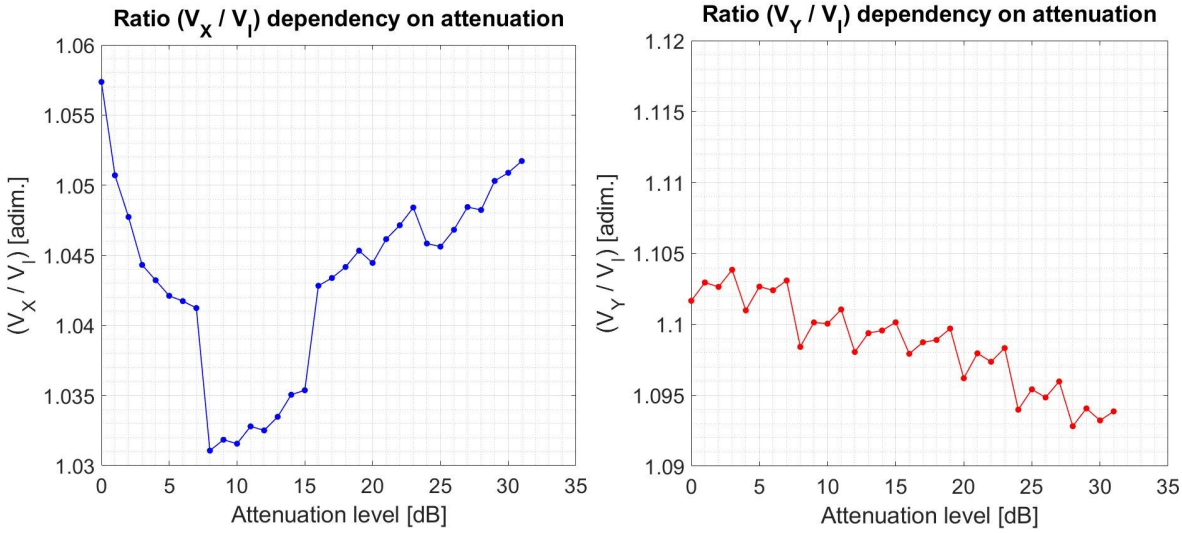

Figure 5.8: Left plot: Amplitudes of the ratio V_X/V_I (left plot) and the ratio V_Y/V_I (right plot) for different attenuation level of the variable attenuators. The attenuation level was applied simultaneously for all the channels.

Based on the measurements performed, we obtained calibration coefficients meant to correct the amplitude for the variable attenuators non-idealities. These coefficients are stored in a look up table in the memory of the "LIBERA Cavity BPM" module and are used automatically for the corresponding attenuator [32]. Same apply for the phase shift in the routine used to calculate the phase difference between the signals on the

channels. Results obtained by applying the calibration coefficients and repeating the same measurements are shown in Figure 5.9 Figure 5.10, where it can be noted that the effects of the non-idealities of the variable attenuators are compensated.

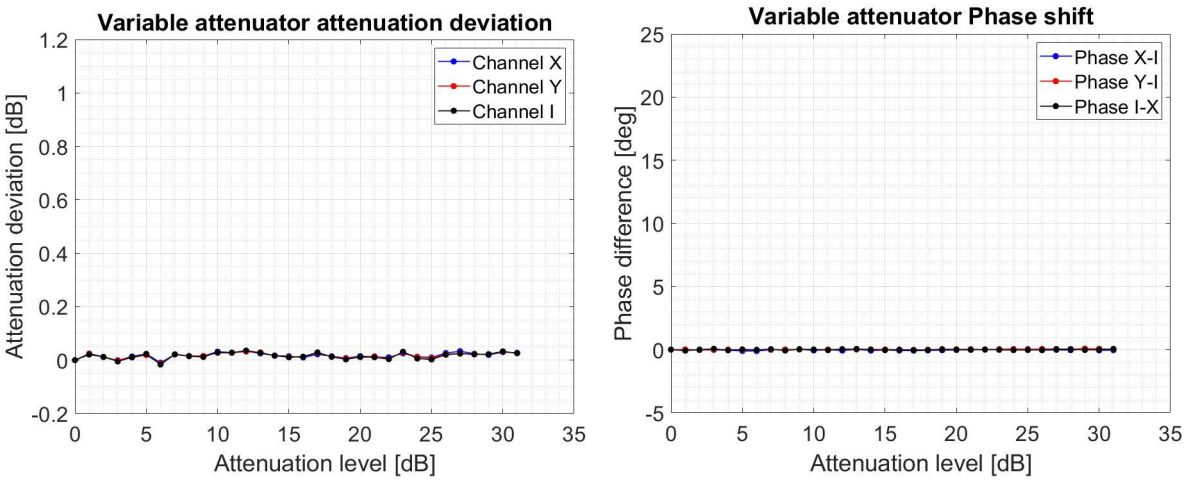

Figure 5.9: Left plot: deviation in attenuation value compared to the nominal value, depending on the value of attenuation applied for the variable attenuators of channel "X", Y", "I" of the "LIBERA Cavity BPM". Right plot: phase shift, calculated as the difference in phase between the three channels ("X-I", "Y-I", I-X"), for different values of attenuation applied for the variable attenuators. Measurements performed after the calibration of the variable attenuators.

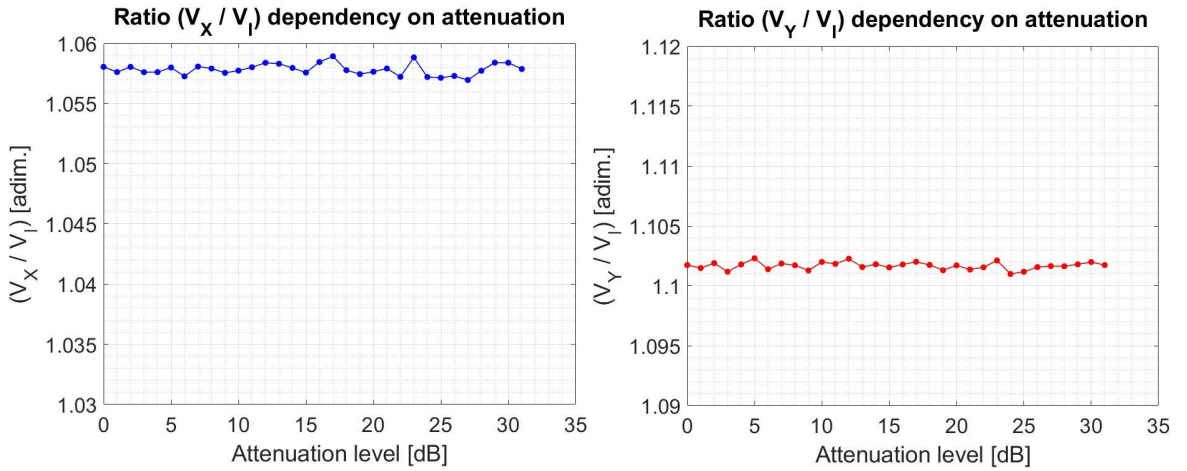

Figure 5.10: Left plot: Amplitudes of the ratio V_X/V_I (left plot) and the ratio V_Y/V_I (right plot) for different attenuation level of the variable attenuators. The attenuation level was applied simultaneously for all the channels. Measurements performed after the calibration of the variable attenuators.

5.3.2 Resolution measurements

Measurements with sinewave signals were performed by using the test-stand shown in Figure 5.4. The sinewave signal generated in laboratory is split by means of a resistive splitter and provided to the Channel “X” and Channel “I” of the “LIBERA CavityBPM” under test. The frequency is 3.284 GHz to resemble the resonance frequency of the resonators of the cBPM, while the amplitude (-9 dBm) is set to exploit all the input range of the measuring system. We used a delay generator at the input of channel “X”, in order to match the phases of the two split signals. The sampled signals are shown in Figure 5.11.

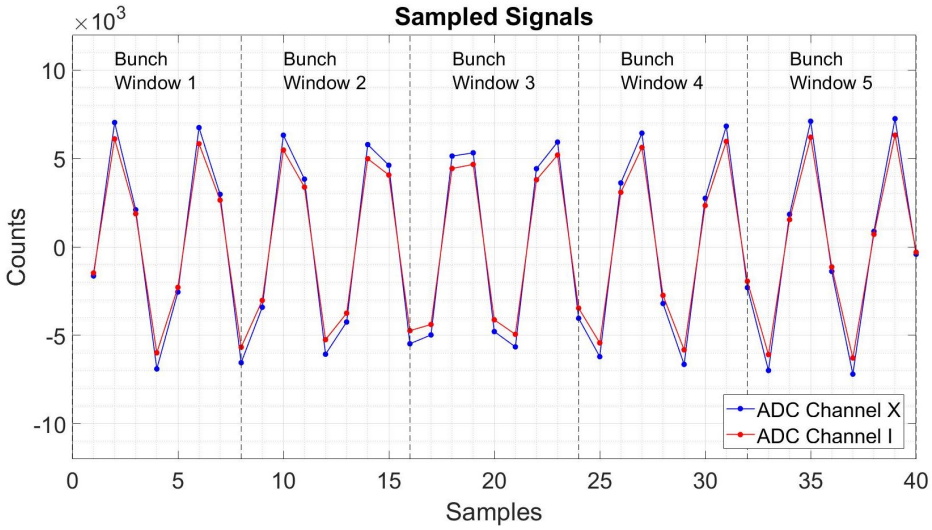

Figure 5.11: Sampled signals on channel “X” and channel “I” of the “LIBERA Cavity BPM”. The waveforms are segmented into “bunch windows” of 8 samples. For each window, the FPGA computes the amplitudes of the two signals and ratio of their amplitudes.

The FPGA was set to separate the sampled signals into “bunch windows” of 8 samples. This is done to mimic the configuration setup that would be used for ELI-NP GBS operation in multi-bunch operation mode 1.2. For each bunch window, the amplitude of the signal for each channel, in this case V_X and V_I, is calculated with Eq.(4.2). The measured values (Figure 5.12) show that the amplitude of the signal on channel “X” is higher than the one on channel “I”. This is due to a non-ideal behaviour of the resistive splitter used during the measurement and/or differences in gain between the two channels.

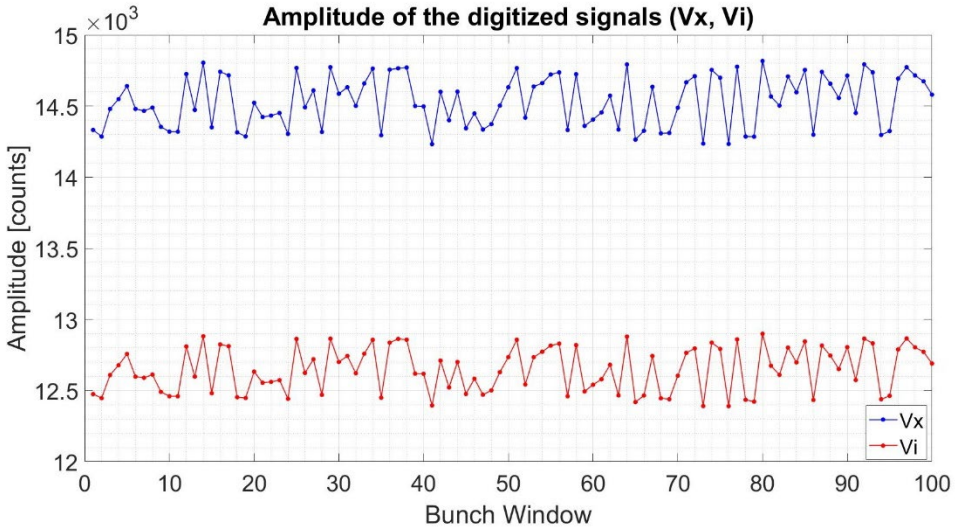

Figure 5.12: Amplitude of the sampled signals (V_X and V_I) of Channel "X" and Channel "I" for each bunch window with sinewave waveforms at the input.

The FPGA calculates the ratio between V_X and V_I for each bunch window (Figure 5.13), according to Eq.(4.3).

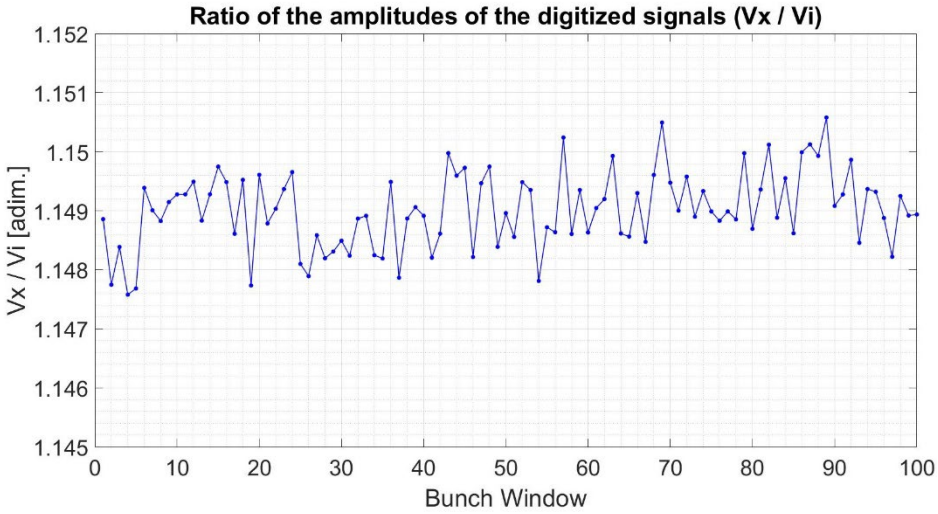

Figure 5.13: Ratio of the amplitudes of the sampled signals of Channel "X" and Channel "I" (V_X / V_I) for each bunch window with sinewave waveforms at the input.

The ratio, in presence of a beam passing through the resonators of the cBPM, would be proportional to the horizontal position of the beam (for the measurements we set the calibration constant K_X equal to 1, see Eq. (4.3)). The standard deviation calculated on V_X, V_I and their ratio V_X/V_I are presented in Table 5.2.

Table 5.2: Mean, standard deviation and relative standard deviation of V_X, V_I and their ratio V_X/V_I for sinewave input signals.

	Mean	**Standard Deviation**	**Relative Standard Deviation**
V_X	14329.1 [counts]	35.7 [counts]	$2.5 \cdot 10^{-3}$ [adim.]
V_I	12648.0 [counts]	28.3 [counts]	$2.3 \cdot 10^{-3}$ [adim.]
V_X / V_I	1.149 [adim.]	$0.47 \cdot 10^{-3}$ [adim.]	$0.4 \cdot 10^{-3}$ [adim.]

The first thing to notice is that the relative standard deviation of the ratio V_X/V_I is much lower than the relative standard deviation of V_X and V_I. This is an indication that noise on V_X and V_I are correlated, which is also visible by comparing the two signals of Figure 5.12. The most obvious consideration is that noise visible on V_X and V_I is dominated by the component introduced along with the sinewave signal. Since it affects both the "X" channel and the "I" channel, this noise component is greatly reduced on the ratio of V_X/V_I, similarly to the case of measuring a noisy signal in differential mode. As such, we can consider the relative standard deviation of the ratio as more pertinent to the resolution of the readout electronics.

5.4 Measurements with single pulse signals

Single pulse measurements were performed by using the test-stand shown in Figure 5.1. The Pulse Generator (Agilent 8133A) was configured in order to generate pulses with a time interval between them of hundreds of ns, in such a way that only the signal produced by the first pulse for every trigger event was captured by the readout electronics. As already explained in section 5.1, the pulses excite the "position" resonator of the cBPM, that acts like a filter, and its output is split in two half and processed by channel "X" and channel "I" of the "LIBERA CavityBPM" module. We used a delay generator at the input of channel "X", in order to match the phases of the two split signals. The analysis of the measurements is performed like the one presented for sinewave signals (refer to section 5.3). The sampled signals and the calculated amplitudes are shown in Figure 5.14 and Figure 5.15.

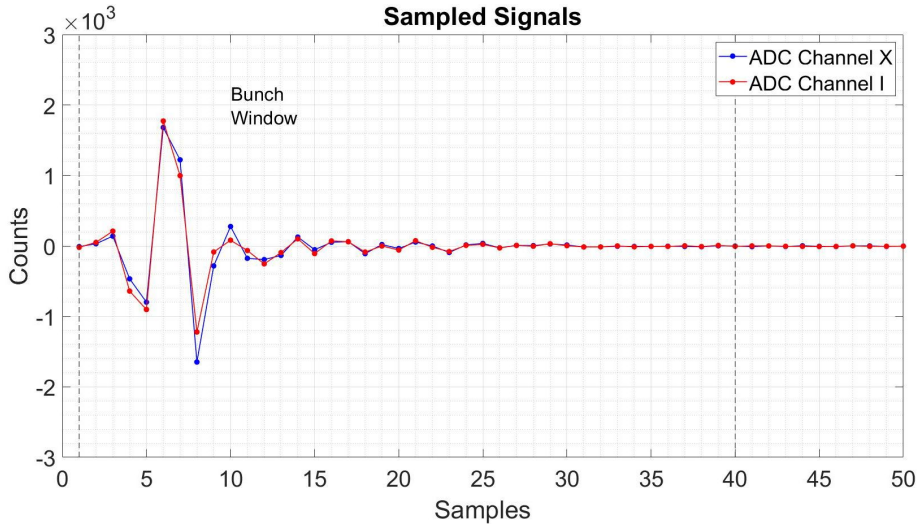

Figure 5.14: Sampled signals on channel "X" and channel "I" of the "LIBERA Cavity BPM". Signals associated with each pulse are digitized with "bunch windows" of 40 samples. For each window, the FPGA computes the amplitudes of the two signals and ratio of their amplitudes. The ADC maximum range is (-8191 - 8192) counts.

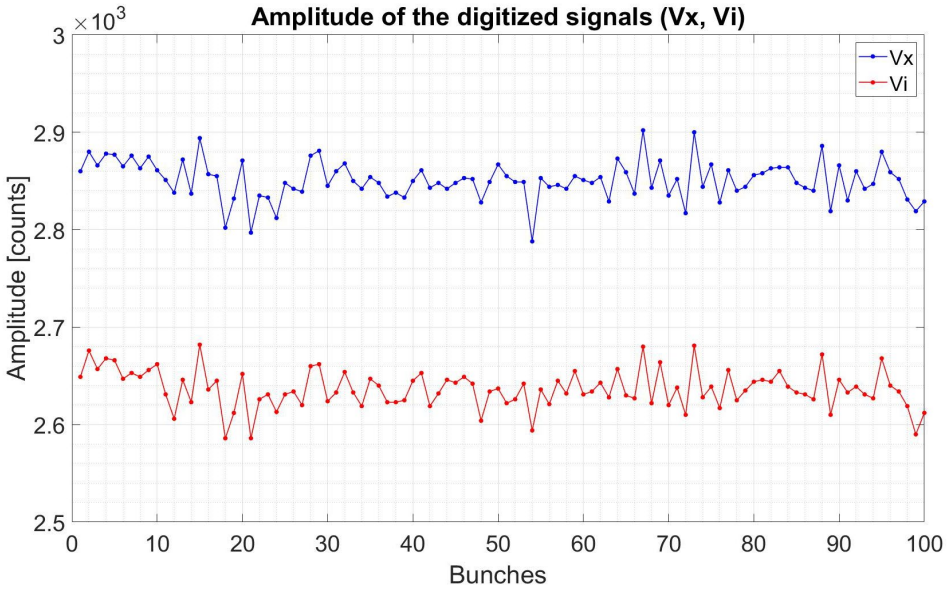

Figure 5.15: Amplitude of the sampled signals (V_X and V_I) of Channel "X" and Channel "I" for each bunch window with signal of the cBPM excited with single pulses.

The standard deviation calculated on V_X, V_I and their ratio V_X/V_I are presented in Table 5.3.

Table 5.3: Mean, standard deviation and relative standard deviation of V_X, V_I and their ratio V_X/V_I, for single pulse signals.

	Mean	**Standard Deviation**	**Relative Standard Deviation**
V_X	2850.8 [counts]	19.9 [counts]	$7.0 \cdot 10^{-3}$ [adim.]
V_I	2636.7 [counts]	19.5 [counts]	$7.4 \cdot 10^{-3}$ [adim.]
V_X / V_I	1.081 [adim.]	$3.32 \cdot 10^{-3}$ [adim.]	$3.0 \cdot 10^{-3}$ [adim.]

Similar to the measurements performed with sinewave signals, the relative standard deviation of the ratio V_X/V_I is lower than the relative standard deviation of V_X and V_I. As already explained, this comes from the fact that the noise component injected along with the input signals is greatly reduced by calculating the ratio (refer to section 5.3).

The standard deviation of the ratio V_X/V_I ($3.32 \cdot 10^{-3}$) is higher than the one calculated with sinewave signals ($0.47 \cdot 10^{-3}$). This is mainly due to the lower signal levels of the single pulse signal, which exploit only ¼ of the max range available. As described in section 5.1, the introduction of external amplifiers was excluded due to high distortion levels. due to the propagation of uncertainty and the fact that V_X and V_I are higher in the case of the sinewave signals. Another consideration is that sinewave amplitude is not reduced in time as the signals produced by the cBPM, which affects the overall SNR of the system.

The effects of the amplitude levels of the input signals on the standard deviation of their ratio is easily explained by looking at the propagation of error for the ratio V_X/V_I, that can be described as:

$$\sigma_{V_X/V_I} = \left|\frac{V_X}{V_I}\right| \cdot \sqrt{\left(\frac{\sigma_{V_X}}{V_X}\right)^2 + \left(\frac{\sigma_{V_I}}{V_I}\right)^2 - 2 \cdot \frac{\sigma_{V_X V_I}}{V_X \cdot V_I}} \qquad (5.3)$$

Since the signals in channel “X” and channel “I” are synchronized and the noise of the source is greatly reduced by calculating the ratio, we could consider only the uncertainty (noise) introduced by the read-out electronics σ_{Vx_el} and σ_{Vi_el}. Thus, we can say in first approximation that the covariance σ_{VxVy_el} is zero, as the channel “X” and “I” are independent. To simplify the formula and adapt it to the measurements performed, we can also say that:

$$\sigma_{V_{Xel}} \approx \sigma_{V_{Iel}} = \sigma_{V_{el}} \qquad (5.4)$$

As such, eq.(5.3) could be simplified as:

$$\sigma_{V_X/V_I el} = \left|\frac{V_X}{V_I}\right| \cdot \sqrt{\left(\frac{\sigma_{V_{el}}}{V_X}\right)^2 + \left(\frac{\sigma_{V_{el}}}{V_I}\right)^2} \qquad (5.5)$$

From the latter, by considering that V_X and V_I have similar values, it is clear that the lower are V_X and V_I, the higher is the standard deviation of the ratio, in line with the experimental data obtained from Table 5.2 and Table 5.3.

It is possible to estimate from the data collected what could be the position resolution (in mm) of the measuring system in presence of beam. In fact, the ratio V_X/V_I is a value which would be proportional to the horizontal beam position, in the case where the cBPM is excited with beam bunches (see Eq. (4.3)). The nominal sensitivity of the "position" resonator (whose signal associated with the horizontal beam position is read by channel "X") and the "reference" resonator (channel "I") for the ELI-NP GBS cBPM are:

$$S_X = 7.07 \ \frac{V}{mm \cdot nC}$$
$$S_I = 135 \ \frac{V}{nC} \qquad (5.6)$$

We could image the case where the beam bunches have a charge of 25 pC and a horizontal offset of 1 mm from the electromagnetic center of the cBPM (which could be a real case during the ELI-NP GBS operations) for a signal amplitude of 176.75 mV for the "X" and 3.375 V for "I".

Considering that in the laboratory measurements we are exploiting only ¼ of the max range (equal to V_{max} = 56 mV), an attenuation of 22 dB on channel "X" and 48 dB on channel "I" would lead to the same amplitude levels obtained in the measurements.

In this scenario, the calibration constant of eq.(4.3) would be K_x = 1 mm and the resolution of the system would be equal to 3.32 µm (see the relative standard deviation of V_X/V_I in Table 5.3), while the maximum observable range for the beam bunches would be approximatively around ±4 mm, as it can be deducted from the fact that the signal on channel "X" occupy only one quarter of the entire input range of the ADC (see Figure 5.14). With signals covering all the available input range, it is possible to expect better results.

5.4.1 Phase dependency

Synchronization of the signal on channel “X” and channel “I” plays an important role on the measurements presented. The effects of changing the phase difference between the signals on the “X” and “I” channels (by means of an installed delay generator) are shown in Figure 5.16. The standard deviation of the ratio is dependent on the phase difference (X-I).

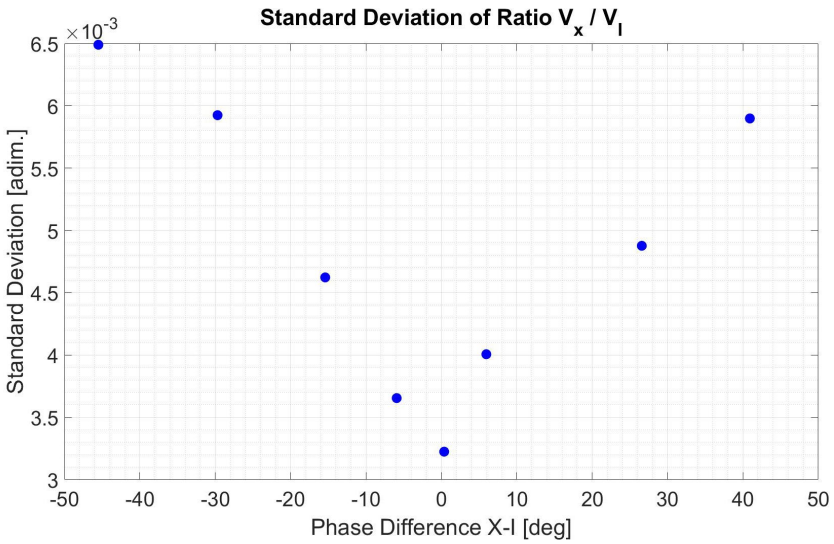

Figure 5.16: Standard deviation of the ratio of the amplitudes of the sampled signals of Channel “X” and Channel “I” (V_X / V_I) for different phase difference between the two signals. For each phase difference value 100 acquisition were taken.

This dependency is mainly due to the fact that by desynchronizing the two signals, the noise of the source will not be decreased anymore by performing the ratio, as the noise “pattern” on one channel will be shifted in time in respect to the other. A similar measurement was also performed in presence of beam during the experiments conducted at DESY. Refer to section 6.6 for a deepening on the topic.

5.5 Measurements with train of pulses

Measurements with train of pulses were performed by using the test-stand shown in Figure 5.1. The gate window generated by the Delay Generator (Standford DG535) was adjusted to fit 32 consecutive bunches, in order to generate a signal that mimic the trains of bunches which would be used during the ELI-NP GBS multi-bunch operations. The trains of pulses (Figure 5.3) are provided with a repetition rate of 100 Hz to the

channel “X” and channel “I” of the “LIBERA Cavity BPM. Measurements performed were conducted in a similar way as the measurements with sinewave signals and single pulses in section 5.3 and 5.4. In this case we also made use of the Deconvolution Filter, that is the digital filter used to compress the ADC data to fit the portion of the signal associated with each bunch in 8 samples, in order to limit the interferences between consecutive pulses (see section 4.2.2). The deconvolution filter was defined before the measurements, in presence of a signal generated by a single pulse.

ADC data in presence of the train of pulses are shown in Figure 5.17 with and without the application of the deconvolution filter.

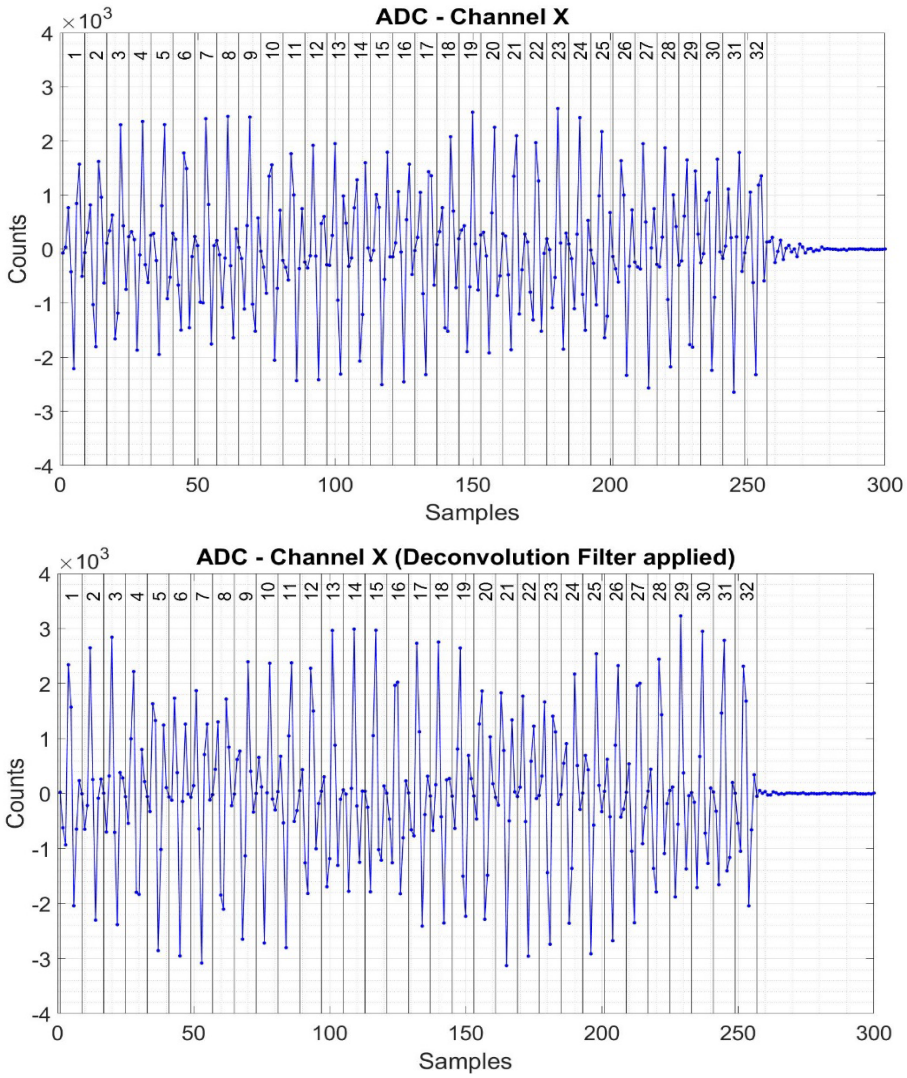

Figure 5.17: Sampled signal on channel “X” of the “LIBERA Cavity BPM” in presence of a multi-pulse signal at the input with (lower plot) and without (upper plot) the Deconvolution Filter. The signal in both cases is divided in “bunch windows” of 8 samples (numbered in the plot). For each window, the FPGA computes its amplitude.

The effect of the deconvolution filter is visible at the end of the signal (bunch window 32), where it is possible to see that the tail of the signal in presence of the filter is truncated, as it is for each bunch window within the train of pulses. The introduction of the deconvolution filter had not significant impact on the resolution and accuracy of the system. Further measurements will be performed on this topic in future. Sampled signals of Channel "I" are similar in shape and amplitude to the one presented for channel "X".

We calculated the phase of the digitized signal on Channel "X and Channel "I" for each bunch window. This was made with an I-Q demodulation algorithm, by considering the signals as "sine-like" and taking the first sample of each "bunch window" as a reference to set the phase as "0" deg. Results are shown in Figure 5.18.

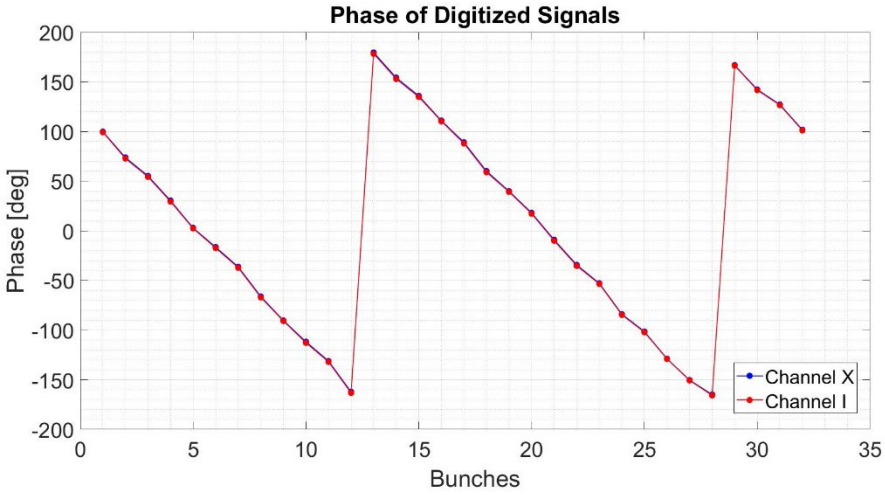

Figure 5.18: Phase of digitized signals for channel "X" and channel "I". Phase is calculated for each bunch window with an I-Q demodulation algorithm.

The average phase advance for each bunch window is -25.46 deg for both channel "X" and channel "I". This is an indication that the ADC sampling clock is not perfectly synchronized with the pulses. By considering that the signal before the down-conversion has a frequency of 3.284 GHz, it is possible to express the phase advance in terms of time shift (TS) for every bunch window:

$$TS = \frac{1}{3.284\ \text{GHz}} \cdot \frac{-25.46}{360} = 21.5\ ps \qquad (5.7)$$

Thus, at the 32th bunch window, the accumulated delay would be:

$$32 \cdot 21.5\ ps = 688\ ps \qquad (5.8)$$

This delay is a possible source of errors and cross-talk between consecutive bunch windows and its effects will be fully analysed in future measurements.

The ratio of the amplitudes (V_X/V_I) calculated by the "LIBERA Cavity BPM" for each bunch window composing the "train" is shown in the left plot of Figure 5.19, as the mean over 100 consecutive acquisitions. As it can be noted, the ratio is lower for the bunch windows from 24 to 32. This behaviour is systematic over all the acquisitions. It could be related to the time shift previously mentioned and it will be also analysed in future measurements.

The relative standard deviation calculated for each bunch window is shown in the left plot of Figure 5.20, showing no big differences between each bunch window.

In the right plots of Figure 5.19 and Figure 5.20 the same measurements are shown but by calculating the mean and the relative standard deviation over the 32 bunch windows of each train of pulses (obtaining the mean and rel. std of each train of pulses for all the acquisitions).

By comparing the results with the ones obtained with single pulses (Table 5.2), it is possible to see that similar results in terms of resolution are achieved. These can be used to estimate the position resolution (in mm) of the measuring system in presence of beam, obtaining similar results as reported in section 5.4.

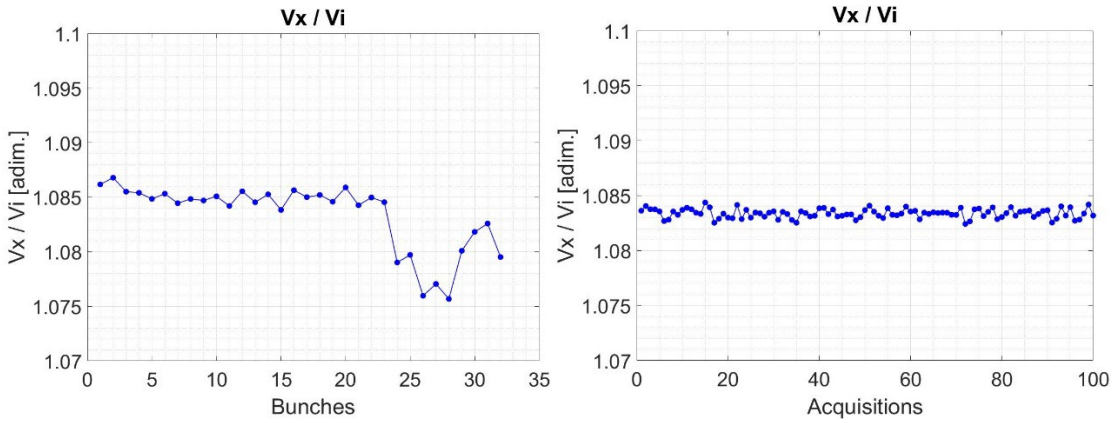

Figure 5.19: Left plot: mean of the ratio of the amplitudes (V_X/V_I) calculated for each bunch window, over 100 acquisitions. Right plot: Mean of the ratio of the amplitudes (V_X/V_I) calculated for the 32 bunch windows composing a single "train", for 100 acquisitions.

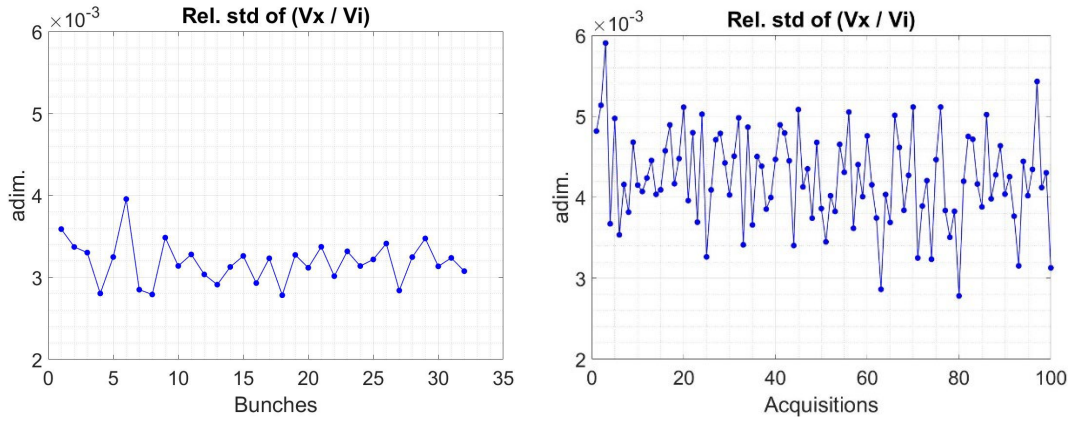

Figure 5.20: Left plot: relative standard deviation of the ratio of the amplitudes (V_X/V_I) calculated for each bunch window, over 100 acquisitions. Right plot: relative standard deviation of the ratio of the amplitudes (V_X/V_I) calculated for the 32 bunch windows composing a single "train", for 100 acquisitions.

5.6 Stability over time

In order to evaluate the stability of the measuring system over a long period of time, a measurement of 50 hours was performed by tracking the amplitude of the signal on channel "X" (V_X) and channel "I" (V_I) every 10 minutes. The signal provided to the system is the same of the one represented in Figure 5.3 and already analysed in section 5.5. The mean amplitude of the entire train of pulses (constituted by 32 bunch windows) for channel "X" and channel "I" and their ratio are showed in Figure 5.21.

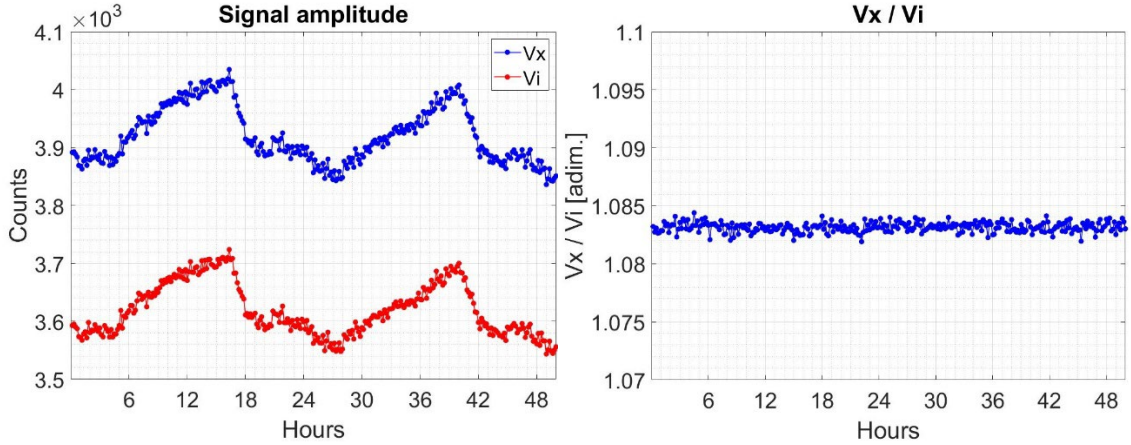

Figure 5.21: Stability over time measurements. Left plot: Amplitude of the signals (left plot) and their ratio (right plot) provided to the measuring system (1 acquisitions every 10 min) for a 50-hours period of time.

The amplitude of the signals, as calculated by the “LIBERA Cavity BPM” show a dependency on the 24-hours cycle, due to temperature excursion. This could depend from the cBPM itself and/or the readout electronics. The ratio is completely unaffected by it. Thus, it is possible to say that temperature dependency would be negligible in terms of accuracy of the calculated beam position. A complete characterization of the stability of the system will be performed once the cBPMs will be installed and working, as other factors should be monitored and taken into accounts, such as the reference signal provided to the readout electronics and the stability over weeks of operation. For an example of this type of investigation on cBPMs, refer to [42].

6 Beam measurements on Cavity BPM and the readout electronics

6.1 Test-stand at FLASH1

The validation and the first measurements on the Cavity BPM and the read-out electronics (LIBERA "CavityBPM") were performed in laboratory at INFN-LNF (see chapter 5). Although all the functionalities were validated and the tests on the measuring performance were promising, the tests were limited by the experimental setup. One of the major limitation, for example, was the impossibility to test the "reference" resonator.

Thus, we performed a second session of tests at DESY, by using a Cavity BPM test stand at FLASH1 [43]. This was performed in collaboration with Instrumentation Technologies and DESY staff. The test stand (see Figure 6.1) was already installed in the FLASH1 beamline and already used for other tests involving Cavity BPMs for EU-XFEL and their related readout electronics [44]. The beam pulses provided at FLASH1 during the three days of measurements had a repetition rate of 10 Hz with a time interval between the bunches of 1 μs or higher. Since the time interval between bunches was much higher than the cavity BPMs signal duration (in the order of tens of nanoseconds), we considered all the measurements taken as in single-bunch mode.

The test stand consists of three Cavity BPMs (EU-XFEL "Undulator" type, see Figure 6.2), installed on independent stages, moveable in both transverse directions (within ±1 mm) by means of remote movers. This gives great flexibility for testing the Cavity BPM, particularly for resolution measurements, as will be described later in this chapter. The three cavity BPMs where labelled cBPM1, cBPM2, cBPM3, where cBPM2 is the central one and cBPM1 and cBPM3 the externals. We installed and connected three "LIBERA CavityBPM" module to the three Cavity BPMs on the test stand. The cables used are the 7/8'' LCF78-50JA with N-type connector from the cBPM side and SMA connector from the readout electronics side. In Table 6.1 the attenuations of the cables are provided.

Figure 6.1: Cavity BPM test-stand at FLASH1 with three EU-XFEL "undulator" Cavity BPMs (on the right) on remote movers. An EU-XFEL "beamline" Cavity BPM is also installed, but it was not used during the tests (on the left).

Table 6.1: Measured attenuation (courtesy of D.Lipka) introduced by the cables connecting the Cavity BPM to the "LIBERA CavityBPM". Attenuations includes also the presence of the patch panels in the rack room and in the tunnel.

	Channel	**Attenuation at 3.3 GHz (dB)**
cBPM1	X	-5.35
	Y	-5.08
	I	-5.07
cBPM2	X	-5.10
	Y	-5.08
	I	-4.94
cBPM3	X	-5.02
	Y	-5.03
	I	-5.10

We did not have the chance to use the ELI-NP Cavity BPM on the test stand. As such, we performed tests on the read-out electronics rather than on the Cavity BPMs

themselves. Nevertheless, the “Undulator” Cavity BPMs are very similar in design and properties compared to the ELI-NP ones (Table 6.2) [45].

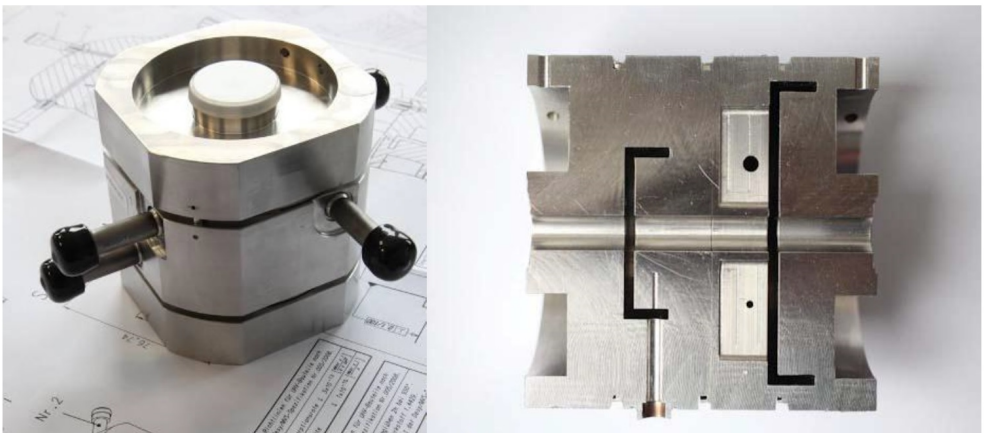

Figure 6.2: EU-XFEL “Undulator” type Cavity BPM, installed at the test-stand in FLASH1 at DESY. The design and properties are similar to the ones of ELI-NP GBS (photos: D. Nölle)

Table 6.2: Nominal Parameters of ELI-NP GBS and EU-XFEL “Undulator” type Cavity BPMs.

Cavity BPM Parameter	**ELI-NP**	**EU-XFEL (Undulator)**
Q_L	40	70
TM_{110} frequency (“Position” resonator) [GHz]	3.284	3.3
TM_{010} frequency (“Reference” resonator) [GHz]	3.284	3.3
“Position” resonator sensitivity [V/mm/nC]	7.07	2.84
“Reference” resonator sensitivity [V/nC]	135	60

From Table 6.2, it is possible to observe that the resonance frequencies are almost the same, while the Q_L is significantly higher for the “Undulator” Cavity BPM and both the sensitivities are lower. In Figure 6.3, it is possible to observe the effects of these differences on the output signals for each type of Cavity BPM. For the simulation, we took into considerations a bunch of 1 nC of charge and a distance of 1 mm on the horizontal axis in respect to the electromagnetic centre of the Cavity BPM.

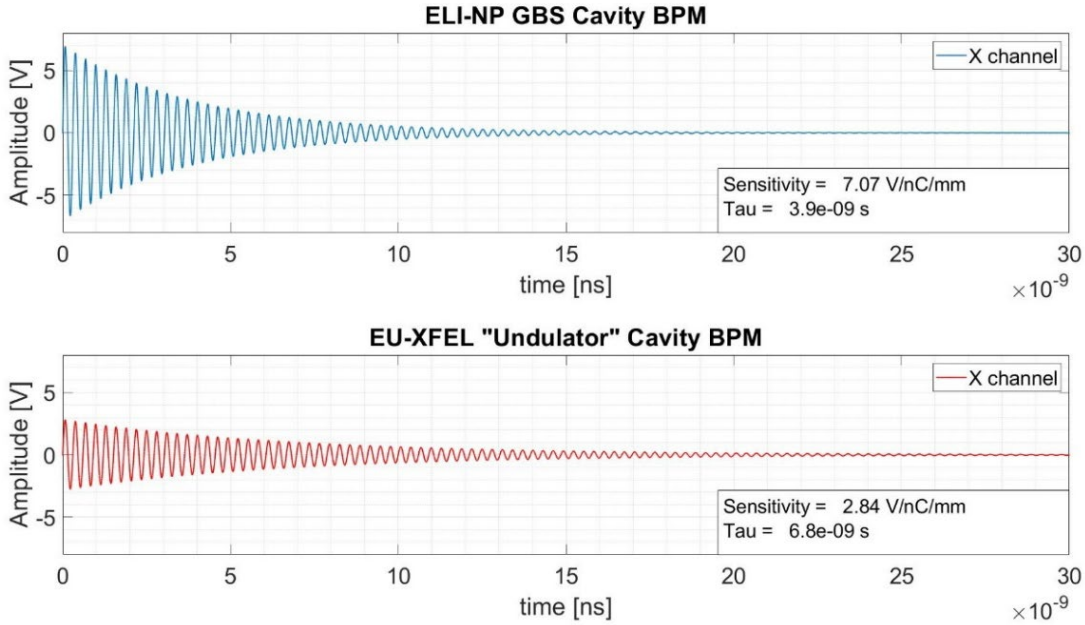

Figure 6.3: Comparison between the output signal of the "X" channel for ELI-NP GBS and EU-XFEL "Undulator" Cavity BPMs. The signals are simulated by taking into consideration a bunch with 1 nC of charge and a distance of 1 mm on the horizontal axis in respect to the electromagnetic center of the Cavity BPM.

In order to test the read-out electronics, we had to adapt our setup to take into considerations the signal features of the "Undulator" Cavity BPMs. The higher Q_L value means that the signals last longer. This was not an issue, because the interval between bunches during the tests was long enough to avoid any inter-bunches interferences (see 4.2.2). As such, we set up the instrument in order to have "bunch windows" of 60 samples. Furthermore, the reference signal provided (for an explanation of it see section 4.1) had a frequency of 216.7 MHz (instead of 62.087 MHz, used in ELI-NP GBS). As such, the PLLs were adjusted in order to work with the new signal and to produce appropriate frequency for the Local Oscillator (3675.3 MHz) and for the ADC (497.53 MHz). The variable attenuators (ranging from 0 to 31dB) for all the three channels ("X","Y","I"), where adjusted accordingly to the expected amplitude of the signal. This means that by deciding the maximum measurable offset range of the beam (typically selected in our case as ±1 mm on both axes) and by knowing the bunch charge, the attenuators were set in order to exploit the dynamic range of the read-out electronics to the best. We also installed a 20 dB external attenuator in front of the "I" channel for each module, in order to match the amplitude of the signals coming from the reference resonators.

We took data for bunch charges of 200 pC and 500 pC. Most of the measurements presented in this chapter have been taken with the configuration setups presented in Table 6.3 and Table 6.4.

Table 6.3: Configuration setup used to collect data set named "500 pC – Range 1300 µm".

Configuration Setup for Data Set "500 pC – Range 1300 µm "	
Parameter	**Value**
Bunch Charge	~500 pC
Internal Attenuators	X, Y: 15 dB; I: 25 dB
Max. Position measurement range	~ ± 1300 µm
Position Range measured	± 800 µm
Position Steps	100 µm – 17 positions
ADC buffer max value	X, I: ~5000 counts
ADC samples per bunch	60

Table 6.4: Configuration setup used to collect data Set named "200 pC – Range 1200 µm".

Configuration Setup for Data Set "200 pC – Range 1200 µm "	
Parameter	**Value**
Bunch Charge	~200 pC
Internal Attenuators	X, Y: 9 dB; I: 16 dB
Max. Position measurement range	~ ± 1200 µm
Position Range measured	- 1100 µm / +800 µm
Position Steps	100 µm – 20 positions
ADC buffer max value	X, I: ~6000 counts
ADC samples per bunch	60

6.2 ADC Output signals and deconvolution filter

The typical sampled signal at the passage of a single bunch is showed in the upper plot of Figure 6.4. The plot is relative to channel "X", with a bunch off-centered on the horizontal plane of approximately 500 pC. Similar signals are captured at channels "Y" and "I". The signal length covers approximately 20 samples (~40 ns). By applying the

digital deconvolution filter (see section 4.2.2), the signal is compressed into 8 samples (lower plot of Figure 6.4). From the measurements performed in single-bunch mode, the effects of the deconvolution filter are negligible in terms of accuracy and resolution.

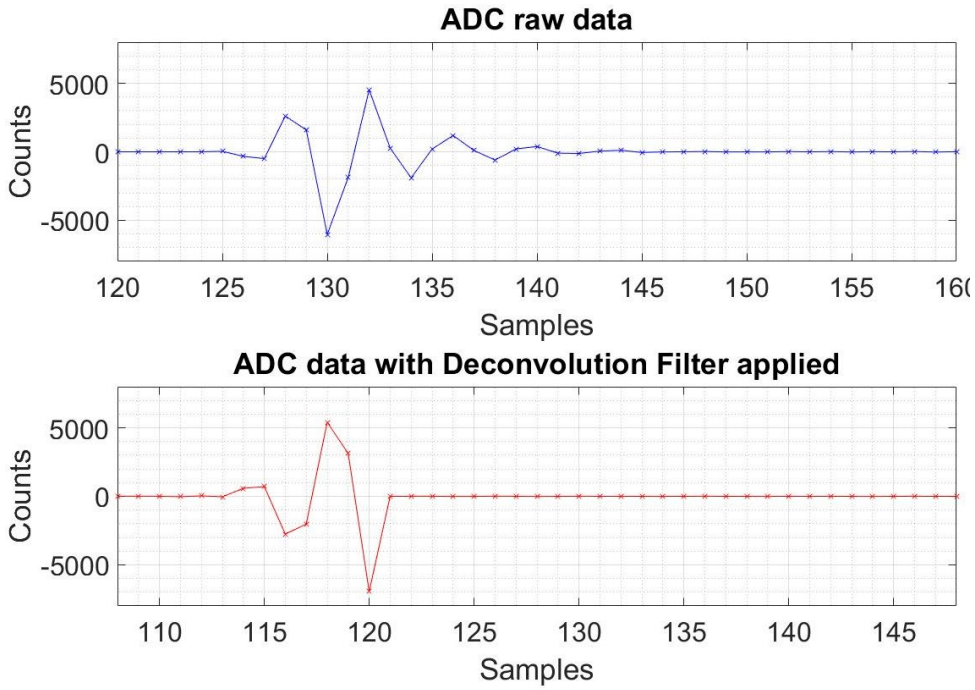

Figure 6.4: Comparison between ADC output without Deconvolution filter (upper plot) and with Deconvolution filter (lower plot) of channel "X" at the passage of an off-centered bunch of approximately 500 pC at FLASH1.

6.2.1 Power Spectrum and frequency measurements

We performed a frequency analysis of the digitized signals, in order to evaluate the quality factors and resonance frequency of the Cavity BPMs. We used the ADC samples of each channel (X,Y,I) of the dataset "200 pC – Range 1200 µm" associated to the passage of beam bunches at a nominal horizontal stage position of 800 µm and vertical stage position of 100 µm (see Figure 6.5, for an example of the signal on the X channel). Power spectra were calculated for each channel for 100 consecutive bunch and then averaged (see Figure 6.6 for the spectra of channel X,Y,I of cBPM2).

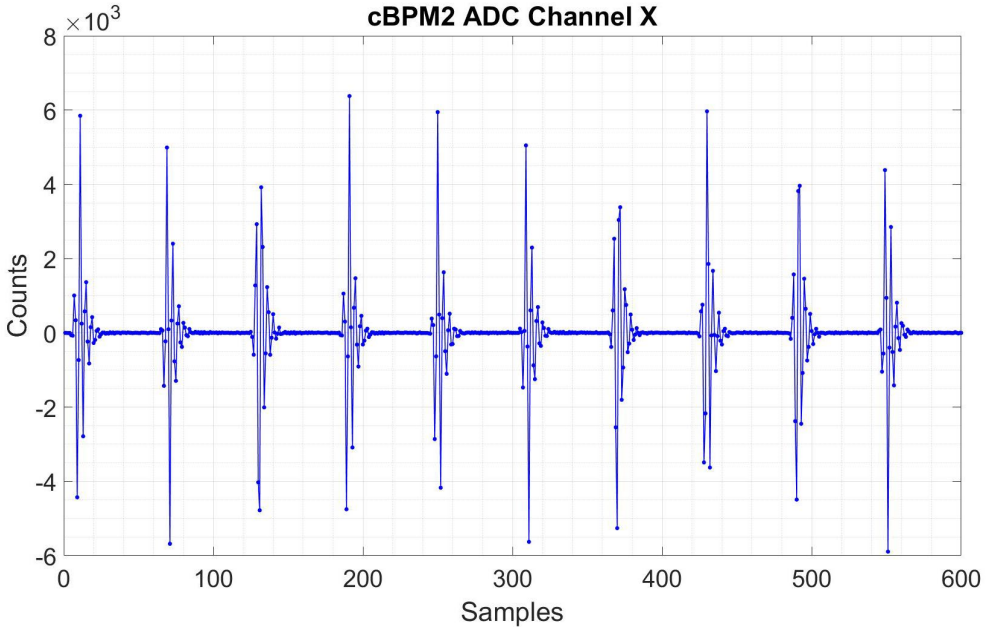

Figure 6.5: ADC output of the signals induced by beam bunch for cBPM2 channel X at a nominal horizontal stage position of 800 µm (Data set: "200 pC – Range 1200 µm").

From the measurements performed it was possible to measure the central frequency (f_{alias}) and the bandwidth at -3dB (Δf) of the digitized signals for each channel and each cBPM, reported in Table 6.5.

Table 6.5: Central frequency and bandwidth of the digitized signals at a nominal stage position of 800 µm (horizontal) and 100 µm (vertical) (Data set: "200 pC – Range 1200 µm").

	Channel	f_{res} [MHz]	Bandwidth [MHz]
cBPM1	**X**	132.15	49.34
	Y	129.97	44.48
	I	123.77	40.79
cBPM2	**X**	128.94	44.44
	Y	129.56	43.88
	I	118.41	38.87
cBPM3	**X**	129.19	45.66
	Y	128.51	46.61
	I	120.23	39.74

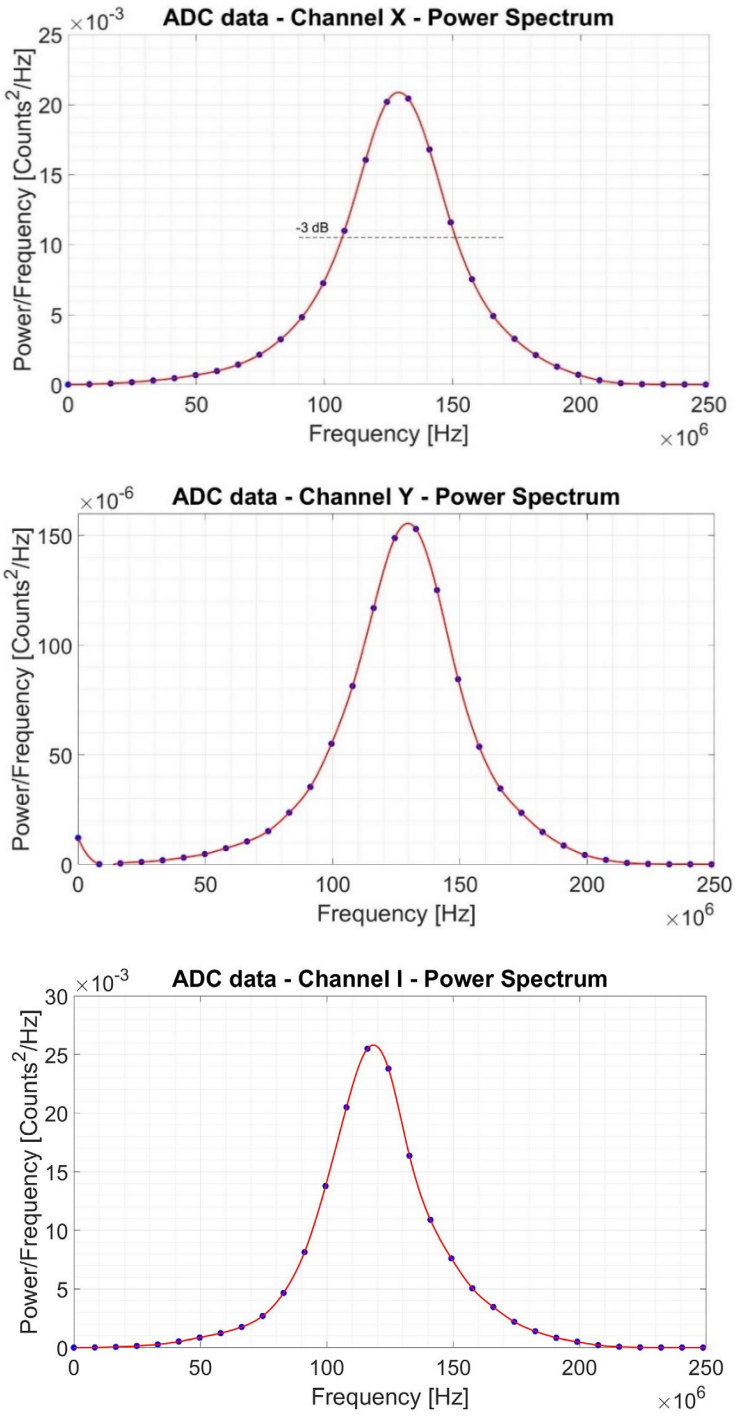

Figure 6.6: Average power spectrum of signals induced by beam bunch for cBPM2 channel X, Y, I at a nominal stage position of 800 µm (horizontal) and 100 µm (vertical). The red plots are the cubic interpolation of the data (blue dots). The dashed black line represents the -3dB level (Data set: "200 pC – Range 1200 µm").

It is also possible to calculate the resonance frequency and the quality factor of the cBPM resonators. As explained in section 4.1.2 the output cBPM signals are down-converted, filtered and under-sampled. As such, to reconstruct the resonant frequencies of the cBPMs (f_{res}) from the measured central frequencies (f_{alias}), the calculation consists of:

$$f_{res} = f_{LO} - \underbrace{(f_{ADC} - f_{alias})}_{f_{IF}} \qquad (6.1)$$

where f_{LO} = 3675.3 MHz and f_{ADC} = 497.53 MHz.

The quality factor can be calculated as:

$$Q = \frac{f_{res}}{\Delta f} \qquad (6.2)$$

From the results obtained (shown in Table 6.6) it can be noted that the resonance frequencies have an average value of 3.305 GHz and are all included in an interval of 14 MHz (±0.4% of the average value).

The loaded Quality factors of the reference resonators (channel "I"), with an average value of 82.9 are significantly higher than the one of the position resonators (channel "X", "Y") with an average value of 72.4. It is interesting to note that for cBPM1, the loaded quality factors for the horizontal and vertical ports ("X" and "Y") differs significantly (a difference of 7.3).

Table 6.6: Calculated cBPM output signal central frequencies and Quality Factors.

	Channel	f_{res} [GHz]	Q_L [adim.]
cBPM1	**X**	3.310	67.1
	Y	3.308	74.4
	I	3.302	80.9
cBPM2	**X**	3.307	74.4
	Y	3.307	75.4
	I	3.296	84.8
cBPM3	**X**	3.307	72.4
	Y	3.306	70.9
	I	3.298	83.0

Values obtained for the loaded quality factors may be slightly higher than the real ones. This is because their values are obtained with signals which have been filtered with a band-pass filter within the LIBERA module. Even if the bandwidth of the filter (116 MHz)

is higher than the bandwidth of the signal (~45 MHz), it is possible that the frequency response of the filter has a slight narrowing effect on the frequency content of the signal, which is translated in a higher calculated quality factor.

6.3 Position measurements

One of the first tests we performed was to observe the position measured by the three Cavity BPMs, for different horizontal positions of the beam. The latter were obtained by moving all the cavity BPMs (by means of the remote movers) with steps of 100 µm (data set "500 pC – Range 1300 µm " and "200 pC – Range 1200 µm ", see Table 6.3, Table 6.4). We measured the horizontal position of 300 bunches at every step.

From the results obtained (see Figure 6.7 and Figure 6.8), it is possible to observe that the overall sensitivities of the three measuring system is not the same.

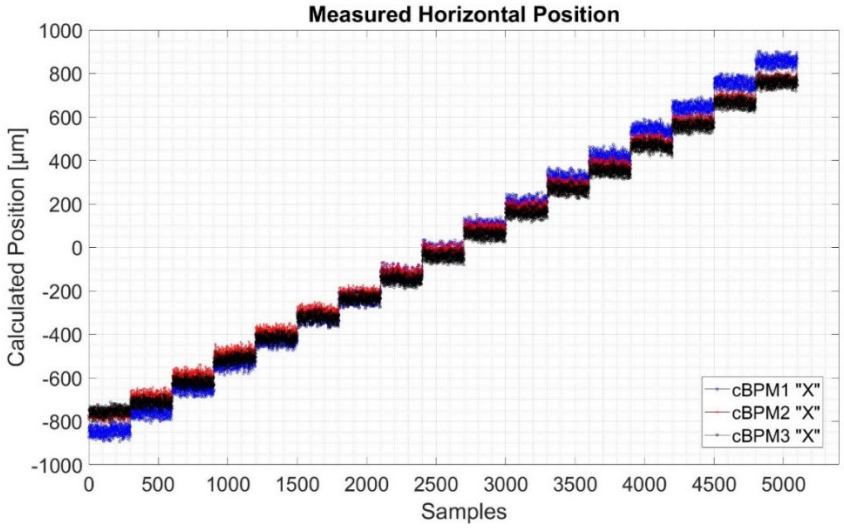

Figure 6.7: Measured horizontal position of the three cBPMs, obtained by moving them with steps of 100 µm in the horizontal plane (Data set: "500 pC – Range 1300 µm").

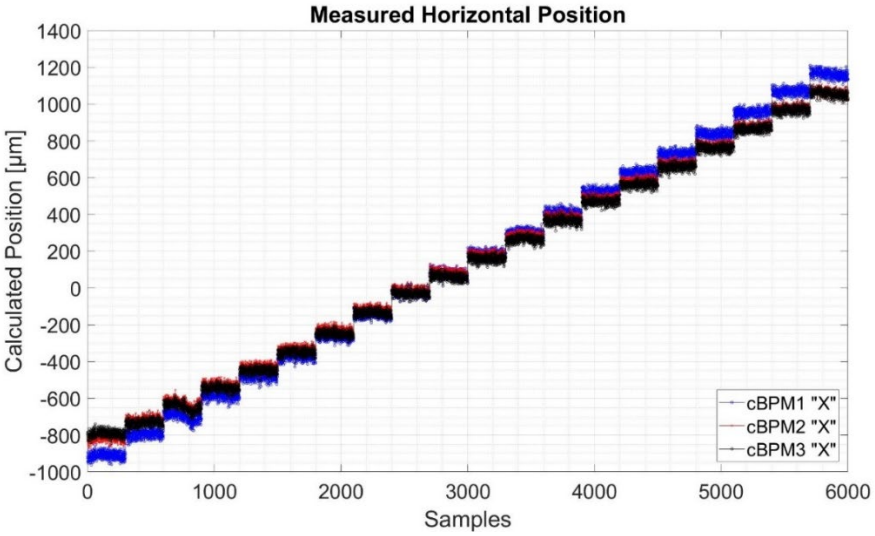

Figure 6.8: Measured horizontal position of the three cBPMs, obtained by moving them with steps of 100 µm in the horizontal plane (Data set: "200 pC – Range 1200 µm").

This is also visible in Figure 6.9 and Figure 6.10, where the data related to the same nominal horizontal stage position (300 acquisitions) have been averaged.

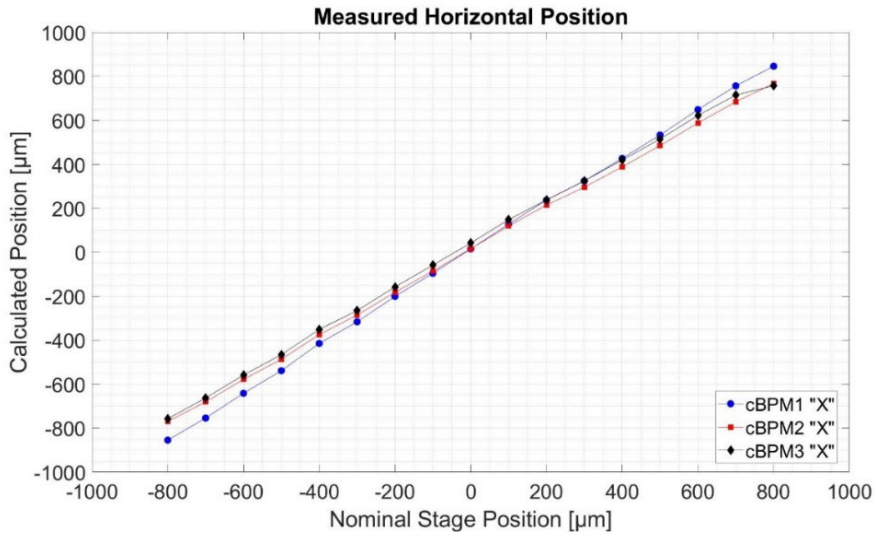

Figure 6.9: Means of the measured horizontal position (performed on sets of 300 samples) of the three cBPMs, obtained by moving them with steps of 100 µm in the horizontal plane (Data set: "500 pC – Range 1300 µm").

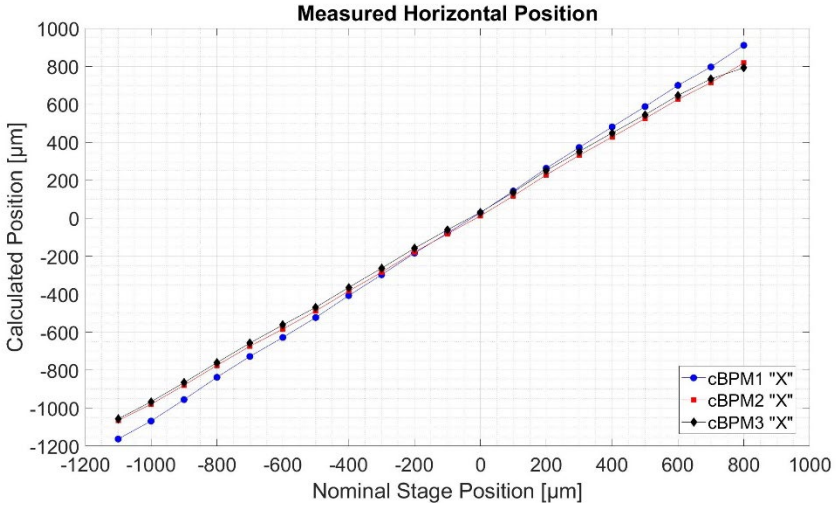

Figure 6.10: Means of the measured horizontal position (performed on sets of 300 samples) of the three cBPMs, obtained by moving them with steps of 100 µm in the horizontal plane (Data set: "200 pC – Range 1200 µm").

We calculate the linear fit with a least squares method between the average positions of cBPM1 and cBPM2 and between cBPM3 and cBPM2. By doing this, we obtained the ratios of sensitivities and offset differences of cBPM1 and cBPM3 position data relatively to the ones of cBPM2 (see Table 6.7 and Table 6.8).

Table 6.7: Coefficients of the linear fit between the mean positions of cBPM1 and cBPM2. Results are displayed in terms of position sensitivity ratio and offset differences between the two Cavity BPMs.

Results of the linear fit between the mean positions of cBPM1 and cBPM2	
Data Set "500 pC – Range 1300 µm"	
Position Sensitivity Ratio	0.9047 [adim.]
Position Offset Difference	1.39 µm
Data Set "200 pC – Range 1200 µm"	
Position Sensitivity Ratio	0.9099 [adim.]
Position Offset Difference	-11 µm

Table 6.8: Coefficients of the linear fit between the mean positions of cBPM3 and cBPM2. Results are displayed in terms of position sensitivity ratio and offset differences between the two Cavity BPMs.

Results of the linear fit between the mean positions of cBPM3 and cBPM2	
Data Set "500 pC – Range 1300 µm"	
Position Sensitivity Ratio	0.9971 [adim.]
Position Offset Difference	-22.8 µm
Data Set "200 pC – Range 1200 µm"	
Position Sensitivity Ratio	1.002 [adim.]
Position Offset Difference	-16.0 µm

The differences in sensitivity could derive from a number of causes, including differences of the Cavity BPMs and/or the read-out electronics or differences on the stage movers. The offset differences could derive from the not perfect alignment of the Cavity BPMs between each other.

For the resolution measurements (see section 6.4), the differences in sensitivity were compensated by applying the coefficients calculated in Table 6.7 and Table 6.8 on the measured positions of cBPM1 and cBPM3 (considering cBPM2 as a reference).

From the data collected it was also possible to measure the standard deviation of the measured position for every step of the horizontal stage (see Figure 6.11 and Figure 6.12). From this measurement it is possible to observe that for every horizontal position (with one exception at position "-900 µm" for the data set "200 pC – Range 1200 µm") the standard deviation is within 17-22 µm for each Cavity BPM. This is not the related to the resolution of the measuring systems (which is much higher, as will be seen in section 6.4), but it is due to the beam fluctuations from shot to shot. The standard deviation at the nominal stage position "-900 µm" (Figure 6.12) is much higher than the other ones, because when we collected that set of data, the beam was slowly shifting on the horizontal axes (see the samples from 600 to 900, corresponding to "-900 µm" in Figure 6.8). Another aspect of this measurement is that the calculated standard deviation of cBPM1 is always higher than the ones of cBPM2 and cBPM3. This is another indication that cBPM1 sensitivity is higher than cBPM2 and cBPM3. In fact, with a higher sensitivity the beam fluctuations measured are also wider resulting in a higher value of standard deviation.

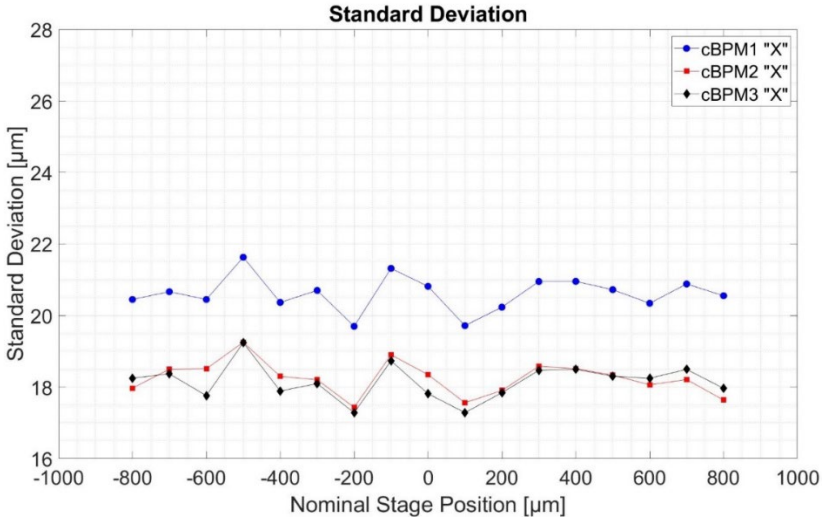

Figure 6.11: Standard deviation of the horizontal measured positions (on sets of 300 samples) of the three Cavity BPMs, for different position on the horizontal axes (Data set: "500 pC – Range 1300 µm").

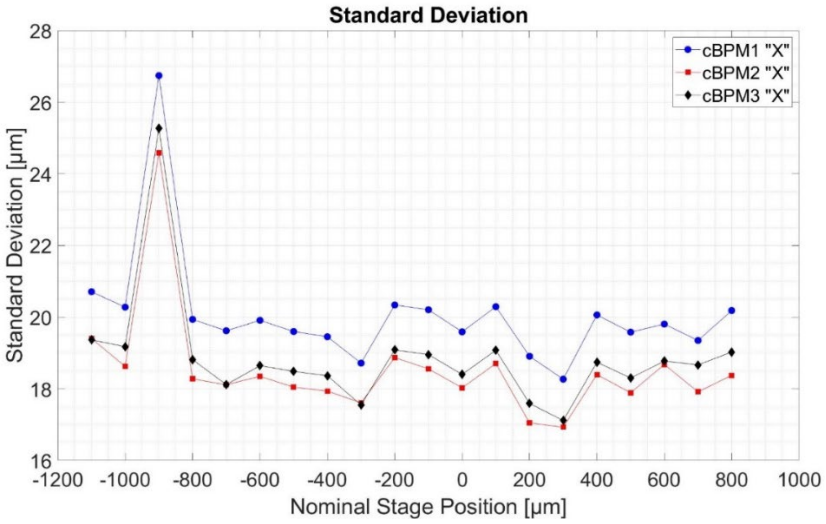

Figure 6.12: Standard deviation of the horizontal measured positions (on sets of 300 samples) of the three Cavity BPMs, for different position on the horizontal axes (Data set: "200 pC – Range 1200 µm").

6.4 Resolution Measurements

6.4.1 Measurement methods

Cavity BPM resolution was determined by measuring the residual, that is the difference between the position of the beam as measured by the cBPM in question and the predicted position as calculated from the beam's position in the two other cBPMs (see Figure 6.13). We used the central cBPM as the device under test (cBPM2) and the external ones (cBPM1, cBPM3) to calculate the predicted position. This method is widely diffused and has been used also for synchrotron BPMs. For comparisons and examples refer to [46], [47] and [48].

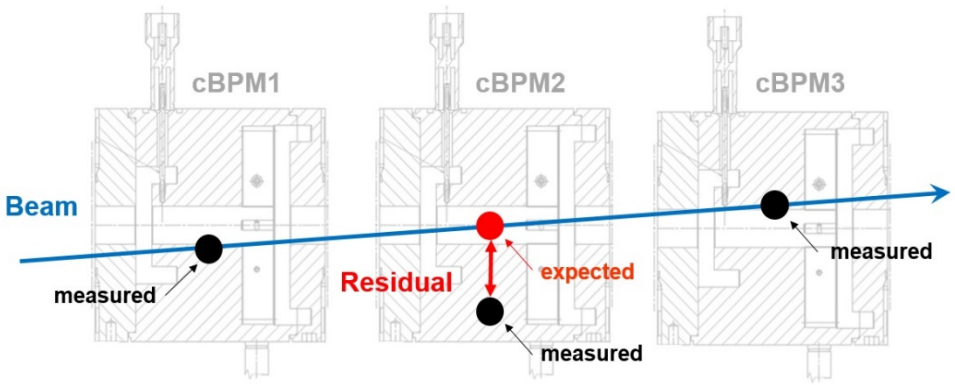

Figure 6.13: Graphical representation of the resolution measurements based on the calculation of the residual for cBPM2.

The distance between cBPM1 and cBPM2 is 179.4 mm, while the distance between cBPM2 and cBPM3 is 178.4 mm. By considering the distance between the cBPMs equal (that is a good approximation of the real case) the residual on the horizontal plane $ResX_2$ is calculated as:

$$ResX_2 = X_2 - \frac{X_1 + X_3}{2} \tag{6.3}$$

where X_1, X_2, X_3 are the horizontal positions of the bunch measured respectively by cBPM1, cBPM2, cBPM3. Same applies for the vertical plane. The standard deviation of the residual is then given by:

$$\sigma_{ResX_2} = \sqrt{{\sigma_{X2}}^2 + \frac{{\sigma_{X1}}^2 + {\sigma_{X3}}^2}{4}} \tag{6.4}$$

By assuming that the cBPMs have the same resolution, we also expect that the standard deviations associated to their position measurement σ_{X1}, σ_{X2}, σ_{X3} are equal. Thus, we can write:

$$\sigma_{ResX_2} = \sqrt{{\sigma_X}^2 + \frac{{\sigma_X}^2 + {\sigma_X}^2}{4}} = \sqrt{\frac{3}{2}} * \sigma_X \qquad (6.5)$$

where we assumed that ($\sigma_{X1,X2,X3} = \sigma_X$). By reversing the equation, the resolution σ_X of the cBPM under test is obtained as:

$$\sigma_X = \sqrt{\frac{2}{3}} * \sigma_{ResX_2} \qquad (6.6)$$

Calculating the resolution of the measuring device (in this case cBPM2) by means of the residual allow to get rid of beam fluctuations from shot to shot on the transversal plane (see Figure 6.12). This is because the beam fluctuations affect in the same way all the cBPMs and the residual is not affected by it. We measured the residual and its standard deviation and calculated the resolution of cBPM2 for different horizontal position of the beam in respect to the electromagnetic center of the cBPMs, by moving the latter with remote movers on the horizontal plane (300 acquisitions for each horizontal position). We decided to move all the cBPMs with the same steps and at the same time.

6.4.2 Measurements for different bunch charges

Resolution measurements performed with configuration setup “200 pC – Range 1200 µm” and “500 pC – Range 1300 µm” are shown in Figure 6.14. From the results shown, it is possible to observe that the resolution is dependent on the beam position and get worse for a beam farther from the electromagnetic center of the cBPM. The same trend with similar values of resolution is present for bunches of 200 pC and 500 pC. By taking into consideration the measurements at 500 pC, the best resolution achieved is at the nominal position “-100 µm”, with a value of 0.37 µm, while the worst resolution is at position “800 µm”, with a value of 5.56 µm.

Another effect to notice is the worsening of the resolution with a beam at the center. The latter behaviour will be explained in section 6.4.5.

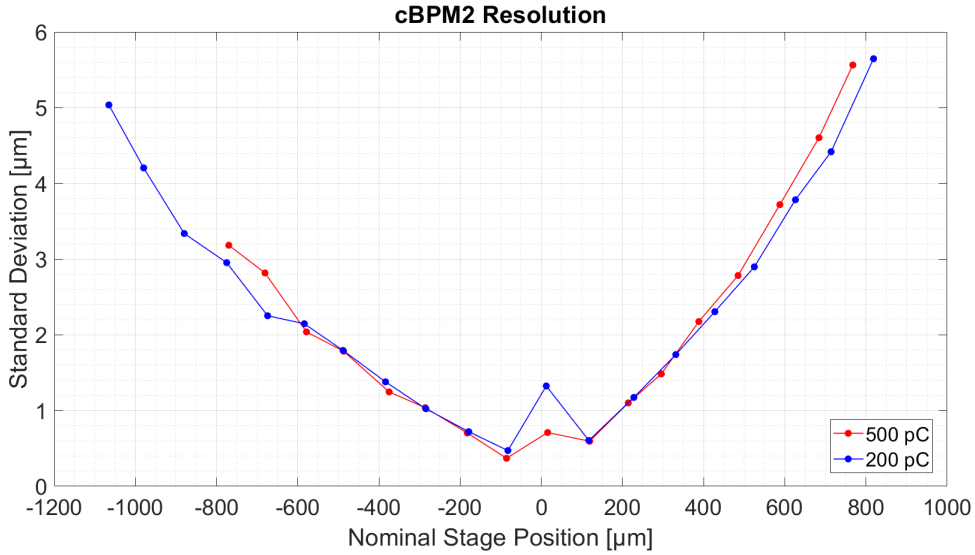

Figure 6.14: Cavity BPM2 horizontal position measurement resolution for different bunch charges and different beam positions. Data set: "200 pC – Range 1200 µm" and "500 pC – Range 1300 µm"

In principle, the resolution of the measurements should be roughly the same for any beam position. This is because thermal noise and electronics noise are independent from the amplitudes of the signals. The position of a single beam bunch (X and Y) is calculated by the readout electronics (see section 4.2.1 and eq.(4.3)) as:

$$X = K_x \frac{V_X}{V_I} \quad Y = K_y \frac{V_Y}{V_I} \tag{6.7}$$

Due to the cBPM behaviour, the amplitude of the output signal of the "position" resonator is higher for larger beam offsets, resulting in a higher V_x (the value calculated by the readout electronics). On the contrary the amplitude of the output signal of the "reference" resonator is dependent only from the beam charge and consequently V_I is constant.

To extend the analysis of the resolution we studied the values and the standard deviation of V_x and V_I. In order to get rid of the effects of beam fluctuations, we measured the standard deviation by calculating the residual for V_x and V_I of cBPM2, with the same steps described in this paragraph. Results are shown in Figure 6.15.

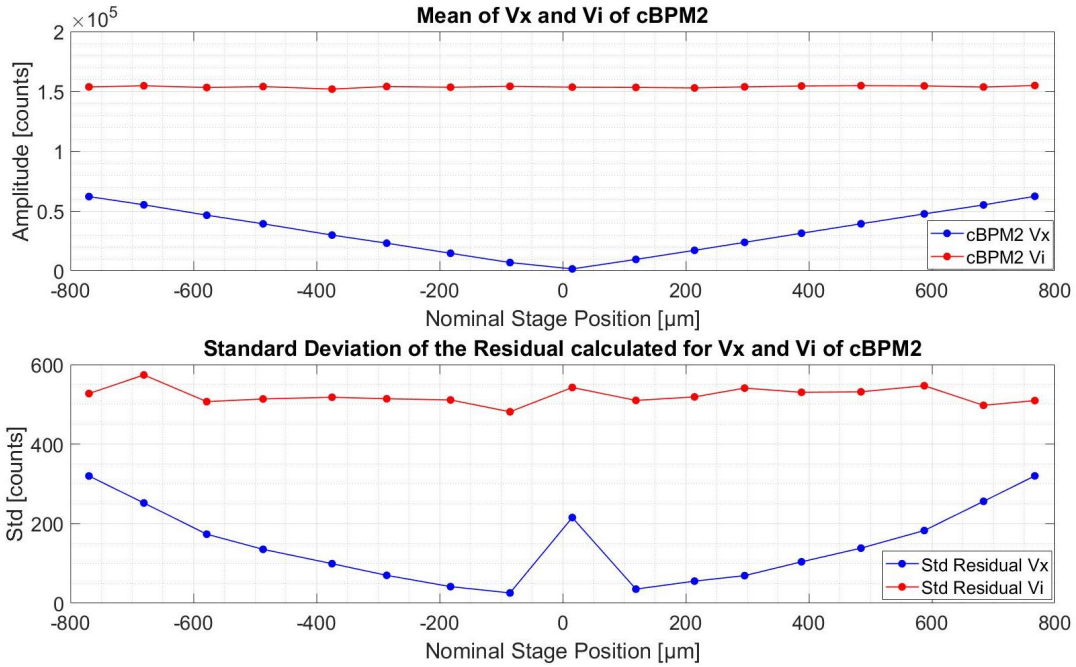

Figure 6.15: Analysis on V_x and V_i data sets for cBPM2 (Data set: "500 pC – Range 1300 µm").

In the upper plot it is possible to observe the mean value (calculated on 300 acquisitions) of V_x and V_I corresponding to the same horizontal stage positions as presented in Figure 6.14. From the figure it is possible to see that V_x increase with the beam offset, while V_i remain constant, as expected. In the lower plot, the standard deviation of the residual of Vx and Vi are shown. As in Figure 6.14, the standard deviation is higher for higher signal amplitudes. This explains the resolution trend on the calculated beam horizontal beam position of Figure 6.14. Concerning the nominal stage position around 0 µm, there is a worsening of the resolution for V_x, similar to Figure 6.14. However, in this case, the effect is expected and is not representative of the actual resolution of V_x, but it is related on how the residual is calculated. In fact, due to minor misalignments of the three Cavity BPMs between each other, the same beam bunch could transit on different sides (left or right) of the X axis in respect of the e.m. center for the three cBPMs. Since V_x (an always positive quantity) is representative of the absolute value of the offset of the beam on the X axis, it will not take into account the sign of it. As such, calculating the residual and its standard deviation in such conditions, will result in a worsening of the calculated resolution. For further readings on resolution measurements performed with cBPM with similar features, refer to [49].

6.4.3 Estimation of thermal/electronic noise on the resolution

From the measurements performed in laboratory and presented in section 5.2, it is possible to estimate the resolution of the horizontal and vertical measured position, in the scenario where the contribution to uncertainty is dominated only by thermal/electronic noise. This is a simplification and does not take into accounts any other type of noise, distortions or interferences.

Horizontal and vertical positions of a single beam bunch are calculated with eq.(6.7). Propagation of uncertainty for the horizontal position (σ_X) can be calculated as [50]:

$$\sigma_X = \left| K_x \frac{V_X}{V_I} \right| \cdot \sqrt{\left(\frac{\sigma_{V_X}}{V_X}\right)^2 + \left(\frac{\sigma_{V_I}}{V_I}\right)^2 - 2 \cdot \frac{\sigma_{V_X V_I}}{V_X \cdot V_I}} \qquad (6.8)$$

where σ_{Vx} and σ_{Vy} are the standard deviation associated to V_X and V_I and σ_{VxVy} is the covariance between V_X and V_I. Same applies for σ_Y.

By recalling the algorithm used to calculate V_x and V_i (see eq.(4.2)) and applying the propagation of uncertainty, it is possible to calculate that the standard deviation σ_{Vx} (associated to V_X) is equal to the standard deviation σ_x associated to each ADC sample x_n.

In eq.(6.8) we considered the covariance σ_{VxVy} to be zero, to simplify the calculation, even though a correlation between V_X and V_I would probably exist, due to possible crosstalk between the two channels and the fact that the reference signal of each "LIBERA Cavity BPM" (used for the down-conversion) is in common between every channel.

In order to estimate the resolution on the horizontal position measurements we used the values measured and reported in Table 5.1 for σ_x and σ_I. For V_x and V_I we used the mean values measured with the configuration setup "500 pC – Range 1300 µm" for different stage positions. For K_x (the calibration constant) we used the same value applied for the configuration setup "500 pC – Range 1300 µm" equal to 1.9078 mm.

The results are displayed in Figure 6.16, where the black dots represents the estimated standard deviation for different horizontal beam position and the red curve is the second order polynomial fit of the data. It is interesting to notice that the estimated resolution presented here, based on the measured thermal/electronic noise reported in section 5.2), is much lower (by at least one order of magnitude) than the measured one with beam (see Figure 6.14). The standard deviation trend for different horizontal beam

position (rising for higher beam offsets) in this case is a consequence of the fact that the position is calculated as the ratio of V_x and V_i, which are both affected by uncertainty. This trend is similar in shape to the one of the real position measurement, but it is negligible in values and cannot justify the fast increase in uncertainty of the real position measurement in relation to the beam position.

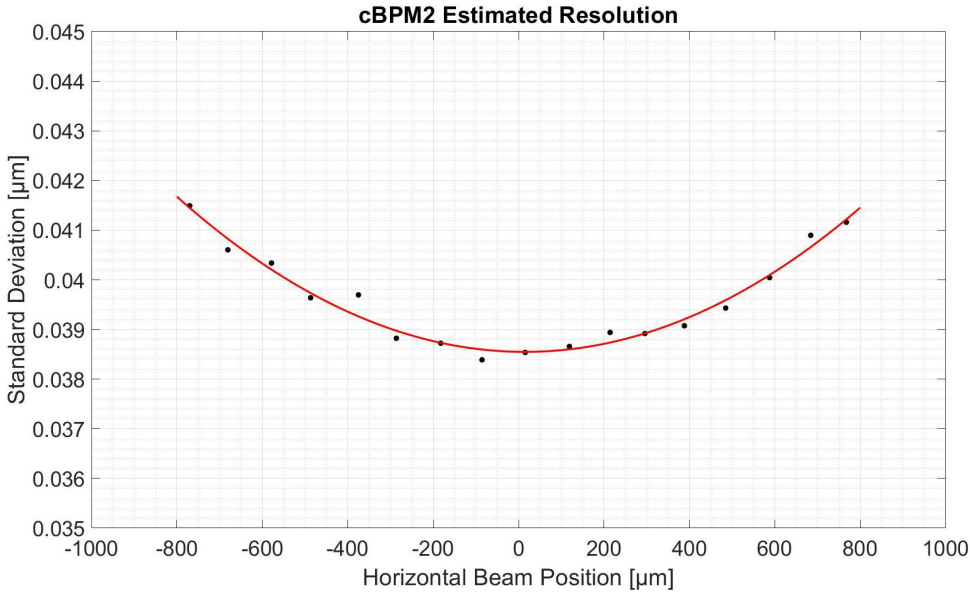

Figure 6.16: Estimation of the resolution of cBPM2, based on the thermal/electronic noise measured in laboratory (see Table 5.1), related to the measurements taken with the setup configuration "500 pC – Range 1300 µm".

6.4.4 Analysis of resolution measurements: Phase Noise

The worsening of resolution with larger beam offsets (Figure 6.14) could be explained by taking into consideration phase noise, which is a known issues for similar measuring systems [17].

The latter is defined (for a sinewave signal with frequency f_{ref}) as the ratio of the noise in a 1 Hz bandwidth at a specified frequency offset to the signal amplitude at frequency f_{ref} and is measured as dBc/Hz.

The effect of phase noise on a signal involves a phase jitter on the signal, which can be expressed both in radians or in seconds [1]:

$$Jiitter_{rms}[rad] = \sqrt{2 * 10^{A/10}}$$
$$Jiitter_{rms}[s] = \frac{\sqrt{2 * 10^{A/10}}}{2\pi * f_{ref}} \quad (6.9)$$

where A is the integrated phase noise power over the spectrum and f_{ref} is the nominal frequency of the signal. For a deepening on phase noise and its effect on sampled systems, refer to [51] and [52].

Contributions to the phase noise on the measuring system could come from the "ADC PLL" and "LO PLL" local oscillators, from the ADC of the "LIBERA for Cavity BPM" and from the reference signal used to lock the ADC and down-mix the cBPM signal (see section 4.1.2). Data sheets of components ([35],[39],[36],[33]) and laboratory tests performed and reported by Instrumentation Technologies during the development of the "LIBERA for Cavity BPM" showed negligible amount of phase noise produced by the local oscillators and the ADC. These behaviour were also not detected during the laboratory measurements presented in chapter 5. As such, the main source of it could come from the reference signal itself, that had a frequency of 216.7 MHz for the experimental setup at FLASH1.

In Figure 6.17, the power spectrum of the reference signal used during the tests and provided to the readout electronics is showed. A jitter of 3.2 ps was measured by integrating the phase noise spectrum from 10 Hz to 10 MHz, according to eq. (6.9).

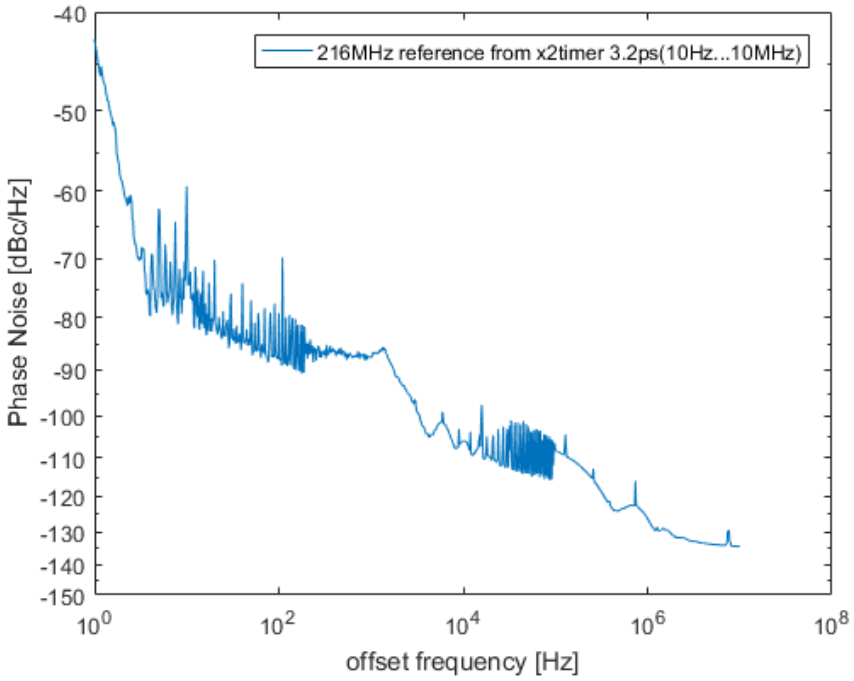

Figure 6.17: Phase noise of the external reference signal used during the tests at DESY for the "LIBERA Cavity BPM". The offset frequency (x-axis) is relative to 216.7 MHz, which is the nominal frequency of the signal (courtesy of Dr. Dirk Lipka)

A jitter on the reference signal is translated to a jitter on the input signals (during the down-conversion process) and on a jitter of the ADC. Both these effects have an impact on the overall resolution of the measuring system.

For example, a jitter on the sampling clock of the ADC, induce an amplitude noise on a digitized sinewave signal of:

$$V_{noise} = 2\pi * V_{max} * f * Jitter_{rms} \qquad (6.10)$$

where V_{max} is the amplitude of the sinewave signal and f is its frequency. This effect is showed in Figure 6.18. Same apply for the cBPM output signals, which can be described as a sinewave signal decaying in time.

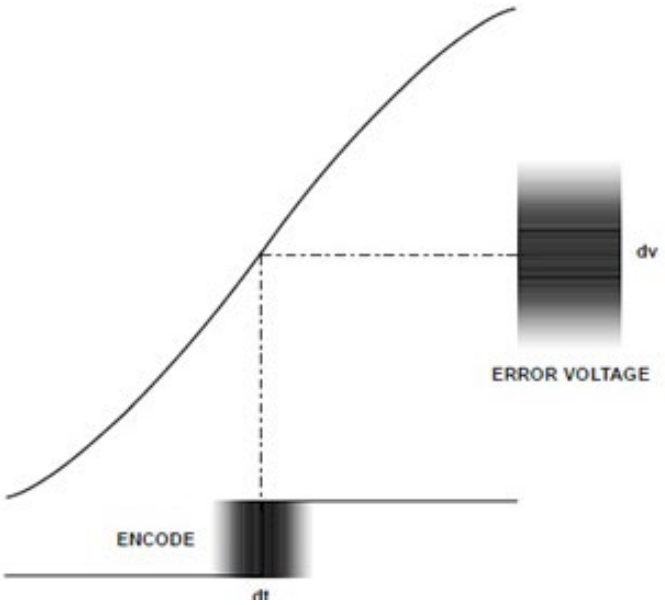

Figure 6.18: Representation of the effect of jitter during the digitization of a signal with an ADC. Jitter on the ADC sampling time directly translates to an error voltage, depending on the slope of the signal [53].

It is difficult to analyse the possible effects of jitter of the reference signal on the position resolution. This is because a full analysis of its impact would be required on the internal components of the LIBERA Cavity BPM, such as the ADC PLL, LO PLL (which could act as a filter for the jitter) and the ADC itself. The effect of the jitter would have an effect both on the down-conversion and the digitization process for the "X" and "Y" and "I" channels. Moreover, all these effects would be correlated and cannot be treated independently, since the source of the jitter would be in common for all the internal components and channels.

Nevertheless, we could provide an estimation of the impact of the jitter on the resolution by considering the simple case where the only source of phase noise is coming from the reference signal and it only affects the ADC sampling clock of one channel.

The reference signal is converted by means of ADC PLL from a frequency of 216.7 MHz to a frequency of 497.5 MHz (reference signal for the ADC sampling clock). By excluding any effect of filtering of the PLL, we can consider that the phase noise is conserved in this conversion. Thus, the jitter of 3.2 ps on the reference signal is translated to a jitter of 1.4 ps on the reference signal for the ADC sampling clock, according to:

$$Jiitter_{refADC} = \frac{f_{ref}}{f_{refADC}} * Jitter_{ref} \qquad (6.11)$$

By using eq.(6.10), the amplitude noise introduced by this jitter can be calculated as:

$$V_{noise} = 2\pi * 1\ V * 375\ MHz * 1.4\ ps = 3.3\ mV \qquad (6.12)$$

where we have considered f = 375 MHz, which is the nominal carrier frequency of the down-converted input signals (see paragraph 4.1.2) and V_{max}= 1 V, which is the maximum input voltage as the ADC input. By comparing the jitter-related noise contribution to the noise at the input of the ADC due to thermal noise (equal to 374.8 µm for channel X, see section 5.2), it is clear that the first is higher than the other. This would justify the noise value and trend on the resolution measurements This analysis gives only a hint on the possible source of the noise. Further measurements will be performed in the future to fully analyse this behaviour.

6.4.5 Analysis of resolution measurements: Beam transiting near the electromagnetic center of the cBPM

As shown in Figure 6.14, there is a worsening of the resolution of the calculated positions at the nominal stage position around 0 µm. At this location the output signals coming from the "position" resonators of the three cBPMs are very low, ideally with zero amplitude. In Figure 6.19, the Channel "X" and "I" digitized signals for cBPM2 with bunches of 500 pC are shown.

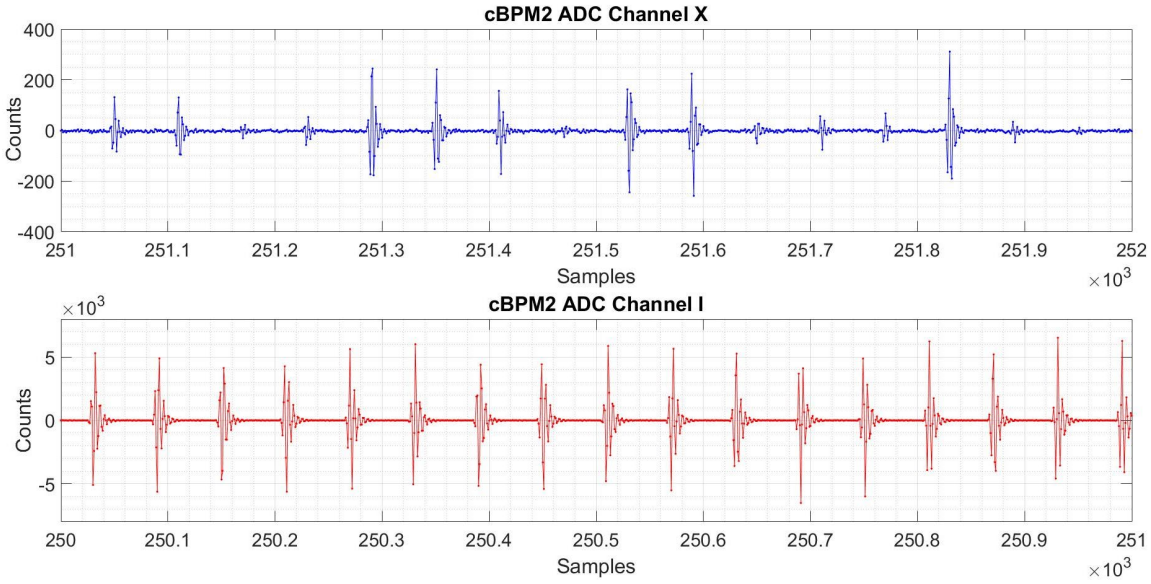

Figure 6.19: ADC signals of Channel X and I of cBPM2 with bunches passing near the e.m. center of the cBPM (Data set: "500 pC – Range 1300 µm").

As expected the Channel I signals have amplitudes of several thousands of counts (ADC limits are 8192 and -8191), because the signal coming from the “reference” resonator is charge-dependent only. Instead, the Channel X signals are very low in amplitude, with fluctuations from shot to shot dependent on the bunch per bunch beam fluctuations. In this case, the algorithm used by the readout electronics to evaluate the sign of the bunch position on the X axes of the transversal plane (see chapter 4.2) could lead to erroneous measurements and the assigned sign for each bunch position near the center could be miscalculated, bringing to an overall worsening of the resolution. This effect is clearly visible in the lower plot of Figure 6.20, where the difference in phase (Phase X-I), bunch by bunch, calculated by the readout electronics between the signals of Channel X and I is shown. Whatever is the difference in phase between the channels for a specific offset on the X axes (left or right from the e.m. center), the readout electronics is configured to interpret a shift of 180° in phase as a change of sign for the position of the beam. When the position of the beam is far enough from the e.m. center, the signals are strong enough (first and third segments of data, at a calculated position of 100 µm and -100 µm in the upper plot) and Phase X-I is properly calculated. In fact, the measured position is calculated to be positive in the first segment (roughly 100 µm) and negative (roughly -100 µm) in the third segment, when a shift of 180° of Phase X-I occurs. When the beam is near the e.m. center, in the second segment of data, it is possible to see that the measured Phase X-I has a lot of variability, bringing the algorithm used to assign the sign of the offset to not properly recognize the correct value, worsening the overall resolution of the measurement system for all the cBPMs (see Figure 6.14).

Another effect which is relevant for small beam offsets is the miscalculation of the beam position due to the presence of electronic offset and noise. This can be seen as a worsening of the accuracy of the measuring system and is related on how the position is calculated, particularly on the computation of the signal amplitudes of the cBPMs output signals (channel X,Y,I of “LIBERA CavityBPM”, see 4.2.1).

This effect is visible by analysing the position measurements for a bunch near the e.m center of the cBPM from the data set “200 pC – Range 1200 µm” (see Figure 6.21.): there is an interval around 0 µm where there are no data points.

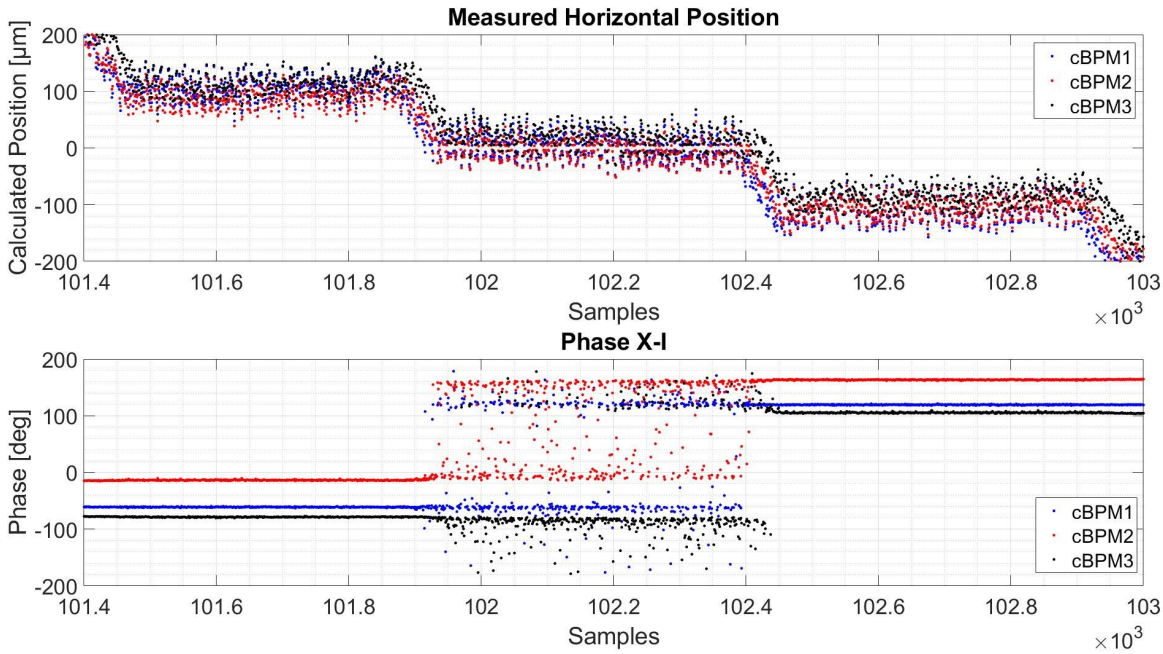

Figure 6.20: Upper plot: measured horizontal position for all the cBPM with bunches of 500 pC passing near the e.m. center of the cBPM. Lower plot: phase difference between the Channel X and I for each cBPM. Each sample represent the passage of a single bunch (Data set: "500 pC – Range 1300 µm").

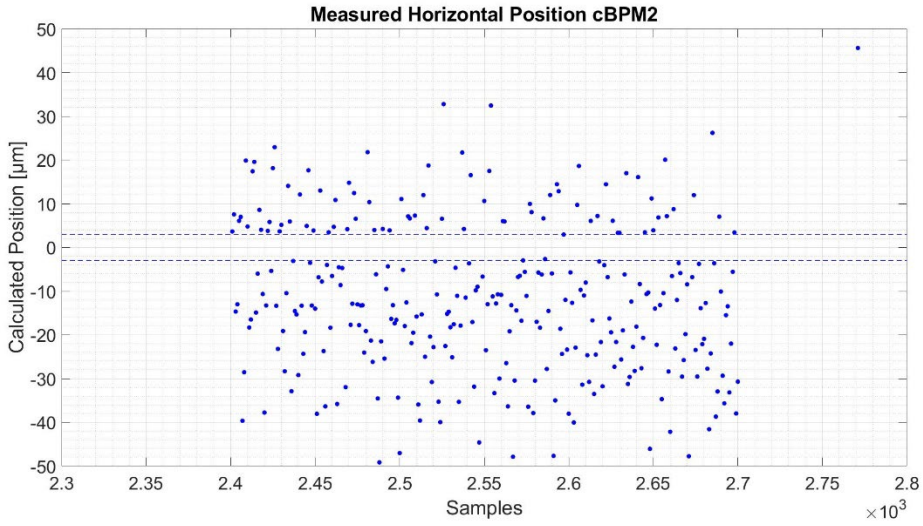

Figure 6.21: Measured horizontal position for cBPM2, for beams passing near the e.m. center of the cBPM (Data set: "200 pC – Range 1200 µm"). The dashed lines are at +3 µm and -3 µm, delimiting the area where there are no measurement points.

The same effect could also be seen on the second segment of data of the upper plot of Figure 6.20 for the data set "500 pC – Range 1300 µm". In the case depicted in the figure, the width of this interval is roughly equal to 6 µm (+3 µm / -3 µm) for each cBPMs.

Although the latter could vary, depending on the configuration set and on the bunch charge, similar width values for this interval were measured also for bunch charges of 500 pC.

This behaviour is due to the presence of noise/electronic offset that is digitized and, even in absence of cBPM signals, leads to a non-zero value of the calculated position.

This is easily explained by recalling how the amplitude of the signals (V_X, V_Y and V_I) and positions (X, Y) are calculated (eq. (4.2) and (4.3)) and observing that V_X, V_Y and V_I, are always positive quantities.

$$V_X = \sqrt{\sum_{bunch\ window} {x_n}^2}$$
$$V_I = \sqrt{\sum_{bunch\ window} {i_n}^2} \qquad (6.13)$$

In eq.(6.13) we reported the same equation of eq.(4.2), for one beam bunch and for the calculation of the horizontal position. x_n and i_n are the n^{th} samples of the "X" and "I" channels respectively. "Bunch window" is the sample window centered on the signals produced by the passage of one beam bunch. V_X and V_I are proportional to the amplitude of the signal associated to the passage of one beam bunch.

The absolute transverse position of each bunch is then obtained as (same as eq. (4.3)):

$$X = K_x \frac{V_X}{V_I} \qquad (6.14)$$

X is the calculated transverse distance of one beam bunch in respect to the electromagnetic center (e.m. center) of the "position" resonator in the horizontal axes. K_x is a user-defined calibration constant which take into accounts the sensitivity of the resonators, the level of input attenuator used and the attenuation of the cables.

The overall effect is that the signal amplitudes for all the channels (X, Y, I) are shifted by the contribution induced by electronic offset and noise.

It is possible to measure and compensate this contribution, by applying a correction on the data points acquired. By measuring V_X, V_Y, V_I in the absence of signals coming from the cBPMs, as:

$$V_{X_N} = \sqrt{\sum_{noise\ window} {x_i}^2}$$	*(6.15)*

where x_i is the i^{th} sample of the X channel; "noise window" is a sample window where only noise and electronic offset is present. Once V_{XN} is calculated, it can be subtracted from the calculated V_X for every bunch, in order to fix the systematic error caused by noise as:

$$V_{X_S} = \sqrt{{V_X}^2 - {V_{X_N}}^2}$$
$$V_{I_S} = \sqrt{{V_I}^2 - {V_{I_N}}^2} \qquad (6.16)$$

where V_{XS} is the contribution to the amplitude coming from the cBPM signals, V_X is the measured amplitude and V_{XN} is the contribution to the amplitude from noise/offset. A similar procedure could be repeated for Channel Y and Channel I of "LIBERA CavityBPM".

It was not possible to implement this correction within the calculation algorithm performed by the FPGA of the "LIBERA CavityBPM". As such we used a post-process script to calculate and use V_{XN}, V_{YN}, V_{IN} from the data already collected. The results of this data compensation in the data set with bunch charge of 200 pC and a nominal stage position of 0 µm are shown in Figure 6.22.

The overall effects for applying this compensation on Channel X and Channel I is a shift of the absolute value of the horizontal positions. From the figure it is possible to see that the fixed data set now presents calculated positions within ±3 µm from the center.

The amplitude of this compensation to the horizontal position for different nominal stage positions is shown in Figure 6.23. It is possible to observe that the effects of noise/offset on the measured position is negligible for high beam offsets.

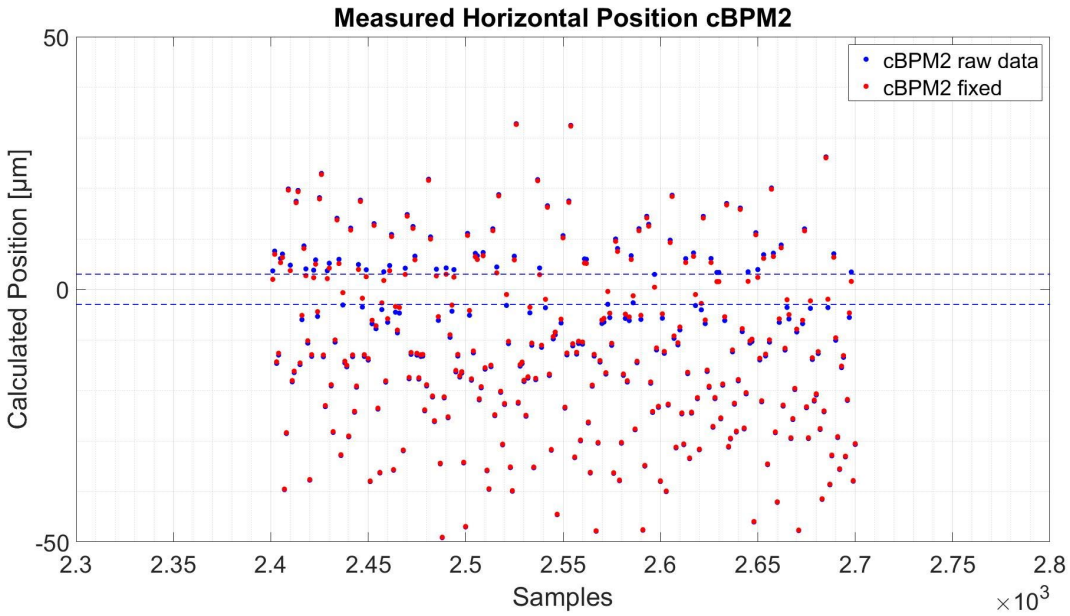

Figure 6.22: Measured horizontal position performed by cBPM2 with bunches of 200 pC, passing near the e.m. center of the cBPM. Blue dots represent the measurements associated with the passage of each bunch. Red dots represent the same measurements with noise/offset compensation. The dashed lines are at +3 µm and -3 µm.

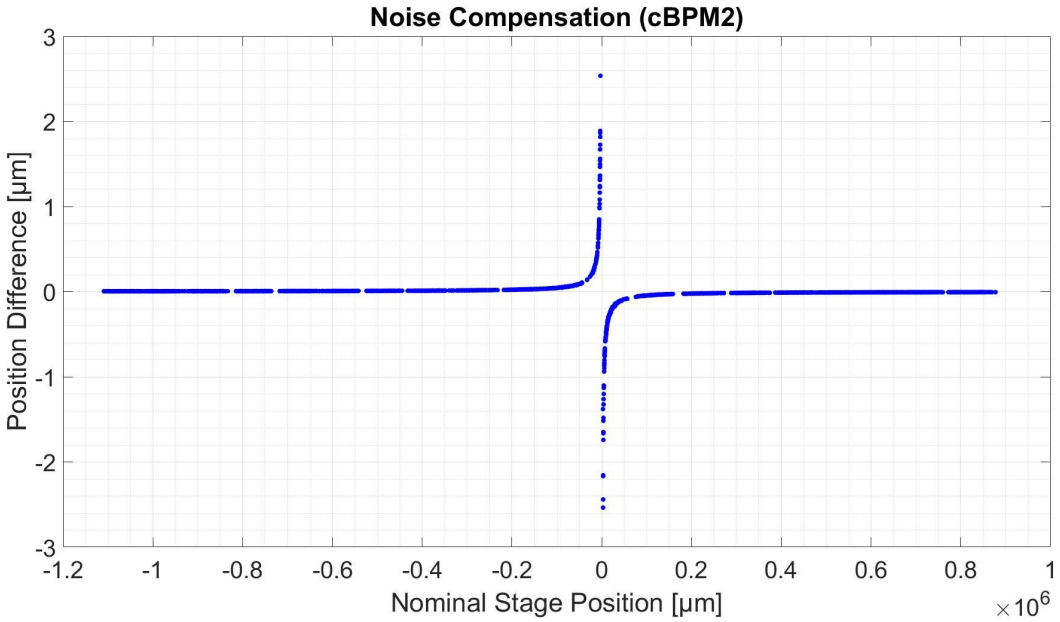

Figure 6.23: Shift of beam position by applying the noise compensation at different nominal stage position. The effects of noise/offset is relevant only for small values of the beam offset.

If there is enough time between bunches, it would be possible to calculate the noise contribution V_{XNb} for every bunch, by taking samples (x_i) on a window centered where

only noise is present ("noise window"), immediately before or after the "signal window". In this case, by subtracting this quantity from V_{Xb} the readout electronics would automatically compensate for the noise. This feature could be considered to be implemented in future upgrades of the readout electronics.

6.4.6 Resolution measurement with lower maximum measurement range

In order to better analyse the behaviour of the measurement system based on cBPMs and "LIBERA Cavity BPM", we performed resolution measurements with the configuration setup presented in Table 6.9.

Table 6.9: Configuration setup used to collect data set named "200 pC – Max Range 400 µm".

Configuration Setup for Data Set "200 pC – Max Range 300 µm"	
Parameter	**Value**
Bunch Charge	~200 pC
Internal Attenuators	X, Y: 0 dB; I: 16 dB
Max. Position measurement range	~ ± 400 µm
Position Range measured	± 150 µm
Position Steps	50 µm – 5 positions
ADC buffer max value	X: ~3000 counts I: ~6000 counts
ADC samples per bunch	60

By comparing it with the configuration setup "200 pC – Range 1200 µm", in Table 6.4, the value of the internal attenuators of the "LIBERA for CavityBPM" for channels X and Y were changed from 9 dB to 0 dB for each cBPM. By decreasing the attenuation, the amplitude of the signals from the "position resonator" of the cBPMs, as measured by the readout electronics, is higher (by a factor of 2.82). Calibration factors were changed accordingly to compensate the removal of attenuation and to guarantee the right conversion value for the position measurements. Nevertheless, by decreasing the input attenuation, there is a decrease by the same factor in the maximum position measurement range (from ~±1200 µm to ~±400 µm), as the latter is limited by the input range of the readout electronics ADC (±1 V). Resolution measurements for cBPM2, performed with the calculation of the residual and by considering 300 acquisitions per nominal stage position value, as described in Section 6.4.1, are presented in Figure 6.24.

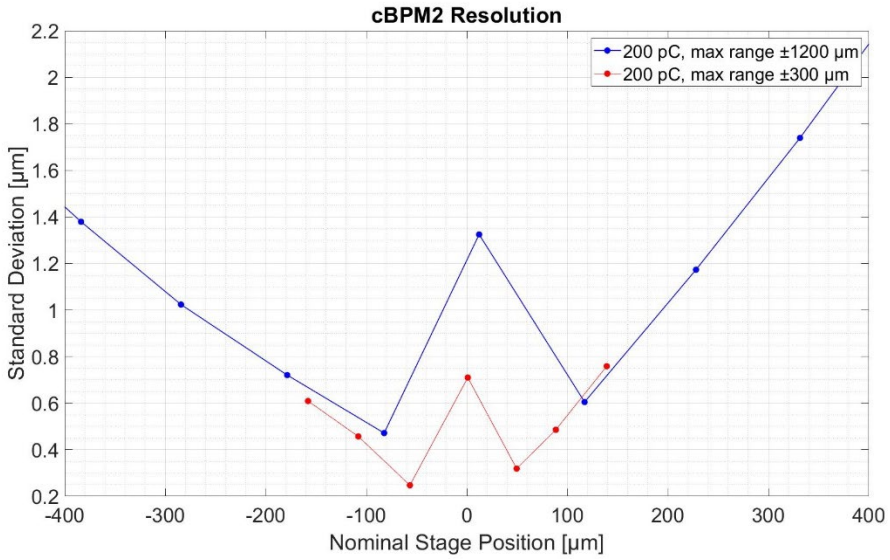

Figure 6.24: Cavity BPM2 horizontal position measurement resolution for different beam positions. Blue plot is relative to data set "200 pC – Max Range 1200 µm"; red plot is relative to data set "200 pC – Max Range 300 µm".

Besides the measurement at position "0 µm", already explained in Section 6.4.5, it is possible to observe that the resolution does not change significantly for data set "200 pC – Max Range 400 µm" and "200 pC – Max Range 1200 µm". This behaviour is compatible with the hypothesis that the resolution is limited by phase noise rather than thermal/electronic noise (see section 6.4.4).

By reducing the attenuation level, the signal for the same beam positon would be stronger and SNR should improve. Nevertheless, under the hypothesis that phase noise is dominant, the overall noise would increase proportionally with the signal, neglecting any resolution improvement.

On the contrary, if thermal/electronic noise would be the dominant one, magnifying the signals should bring an improvement on the resolution, as the noise would be smaller relative to the signals.

6.4.7 Resolution measurement by using I-Q demodulation

As described in section 4.2.1 and depicted in Figure 4.5, the "LIBERA Cavity BPM" uses two different algorithm path to calculate amplitude and phase of the digitized signals for each channel. For phase calculation, the digitized signals are I-Q demodulated and processed by the CORDIC algorithm.

We investigated the possibility to use an algorithm based on I-Q demodulation to calculate, not only the phase, but also the amplitude of the signals (and consequently the beam position). The aim was to find an algorithm more "robust" to noise and obtaining an improvement on the resolution. For a detailed description of digital I-Q demodulation and I-Q sampling see [54]. I-Q demodulation is one of the most diffused methods to analyse the cBPMs signals. Refer to [55] and [56], for examples of similar systems based on I-Q demodulation.

The "LIBERA Cavity BPM" does not allow to calculate the amplitude of the signals using I-Q demodulation, as such, we performed an offline analysis on the ADC data collected with the setup configuration "200 pC – Max Range 1200 µm".

The algorithm, based on the I-Q demodulation, relies on the fact that the output signals of the cBPMs (f_{res} = 3300 MHz, down-converted to f_{IF} = 375.3 MHz) and the ADC sampling (f_{ADC} = 497.53 MHz) are synchronized (see section 4.1). The phase advance Δφ (i.e. the phase advance of the down-converted signal in the interval between two consecutive sample is:

$$\Delta\varphi = 2\pi \cdot \frac{f_{IF}}{f_{ADC}} = 4.74\ rad \qquad (6.17)$$

The values I and Q can be calculated as [54]:

$$\begin{pmatrix} I_n \\ Q_n \end{pmatrix} = \frac{1}{sin\Delta\varphi} \cdot \begin{pmatrix} cos(n\Delta\varphi) & -cos((n+1)\Delta\varphi) \\ -sin(n\Delta\varphi) & sin((n+1)\Delta\varphi) \end{pmatrix} \cdot \begin{pmatrix} x_{n+1} \\ x_n \end{pmatrix} \qquad (6.18)$$

Where I_n and Q_n are the "in-phase" and "quadrature" components of the signal calculated with x_n and x_{n+1}, which are the n^{th} and $(n+1)^{th}$ samples of the Channel X.

By performing the calculation of I_n and Q_n on the first 30 ADC samples (out of 60) associated to the signal produced from a single bunch and applying the mean, it is possible to calculate I_b and Q_b, which are the components associated to the signal of the b^{th} bunch.

$$I_b = \sum_{n=1}^{30} \frac{I_n}{30} \quad for\ the\ b^{th}\ bunch\ window$$
$$Q_b = \sum_{n=1}^{30} \frac{Q_n}{30} \quad for\ the\ b^{th}\ bunch\ window \qquad (6.19)$$

The amplitude of the signal A_b and its phase ϕ_b are then calculated as:

$$A_b = \sqrt{I_b^2 + Q_b^2}$$
$$\Phi_b = atan\left(\frac{Q_b}{I_b}\right) \qquad (6.20)$$

The same algorithm can be applied for all channels (X, Y, I), obtaining A_{Xb}, A_{Yb}, A_{Ib} and ϕ_{Xb}, ϕ_{Yb}, ϕ_{Ib}. By doing this, it is possible to obtain the calculated position as:

$$X_b = K_x \frac{A_{X_b}}{A_{I_b}} \quad Y_b = K_y \frac{A_{Y_b}}{A_{I_b}} \qquad (6.21)$$

Which has the same structure as eq.(4.3) (including K_x and K_y which have the same value).

We tested this algorithm on the data set "200 pC – Max Range 1200 µm". By comparing the two algorithm (the one implemented in the FPGA of the "LIBERA for Cavity BPM" and the one based on I-Q demodulation) on the same data set, we obtained the differences on the calculated positions, shown in Figure 6.25.

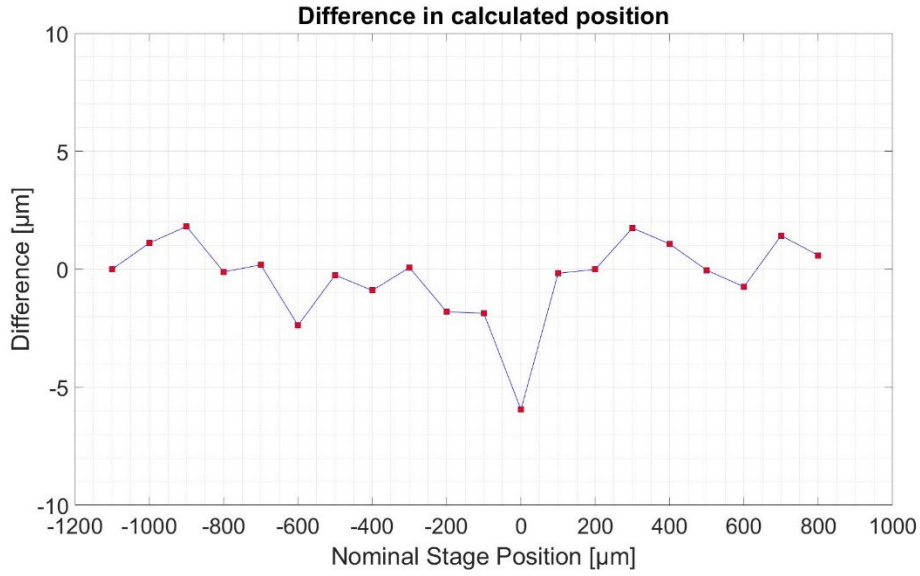

Figure 6.25: Difference in calculated horizontal position of Cavity BPM2 performed with two different algorithms. The first algorithm is the one implemented in the FPGA of "LIBERA Cavity BPM", the other is based on I-Q demodulation. Both algorithms were used with data set "200 pC – Max Range 1200 µm".

By using the same procedure, based on the calculation of the residual for cBPM2 (see section 6.4.1), we obtained resolution measurements, shown in Figure 6.26 and compared to the one obtained with the LIBERA algorithm (already shown in Figure 6.11).

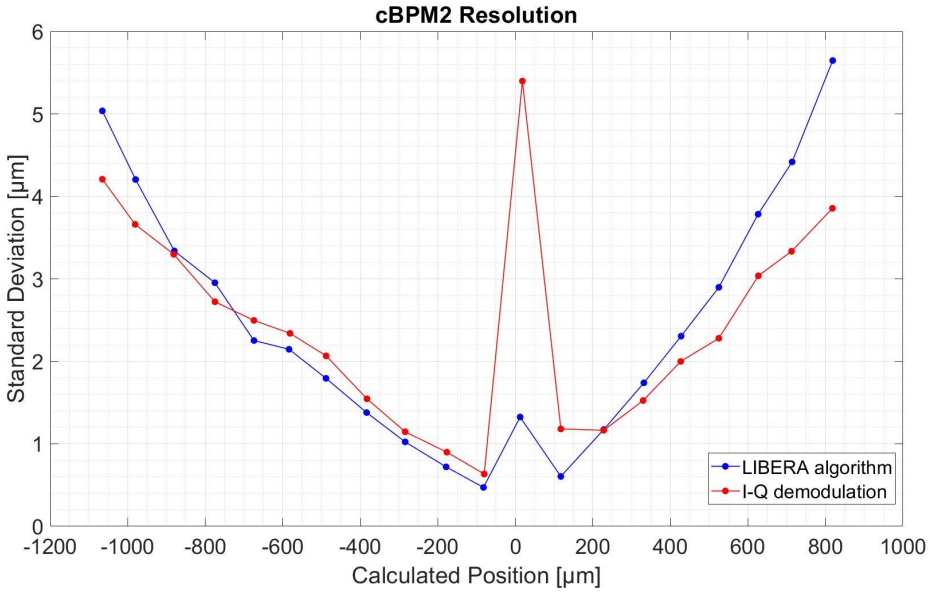

Figure 6.26: Cavity BPM2 horizontal position measurement resolution for different beam positions. Blue plot is relative to the algorithm implemented in the FPGA of "LIBERA Cavity BPM". Red plot is relative to the algorithm based on I-Q demodulation. Data set used: "200 pC – Max Range 300 µm".

As it can be seen from the results (as usual by not taking into account the measurements at the center), the differences on the calculated positions are in the order of few µm. Concerning the resolution, we obtained a small improvement for beam bunch positions far from the center (≥200 µm and ≤-800 µm) and a worsening for all the other values. We can conclude that the two algorithms are equivalent in terms of resolution achievable.

6.5 Crosstalk

If the BPMs are not perfectly machined but rather the cavities have a degree of eccentricity, excitations of the cavities antisymmetric modes in the X direction may become coupled with those in the Y direction. In Figure 6.27, four different cavity geometries are shown. In a perfectly round cavity (case (a)), the x and y antisymmetric modes are not coupled. If the cavity has a non-zero eccentricity, but the waveguides are aligned with the semi-major and semi-minor axes (case (b)), the modes are still not coupled, although the resonance frequency and the quality factor may differ between the two axes. If, however, the waveguides are not aligned, like in the previous case and/or they are not perfectly orthogonal (case (c) and (d)), a crosstalk between the

signals associated to the x axes and y axes may appear, as a consequence of a mix between the antisymmetric modes on the two axes [57].

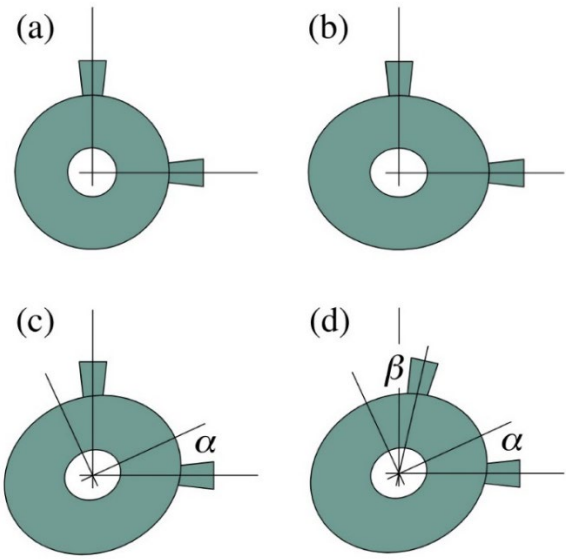

Figure 6.27: (a) A perfectly circular cavity with the wave guides at right angles. (b) An elliptical cavity with the semi-major and semi-minor axes aligned with the wave guides. (c) An elliptical cavity with the semi-major and semi-minor axes rotated by an angle α relative to the wave guides. (d) An elliptical cavity with the semi-major and semi-minor axes rotated by an angle α relative to the x-wave guide and by an angle β relative to the y-wave guide [57].

Crosstalk between the channels could also be introduced in the front-end electronics, since the output signals of the cBPM (X, Y, I) are processed independently, but within the same hardware platform.

Another possible source of crosstalk is related to the moveable stages, upon where the cBPMs are installed. This would be not a crosstalk related to the measuring system, but rather, a limitation of the test-stand. For example, if the cBPM waveguides are not aligned to the stages, moving the cBPM along one axes could enforce a misplacement on the other axes.

In order to investigate the crosstalk, we performed a specific set of measurements, by moving only cBPM2 on the horizontal axes from a nominal stage position of -800 µm to +800 µm with steps of 100 µm, leaving cBPM1 and cBPM3 to a fixed horizontal position and taking 300 acquisitions for each stage position. The vertical position for each cBPMs was left untouched near the “0 µm” nominal vertical position. The other configuration parameters were the same as the configuration setup “500 pC – Range 1300 µm”, reported in Table 6.3.

In order to get rid of beam fluctuations on the y axes, we calculated the residual for cBPM2, with the same procedure as described in section 6.4.1.

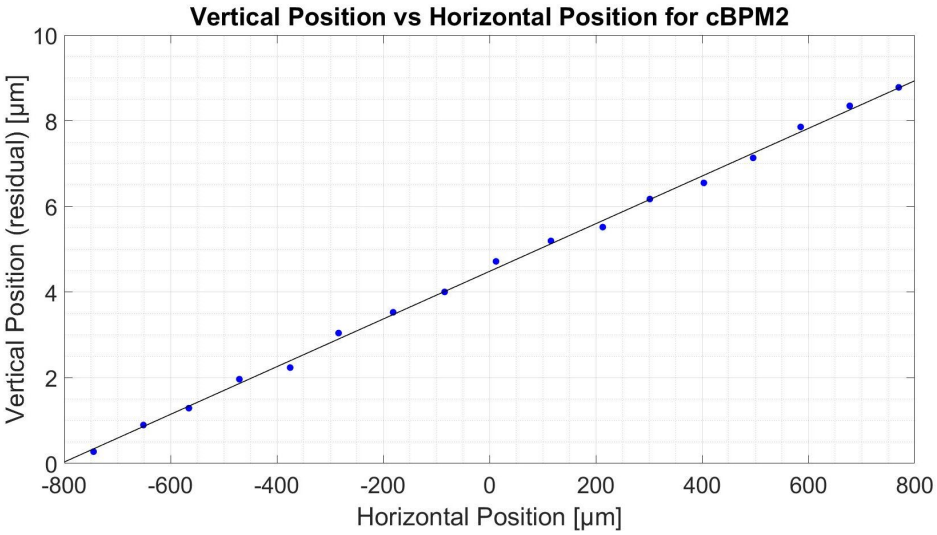

Figure 6.28: Calculated beam vertical position for different horizontal position for cBPM2. The vertical position was calculated as the residual of cBPM2, taking into accounts all the measured vertical position of each cBPM. Data represented (blue dots) are the mean values between 300 acquisitions. Black curse is a linear fit of the data. A dependency between the two axes is clearly visible.

Measurements demonstrate (see Figure 6.28) that there is a correlation between the calculated horizontal and vertical position: the coupling coefficient, calculated by means of a linear fit, is 0.0056 (-45 dB). However, it was not possible to determine if the crosstalk is caused by the cBPM geometry, the electronics or the test-stand.

6.6 Dependency on phase

Based on the observation already reported in section 5.4.1 for the laboratory measurements,, we studied the behaviour of the measuring system by modifying the phase of the output signals of cBPM2. More specifically, we installed a programmable delay generator immediately before the input port of Channel X of cBPM2 in order to modify the phase of the signal on channel X in respect to the phase of the signal on channel I. The horizontal position calculated by each cBPM and the measured phase difference between Channel X and I are reported in Figure 6.29. Figure 6.29Cavity BPMs were positioned near the "-500 µm" position and left untouched during the measurements. We used the delay generator to change the phase with steps of 30°

(300 acquisitions for each step). The other configuration parameters were the same as the configuration setup “500 pC – Range 1300 µm”, reported in Table 6.3.

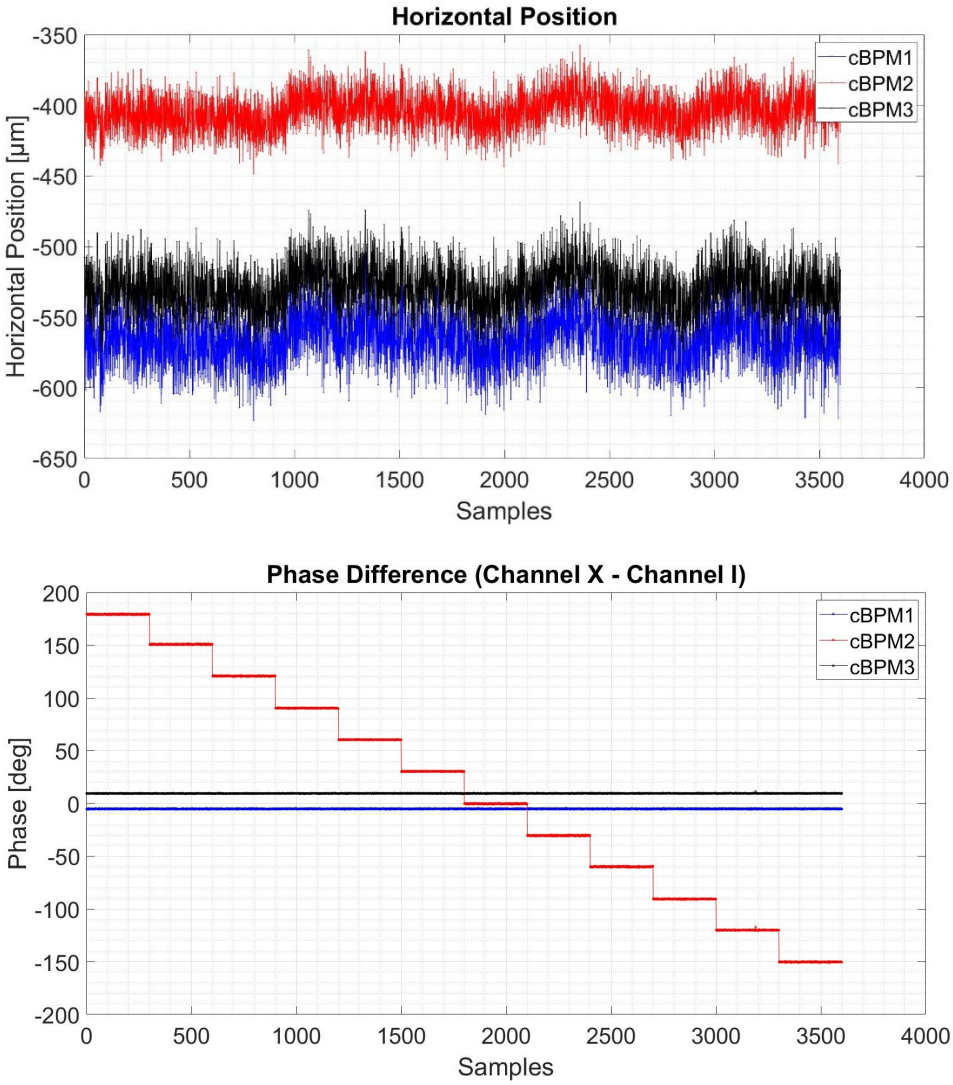

Figure 6.29: Upper plot: calculated horizontal position for each cBPM for different phase difference (see lower plot). Lower plot: calculated phase difference between signals on channel X and I for each cBPM. The phase difference was modified by mean of a delay generator device installed at the cBPM2 Channel X input.

In order to investigate the effect of a phase change on the calculated position and its resolution, we calculate the residual of the horizontal position of cBPM2, with the same procedure as described in section 6.4.1.

The mean and the standard deviation of Horizontal Position Residual of cBPM2 (obtained averaging 300 samples for each phase value) are reported in Figure 6.30.

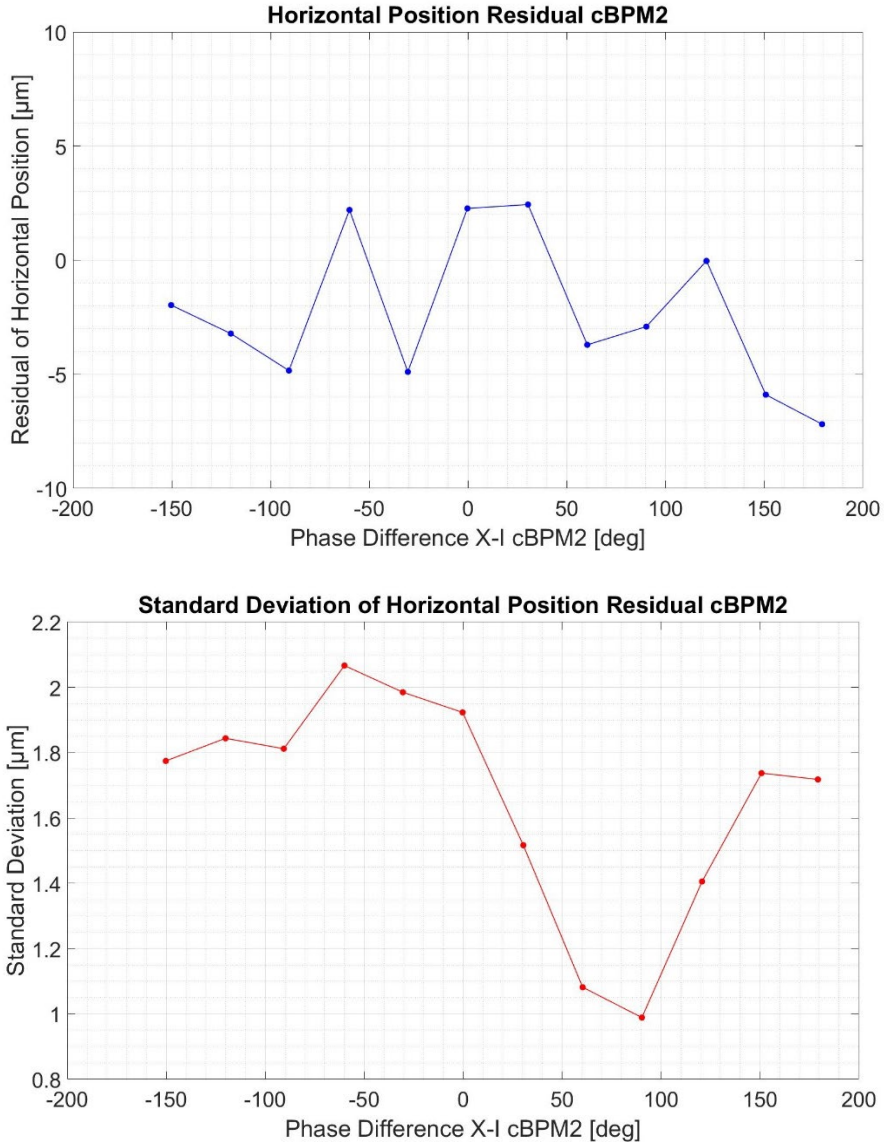

Figure 6.30: Mean (upper plot) and standard deviation (lower plot) of the horizontal position Residual of cBPM2 for different Phase differences between signal on Channel X and Channel I.

It is possible to notice that both the mean value and the standard deviation of the residual show a dependency on the phase difference between X and I signal. The mean value varies within an interval of approximately 10 µm and can be accounted as a degradation in accuracy of the measuring system. The cause is probably related to the synchronization between the sampling time and the signal. Further measurements are required to fully investigate this dependency

The standard deviation varies by approximately a factor of two. In contrast to the laboratory measurements, where the dependency was basically caused by the noise on

the input signal (see section 5.4.1), this could be related to jitter (see section 6.4.4). The latter introduces an uncertainty which is proportional to the gradient of the waveform. As such, by changing the phase of the signal to be digitized, the ADC captures samples at different time with different waveform gradients. The overall effect is that the phase noise contribution is dependent on the phase of the signal.

7 Conclusion and future work

The aim of the work presented in this thesis was to study, develop, characterize and put into operation a beam position monitor system, based on Cavity Beam Position Monitors (cBPM) for the ELI-NP GBS Linac. As explained in chapter 1, the cBPM are used at the interaction points of ELI-NP GBS, where the gamma beams are produced and where the accuracy and the resolution on the beam position are more compelling, in order to match the strict requirements for the produced photons. In particular, a resolution of 1 μm over a maximum observable range of ±1 mm and the possibility to measure the position of each beam bunch are the most challenging tasks. The work was focused particularly on the read-out electronics (Chapter 4), represented by the module "LIBERA Cavity BPM". The latter was developed by Instrumentation Technologies in strict collaboration with INFN-LNF and represent part of the work discussed in this thesis. The cBPMs used are the model "PSI BPM16", that has a design that fit well for the ELI-NP GBS requirements. In particular, the low value of the loaded quality factor allows the measurements of each bunch composing the beam during the multi-bunch operation mode. The crosstalk between bunches, induced by the tail of the signals induced by the passage of the bunch (relatively small, thanks to the low value of Q_L) was fixed with the implementation of a digital filter within the read-out electronics, called deconvolution filter, capable of decoupling the signals (see section 4.2.2). Another interesting feature of the readout electronics is the implementation of variable attenuators (which can also be calibrated), which allows to exploit all the dynamic range (and thus enhancing SNR), for any operational mode of ELI-NP GBS. Thus, the measuring system is adaptable for different bunch charges and different observable ranges of position. A lot of effort was put into the characterization of the position resolution of the system and in the signal analysis. The aim was not only to characterize the system, but also searching for different algorithms for signal treatment, which can enhance the performances of the measuring system.

In Chapter 5, measurements in laboratory with a cBPM and its readout electronics were presented. The test bench developed was revealed to be useful and can be used for future applications, when characterization of devices in presence of beam is not possible or practical. Although it allows to perform measurements only for the position "resonator", it gave us the possibility to test the readout electronics with cBPM signals and to estimate the resolution of the system. Splitting the output signal of the "position" resonator in two parts, one for the horizontal signal ("X") and the other for the reference signal ("I") (mimicking the signal of the "reference" resonator) had the advantage of

drastically reduce the noise coming from the signal generator used. All the functionalities of the LIBERA Cavity BPMs were successfully tested, including the effects of the variable attenuators, the deconvolution filter and the stability over time. Noise measurements and analysis show that for the signal levels expected for ELI-NP GBS application, the main source of noise are the active components of the readout electronics, particularly the ADC.

Resolution of the system was tested for different modes, including trains of pulses, which resemble the multi-bunch operation mode for ELI-NP GBS. We obtained a relative standard deviation of $0.4 \cdot 10^{-3}$ with sinewave signals, that, if translated into a position measurement, is below the aforementioned resolution of 1 μm over ±1 mm range. With pulse-like signal (both in single mode and for trains of pulses) we obtained worse resolutions for the fact that we did not used all the input range of the ADC, due to technical difficulties (which will be fixed in the future). Nevertheless, a sample scenario was presented where, by translating the measurement to beam position information, an estimation of 3.32 μm of resolution for a range of approximately ±4 mm is expected. By considering the resolution relative to the maximum observable range, the latter is also within the requirements of ELI-NP GBS. While the measurements with trains of pulses show the same results in terms of resolution, potential problems of desynchronization between the sample frequency and the signals digitized were detected. This requires further study as it could lead to a worsening of the accuracy of the system for trains of beam bunches.

In Chapter 6, measurements in presence of beam were presented. These were performed with three cBPM (with similar features of the cBPMs under study) already installed on a test-bench at FLASH1 in DESY. These measurements gave us the possibility to test the readout electronics during beam operations for bunch charges of 200 pC and 500 pC. The resolution, obtained through the calculation of residuals, showed a dependency on the beam position: for higher beam offsets (relative to the e.m. center of the cBPM), the measurement resolution was worse. For bunch charge of 500 pC and a maximum observable range of ±1.3 mm, the best resolution achieved was with the beam near the e.m. center of the cBPM (at 100 μm), with a value of 0.37 μm, while the worst resolution was at position “800 μm”, with a value of 5.56 μm. The hypothesis for this behaviour is that jitter of the reference signal used during the measurements introduced phase noise into the system, which is dominant in respect to thermal/electronic noise, worsening the overall position resolution. Worsening of the resolution was also found for beam position within a small range near the e.m. center of the cBPM (about ±3 μm). This problem was fully analysed and was revealed to be

caused by the algorithm which detects the phase of the cBPM signals. The latter is used for determining the direction of the beam offset. In the analysis of the measurements performed, proposals for different signal treatment were discussed with the aim of enhancing the accuracy and the resolution of the system. Moreover, a correlation between the phase of the cBPM signals and the resolution of the beam position was detected. The reason for this has to be fully investigated, while a possible solution could be the installation of programmable phase delay devices on the input channels of the readout module.

To summarize, the required resolution of 1 µm for ELI-NP GBS can be easily obtained with the cBPM and the readout module under study. Nevertheless, some of the issues exposed (such as the worsening of the resolution at the e.m. center, the resolution dependency on the phase of the cBPM signals and on the beam position) requires further testing and analysis. This is particularly true because the studies proposed here represents one of the first steps carried out for the design of beam position monitor systems for the linac under study for the EuPRAXIA project [4].

As such, a new test bench for cBPMs at SPARC-LAB at INFN-LNF, was designed and will be used in the immediate future. The test bench, based on the same design of the one used at DESY for the measurements presented in this dissertation, is already installed at the linac of SPARC-LAB, at INFN-LNF (see Figure 7.1).

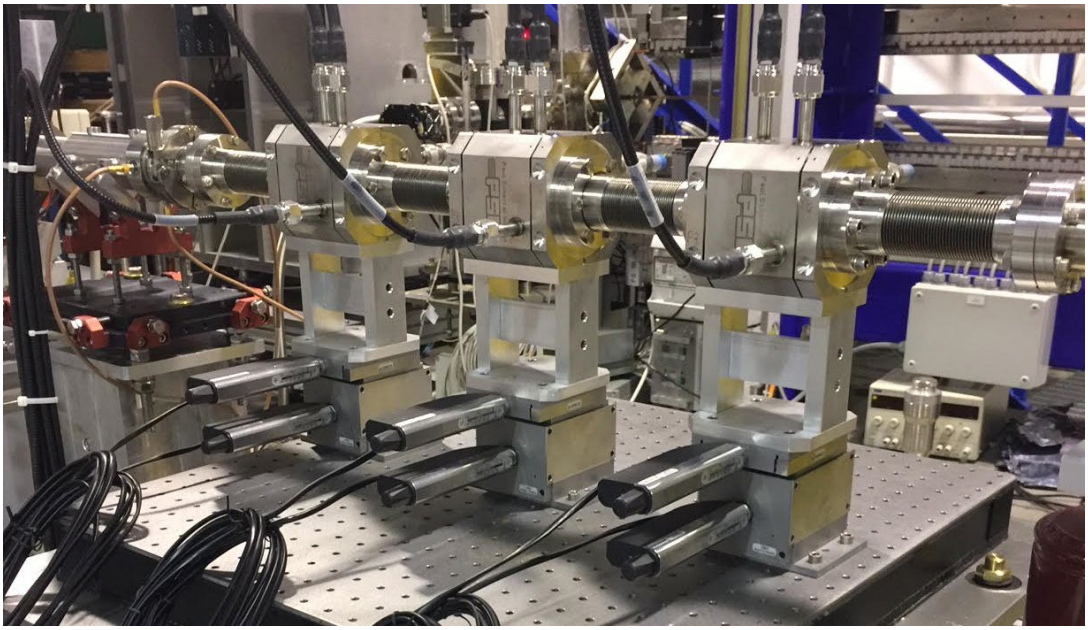

Figure 7.1: Test-bench with the three cBPM, model "PSI BPM16", installed at the linac of SPARC-LAB.

The test-bench consists of three Cavity BPMs (model “PSI BPM16”), installed on independent stages, moveable in both transverse directions by means of remote movers. Immediately after the three cBPMs, a stripline BPM [58] is also installed to perform comparison measurements.

Aim of the test bench is to perform measurements on the cBPMs similar to the ones carried out at FLASH1. The main reason for these is to further investigate the issues presented in this dissertation and to search possible solutions for them, dealing also with the new challenges related to the design of beam diagnostics for the EuPRAXIA.

8 Bibliography

[1] P.Forck, “Lecture Notes on Beam Instrumentation and Diagnostics”, Joint University Accelerator School (JUAS), 2007.

[2] P. Forck et al. “Beam Position Monitors”. Synchrotron Radiation News, 1(3), 2008

[3] L. Serafini et al., “Technical Design Report EuroGammaS. Proposal for the ELI-NP Gamma Beam System”, arXiv:1407.3669, 2014.

[4] P. A. Walker et al., 'Horizon 2020 EuPRAXIA design study', J. Phys.: Conf. Ser. 874, 012029, 2017.

[5] A. Giribono et al., “ELI-NP GBS status”, Proceedings of International Particle Accelerator Conference 2017 (IPAC2017), Copenhagen, Denmark, pp. 880-883, ISBN 978-3-95450-182-3, 2017.

[6] G.Korn et al., “ELI – Extreme Light Infrastructure – Whitebook”, THOSS Media GmbH, 2011

[7] B. Rus et al., “Outline of the ELI-Beamlines facility”, Proceedings of SPIE 8080 (June 9, 2011). DOI:10.1117/12.890392

[8] S. Kuhn et al. “The ELI-ALPS facility: The next Generation of Attosecond sources”, Journal of Physics B: Atomic, Molecular, Optical Physics 50, DOI: 10.1088/1361-6455/aa6ee8, 2017.

[9] G. Wormser et al., “The White Book of ELI Nuclear Physics Bucharest-Magurele, Romania”, www.researchgate.net, 2010

[10] K. Cassou et al. “Low power commissioning of an innovative laser beam circulator for inverse Compton scattering γ-ray source”, Phys. Rev. Accel. Beams Vol. 22, Iss. 9, doi.org/10.1103/PhysRevAccelBeams.22.093501, 2019

[11] F. Cardelli, “Design, realization and commissioning of RF Power system and accelerating structures for a Gamma Source”,
Doctoral Thesis - Scuola di Dottorato in Fisica degli Acceleratori, Università di Roma, a.a. 2016/2017.

[12] P. Tracz, “ELI-NP Gamma Beam System — New Facility for Nuclear Physics Research”,
Proceedings of IEEE 21st International Conference on Pulsed Power (PPC), 10.1109/PPC.2017.8291290, 2011

[13] C. Sun et al., “Theoretical and Simulation Studies of Characteristics of a Compton Light Source”,
Physical Review Special Topics - Accelerators and Beams 14.4, 10.1103/PhysRevSTAB.14.044701, 2011.

[14] A. Giribono, “6D Phase space optimisation for high brightness electron beams in RF linacs as drivers for high brilliance inverse compton X and Y ray sources”,
Doctoral Thesis - Scuola di Dottorato in Fisica degli Acceleratori, Università di Roma, a.a. 2016/2017.

[15] G. Franzini et al., “Beam Diagnostics for Charge and Position Measurements in ELI-NP GBS”,
Proceedings of International Beam Instrumentation Conference 2016 (IBIC2016), Barcelona, Spain, pp. 682-685, ISBN 978-3-95450-177-9, 2016.

[16] A.A. Nosych et al., “Measurements and Calibration of the Stripline BPM for the ELI-NP Facility with the Stretched Wire Method”,
Proceedings of International Beam Instrumentation Conference 2015 (IBIC’15), Melbourne, Australia, p. 423-427, 2015.

[17] G.Franzini et al., “Analysis and Correction of Geometrical Non-Linearities of ELI-NP BPMS on Position and Current Measurements”,
Proceedings of International Particle Accelerator Conference 2017 (IPAC’17), Copenhagen, Denmark, p. 235-237, 2017.

[18] F. Marcellini et al., “Design of Cavity BPM Pickups for SwissFEL”,
Proceedings of International Beam Instrumentation Conference 2012 (IBIC2012), Tsukuba, Japan, pp. 390-393, ISBN 978-3-95450-119-9, 2012.

[19] B. Keil et al. “Design of the SwissFEL BPM system”,
Proceedings of the 2nd International Beam Instrumentation Conference (IBIC 2013), Oxford, UK, pp. 427–430, 2013

[20] T. Shintake, “Development of nanometer resolution RF-BPMs”,
Proceedings of HEAC’99, 1999.

[21] S. Walston et al., “Performance of a high resolution cavity beam position monitor system”,
Nuclear Instruments and Methods in Physics Research - Section A, Accelerators, Spectrometers, Detectors and Associated Equipment, 578(1), pp 1-22. doi:101016/jnima200704162, 2007.

[22] E. Jensen, “Cavity basics”,
Proceedings of Cern Accelerator School 2010 (CAS ’10): RF for Accelerators, Ebeltoft, Denmark, arXiv:1201.3202, 2010.

[23] D. Whittum et al., “Analysis of an asymmetric resonant cavity as a beam monitor”,
Review of Scientific Instruments. Vol.70 pp 2300 - 2313. 10.1063/1.1149756, 1999.

[24] M.Dal Forno, “Theoretical and experimental analysis of interactions between electromagnetic fields and relativistic electrons in vacuum chamber”,
Doctoral Thesis - Scuola di Dottorato di Ricerca in Ingegneria dell’Informazione - Università degli Studi di Trieste, a.a. 2011/2012.

[25] T. Nakamura, "Development of Beam-position Monitors with High Position Resolution”,
Master Thesis, The University of Tokyo, 2008.

[26] N. Y. Joshi, “Design and Analysis Techniques for Cavity Beam Position Monitor Systems for Electron Accelerators”,
Doctoral Thesis - Department of Physics- Royal Holloway, University of London, 2013.

[27] D. Lipka, “Cavity BPM designs, related electronics and measured performances”.
Proceedings of European Workshop on Beam Diagnostics and Instrumentation for Particle Accelerators (DIPAC ’09), Basel, Switzerland, 2009.

[28] S. Shin et al. “Design of a Low-Q S-Band Cavity Beam Position Monitor”, Journal of The Korean Physical Society, Vol. 52, No. 4, April 2008, pp. 992-998, 2008.

[29] Y. Inoue et al. “Development of a high-resolution cavity-beam position monitor”, Physical Review Special Topics - Accelerators and Beams, 11. 10.1103/PhysRevSTAB.11.062801, 2008.

[30] B. Keil et al. “First beam commissioning experience with the SwissFEL cavity BPM system”, Proceedings of International Beam Instrumentation Conference (IBIC2017), Grand Rapids, USA, pp.251-254, https://doi.org/10.18429/JACoW-IBIC2017-TUPCF17, 2017.

[31] M. Cargnelutti et al., “Design and simulations of the cavity BPM readout electronics for the ELI-NP Gamma Beam System”, Proceedings of International Particle Accelerator Conference 2016 (IPAC2016), Busan, Korea, pp. 264-266, ISBN: 978-3-95450-147-2, 2016.

[32] “User Manual and Specifications for Libera Cavity BPM”, Instrumentation Technologies, www.i-tech.si, 2017.

[33] “EPICS-IOC User Manual for Libera Cavity BPM”, Instrumentation Technologies, www.i-tech.si, 2017.

[34] “ADL5611 Data Sheet”, Analog Devices, Inc., www.analog.com

[35] “AD9528 Data Sheet”, Analog Devices, Inc., www.analog.com

[36] “ADF4107 Data Sheet”, Analog Devices, Inc., www.analog.com

[37] C. Pearson, "High-speed analog-to-digital converter basics", Texas Instruments, Application Report, www.ti.com, 2011

[38] P. Poshala et al., "Why Oversample when Undersampling can do the job?", Texas Instruments, Application Report, www.ti.com, 2013

[39] “AD9680 Data Sheet”, Analog Devices, Inc., www.analog.com

[40] M. Cargnelutti et al., “S-Band Cavity BPM Readout Electronics for the ELI-NP Gamma Beam Source”,
Proceedings of International Beam Instrumentation Conference 2017 (IBIC2017), Grand Rapids, MI, USA, ISBN 978-3-95450-192-2, 2017.

[41] “Fundamentals of RF and Microwave Noise Figure Measurements”,
Keysight Technologies, Application Note, www.keysight.com, 2019.

[42] A. Lyapin et al., “Cavity BPM System for ATF2”,
Proceedings of European Workshop on Beam Diagnostics and Instrumentation for Particle Accelerators (DIPAC ’11), Hamburg, Germany, 2011.

[43] G. Franzini et al., “Measurements with the ELI-NP Cavity Beam Position Monitor Read-Out Electronics at FLASH”,
Proceedings of International Particle Accelerator Conference 2018 (IPAC2018), Vancouver, Canada, 4 pp., doi:10.3204/PUBDB-2018-02065, 2018.

[44] D.Lipka et al., “FLASH Undulator BPM Commissioning and Beam Characterization Results”,
Proceedings of International Beam Instrumentation Conference 2014 (IBIC’14), Monterey, USA, p. 315-319, 2014.

[45] B.Keil et al., “The European XFEL Beam Position Monitor System”,
Proceedings of International Particle Accelerator Conference 2010 (IPAC’10), Kypto, Japan, p.1125-1127, 2010.

[46] A. Stella et al., “Beam Tests with LIBERA in Single Pass Mode”,
Proceedings of the 9th European Workshop on Beam Diagnostics and Instrumentation for Particle Accelerators (DIPAC2009), Basel, Switzerland, pp. 306-308, 2007.

[47] M. Stadler et al., ”Beam Test Results of Undulator Cavity BPM Electronics for the European XFEL”,
Proceedings of International Beam Instrumentation Conference 2012 (IBIC2012), Tsukuba, Japan, p. 406, 2012.

[48] V. Balakin et al., “Experimental results from a microwave cavity beam position monitor”,
Proceedings of Particle Accelerator Conference (PAC ’99), New York, USA, 1999.

[49] H. Maesaka et al., “Performance of the RF Cavity BPM at XFEL/SPring-8 ``SACLA''”, Proceedings of 33rd Int. Free Electron Laser Conf. (FEL'11), Shanghai, China, pp. 539-542, 2011.

[50] L. De Nardo, “On the Propagation of Statistical Errors”, www.phenix.bnl.gov, 2002

[51] B. Brannon, "Sampled systems and the effects of clock phase noise and jitter", Analog Devices, Application Note, vol. AN-756, 2004.

[52] W. Kester, “Converting Oscillator Phase Noise to Time Jitter”, Analog Devices, Tutorial MT-008, , www.analog.com, 2009

[53] B. Brannon et al. “Aperture Uncertainty and ADC System Performance.”, Analog Devices, Applications Note, vol. AN-501, www.analog.com, 2006

[54] T.Schilcher, “RF applications in digital signal processing”, CAS 2007 - CERN Accelerator School: Digital Signal Processing, Proceedings, 2008.

[55] S.T. Boogert et al., “Cavity beam position monitor system for ATF2”, Proceedings of International Particle Accelerator Conference 2010 (IPAC’10), Kyoto, Japan, pp. 1410-1412, 2010.

[56] M. Stadler et al., “Low-Q Cavity BPM Electronics for E-XFEL, FLASH-II and SwissFEL”, Proceedings of 3rd Int. Beam Instrumentation Conf. (IBIC'14), Monterey, CA, USA, pp. 670-674, 2014.

[57] V. Vogel et al. “Performance of a Nanometer Resolution BPM System”, UCRL-CONF-216283, Nanobeam, 2005.

[58] A.Stella et al. “Stripline bpm with integral in-vacuo termination” Proceedings of 3rd Int. Particle Accelerator Conf. (IPAC'12), New Orleans, LA, USA, pp. 828-830, 2012.